

DOKUZ EYLÜL UNIVERSITY
GRADUATE SCHOOL OF NATURAL AND APPLIED
SCIENCES

APPLICATION OF NEW MATRIX MATERIALS
FOR DISSOLVED AND GASEOUS CARBON
DIOXIDE SENSING AND FIBER OPTIC CO₂
SENSOR DESIGN

by
Sibel DERİNKUYU

February, 2010
İZMİR

**APPLICATION OF NEW MATRIX MATERIALS
FOR DISSOLVED AND GASEOUS CARBON
DIOXIDE SENSING AND FIBER OPTIC CO₂
SENSOR DESIGN**

**A Thesis Submitted to the
Graduate School of Natural and Applied Sciences of Dokuz Eylul University in
Partial Fulfillment of the Requirements for the Degree of Doctor of
Chemistry in
Chemistry, Applied Chemistry Program**

**by
Sibel DERİNKUYU**

**February, 2010
İZMİR**

Ph.D. THESIS EXAMINATION RESULT FORM

We have read the thesis entitled “**APPLICATION OF NEW MATRIX MATERIALS FOR DISSOLVED AND GASEOUS CARBON DIOXIDE SENSING AND FIBER OPTIC CARBON DIOXIDE SENSOR DESIGN**” completed by **SIBEL DERINKUYU** under supervision of **ASSOCIATED PROFESSOR KADRIYE ERTEKIN** and we certify that in our opinion it is fully adequate, in scope and in quality, as a thesis for the degree of Doctor of Chemistry.

Doç. Dr. Kadriye Ertekin

Supervisor

Prof. Dr. Ali Celik

Committee Member

Doç. Dr. Erdal Celik

Committee Member

Examining Committee Member

Jury Member

Prof.Dr. Cahit HELVACI

Director

Graduate School of Natural and Applied Sciences

ACKNOWLEDGMENTS

I would like to express sincere gratitude to my supervisor Associated Professor Dr. Kadriye Ertekin for providing the fascinating subject, for her valuable support during this thesis and for the great working conditions at our laboratory.

I want to thank to Associated Professor Dr. Yavuz Ergun for his valuable support.

I gratefully acknowledge the extensive helps of my colleagues Ozlem Oter, Sibel Kacmaz, Merve Zeyrek and Sibel Aydogdu.

Finally, I want to thank to my parents for their tolerant attitude to my working effort during the elaboration of this dissertation and for their incessant support during all the years of my studies.

Sibel DERİNKUYU

APPLICATION OF NEW MATRIX MATERIALS FOR DISSOLVED AND GASEOUS CARBON DIOXIDE SENSING AND FIBER OPTIC CARBON DIOXIDE SENSOR DESIGN

ABSTRACT

In most of the optical CO₂ sensor designs, pH probes with different absorption or emission maxima were embedded in a polymer or sol-gel matrix material. Immobilization of the dye in the matrix material effectively induces spectral characteristics of the sensing agent. In this work, polyvinyl chloride (PVC), ethyl cellulose (EC) and polymethylmethacrylate (PMMA) were used together with different types of additives for CO₂ or dissolved CO₂ sensing purposes. Carbon dioxide carriers of perfluorochemicals or room temperature ionic liquids were employed and tested as polymer additives. Newly synthesized azomethine (AZM) dyes 4,4'-[hydrazine-1,2-dilidendimethylidene]bis N,N-dimethylaniline, 4-[(4-(dimethylamino)phenyl)methylidene hydrazono] methyl benzonitrile and N,N'-bis-(4-metoxifenyl) methylidene-benzene-1,4-diamine were characterized by spectroscopic ways in thin film or micro fiber form in the polymer matrix materials. Quantum yield and acidity constant (pKa) calculations of the AZM dyes were performed in the conventional solvents and/or in the employed solid matrices. Their fluorescence based response to CO₂ or dissolved CO₂ were examined in flow systems with fiber optics. To our knowledge this is the first attempt to produce electrospun sensor fibers for CO₂ sensing purpose. The potential use of some of azomethine molecules as optical switches for the realization of artificial functions at the molecular level was also investigated. Their cross sensitivities to anions, metal cations and effect of ionic strength were tested. Except that of azomethine dyes, three potential fluorescence Schiff bases were also investigated for CO₂ and pH sensing in plasticized PVC and EC, with or without additives.

Absorption and emission based spectral data and acidity constants (pK_a) of the schiff bases were determined in conventional solvents such as PVC and EC.

Keywords: Fiber optic CO₂ sensor, optical CO₂ sensor, dissolved CO₂, fluorescent pH indicator, carbon dioxide.

ÇÖZÜNMÜŞ VE GAZ KARBON DİOKSİT TAYİNİ İÇİN YENİ MATRİKS MALZEMELERİNİN UYGULAMASI VE FİBER OPTİK KARBON DİOKSİT SENSÖR TASARIMI

ÖZ

Çoğu optik CO₂ sensör tasarımında farklı absorpsiyon veya emisyon maksimumlarına sahip olan pH problemleri polimer ya da sol-jel matrikse hapsedilmiştir. Boyanın matriks materyaline immobilizasyonu sensör materyalin spektral özelliklerini etkiler. Bu çalışmada, polivinil klorür (PVC), etil selüloz (EC) ve polimetilmetakrilat (PMMA) gaz haldeki ve çözünmüş CO₂'in analizi için farklı katkı maddeleri ile birlikte kullanılmıştır. Karbon dioksit taşıyıcı perfloro bileşikler veya oda sıcaklığında sıvı halde bulunan iyonik sıvıların polimer katkı maddeleri olarak kullanılmasının etkileri araştırılmıştır. Yeni sentezlenen azometin (AZM) boyaları 4,4'-[hidrazin-1,2-dilidendimetiliden]bis N,N-dimetilanilin, 4-[(4-(dimetilamino)fenil)metiliden hidrazono] metil benzonitril ve N,N'-bis-(4-metoksifenil) metiliden-benzen-1,4-diamin polimer matriks materyallerinde mikro fiber formunda veya ince film olarak spektroskopik çalışmalarla karakterize edilmiştir. AZM boyalarının kuantum verimi ve asitlik sabiti (pKa) hesaplamaları bilinen çözücülerde ve/veya kullanılan katı matrikslerde gerçekleştirilmiştir. İndikatörlerin kullanılan matrikslerde gaz haldeki veya çözünmüş karbon dioksit floresans esaslı yanıtları fiber optikli akışkan sistemde incelenmiştir. Bu çalışma CO₂ ölçüm çalışmaları için elektro eğirme yolu ile elde edilmiş sensör özellikteki fiberlerin üretimi için ilk çalışmadır. AZM moleküllerinin, yapay fonksiyonların gerçekleşmesinde optik anahtar olarak kullanılma potansiyeli de moleküler düzeyde araştırılmıştır. İndikatör kompozisyonunun anyonlara, metal katyonlarına ve iyonik şiddete karşı duyarlılıkları incelenmiştir. Bu çalışmada CO₂ analizi ve pH ölçümü için azometin boyalarının dışında katkı maddesi içeren ya da içermeyen polimer matrikslerde (PVC ve EC) üç farklı floresans schiff bazının cevabı araştırılmıştır. Bu schiff bazlarının absorpsiyon ve emisyon esaslı spektral yanıtları ve asitlik sabiti (pKa) değerleri bilinen çözücülerde, PVC ve EC ortamlarında incelenmiştir.

Anahtar Sözcükler: Fiber optik CO₂ sensörü, optik CO₂ sensörü, çözünmüş CO₂, floresans pH indikatörü, karbon dioksit.

CONTENTS

	Page
THESIS EXAMINATION RESULT FORM	ii
ACKNOWLEDGEMENTS	iii
ABSTRACT	iv
ÖZ	vi
CHAPTER ONE-INTRODUCTION	1
1.1 Chemical Sensors	1
1.2 Sensor Classification	1
1.3 Optical Sensors	2
1.3.1 Advantages and Disadvantages of Optical Sensors	2
1.4 Fiber Optic Sensors	3
1.4.1 Theory of Absorption and Fluorescence.....	5
1.4.1.1 Principle of UV/VIS Absorption Spectroscopy.....	5
1.4.1.2 Principle of Fluorescence Spectroscopy	6
1.5 Luminescence	7
1.5.1 Mechanism of Luminescence	7
1.5.2 Stoke's Shift	9
1.5.3 Quantum Yield.....	9
1.5.4 Solvatochromism	10
1.6 Absorption-Based Sensors	11
1.6.1 Beer-Lambert Law.....	12
1.6.2 Instrumentation	15
1.7 Fluorescence-Based Sensors	15
1.7.1 Fluorescence Based Gas Sensors.....	15
1.7.1.1 Optical Oxygen Sensors.....	16
1.7.1.2 Optical NO _x sensors	17
1.7.1.3 Optical CO ₂ sensors	17

1.7.1.3.1 Gas Phase CO ₂ Measurements	18
1.7.3.1.2 Dissolved CO ₂ Measurements.....	19
1.8 Polymers for Optical Sensors	21
1.8.1 Polymers as Matrix Materials.....	21
1.8.2 Requirements for Polymer Matrix Materials.....	22
1.8.3 Types of Polymers Used in Optical Sensing	22
1.8.3.1 Lipophilic Polymers and Plasticizers.....	22
1.8.3.2 Hydrophilic Polymers	24
1.8.3.3 Ionic Polymers (Polyelectrolytes).....	24
1.8.3.4 Sol-Gel Glass	25
1.8.3.5 Molecularly Imprinted Polymers (MIPs).....	26
1.8.4. Immobilisation of Indicator Chemistry in Polymers	28
1.8.4.1 Hydrophobic Interactions.....	28
1.8.4.2 Ion-Exchange	29
1.8.4.3 Covalent Immobilisation.....	30
1.8.5 Polymer Effect on Indicator Chemistry.....	33
1.8.5.1 Co-Extraction and Ion-Exchange.....	33
1.8.5.1.1 Measurement of Cations.....	34
1.8.5.1.2 Measurement of Anions	35
1.8.5.2 Potential Sensitive Dyes (PSDs).....	36
1.8.5.2.1 Measurement of Cations.....	37
1.8.5.2.2 Measurement of Anions	38
1.8.5.3 Chromogenic and Fluorogenic Indicators.....	40
1.8.5.3.1 Measurement of Ions.....	40
1.8.5.3.2 Measurement of Cations.....	41
1.8.5.3.3 Measurement of Anions	42
1.8.5.3.4 Measurement of Neutral Analytes.....	42
1.9 Combination of Sensor Materials with Transducers	44

CHAPTER TWO-INTRODUCTION 46

2.1 Carbon Dioxide 46
2.2 Dissolved CO₂ Equilibria 46
2.3 pH Calculations in a H₂CO₃ Solution..... 50

CHAPTER THREE-EXPERIMENTAL METHOD AND INSTRUMENTATION 52

3.1 Construction of Fiber Optic Measurement System 53
3.2 Combination of the Flow System with Fiber Optic System 54
3.3 Mixing of the Gases 56
3.4 Construction of the Sensing Films 56
 3.4.1 PVC Cocktail Preparation 56
 3.4.2 Ethyl Cellulose Cocktail Preparation..... 58
 3.4.3 PMMA Cocktail Preparation 59
3.5 Quantum Yield Calculations 59
3.6 Preparation of the Employed Buffer Solutions 60
 3.6.1 Preparation of 0.005 M Acetic Acid/Acetate Buffer 60
 3.6.2 Preparation of 0.005 M NaH₂PO₄·2H₂O and 0.005 M Na₂HPO₄·12H₂O Buffer..... 61

CHAPTER FOUR-SPECTRAL CHARACTERIZATION OF AZOMETINE DYES IN DIFFERENT MATRIX MATERIALS..... 62

4.1 Photophysical Characterization of Azometine Dyes..... 62
4.2 Structural Identification of AZM-I, AZM-II and AZM-III..... 62
4.3 Thin Film Preparation Protocols 63
4.4 Results and Discussion 64
 4.4.1 Absorption Based Spectral Characterization..... 64

4.4.2 Spectral Evaluation, Fluorescence Quantum Yield Calculations and Interpretation of Emission Spectra	68
4.4.3 Acid–Base Behavior of the Schiff Bases.....	72
4.4.3.1 Acid–Base Behavior of the AZM Derivatives in Ethanol	72
4.4.4 pK _a Calculations of AZM-I, AZM-II and AZM-III in PVC Matrix Acid–Base and Molecular Switch Behavior of The AZM Derivatives in PVC Matrix.....	77
4.4.5 Acid–Base and Molecular Switch Behavior of the AZM Derivatives in EC Matrix	85
4.4.6 Reproducibility of the Response.....	87
4.4.7 Cross Sensitivity to Acidogenic Species, Anions, Metal Cations and Effect of Ionic Strength	89
4.5 Conclusion.....	92

CHAPTER FIVE-DISSOLVED CO₂ STUDIES IN IONIC LIQUID AND ETHYL CELLULOSE MATRIX..... 93

5.1 Experimental Studies.....	93
5.2 Synthesis of the AZM-I, AZM-II	93
5.3 Dissolved CO ₂ Sensing Studies	94
5.4 Results and Discussion	95
5.4.1 Spectral Evaluation, Interpretation of Emission Spectra.....	95
5.5 Conclusion.....	102

CHAPTER SIX-EMISSION BASED FIBER OPTIC CO₂ and pH SENSING WITH LONG WAVELENGTH EXCITABLE SCHIFF BASES 103

6.1 Introduction	103
6.2 Synthesis of the Schiff Bases (CY–1, CY–2 and CY–3)	104
6.3 PVC Cocktail Preparation	105
6.4 Ethyl Cellulose Cocktail Preparation	105
6.5 Results and Discussion	106
6.5.1 Spectral Characterization Studies in Solvents	106

6.5.2 Spectral Evaluation, Interpretation of Emission Spectra.....	109
6.5.3 pK _a Calculations of CY-1, CY-2 and CY-3 in PVC Matrix.....	110
6.5.4 Gas Phase Sensing Studies for EC Doped CY-1, CY-2 and CY-3.....	116
6.5.5 Dissolved CO ₂ Sensing Studies CY-1, CY-2 and CY-3 in EC.....	122

CHAPTER SEVEN- CO₂ SENSING STUDIES WITH ELECTROSPUN PMMA FIBERS.....131

7.1 Introduction	131
7.2 Materials and Equipment.....	133
7.3 Gaseous and Dissolved CO ₂ Sensing Studies in PMMA	135
7.4 Results and Discussion	135
7.5 Conclusion.....	139

CHAPTER EIGHT-CONCLUSION..... 141

REFERENCES..... 142

CHAPTER ONE

INTRODUCTION

1.1 Chemical Sensors

Simply, an optical chemical sensor is a device that measures a physical quantity or the concentration of a chemical or biochemical species and converts it into a signal which can be read by an observer or by an instrument. The most widely used basic measuring techniques in optical chemical sensors are optical absorption and luminescence, but sensors based on other optical parameters, such as refractive index and dispersion, have also been developed. However, sometimes the term “sensor” is being used to refer to a cation or anion-selective molecular probe or a pH indicator.

According to the way of signal transmission sensors can be classified into two main types, namely electrochemical sensors and optical sensors. The typical examples are ion selective electrodes and pH papers. The former was developed at the early 1950's, but have some disadvantages such as sensitivity to electrical interferences (Janata, 1990). The latter were developed at the beginning of thirties and found a widespread application, particularly in the 1980's after their combination with optical fiber technology and solid-state components.

1.2 Sensor Classification

According to their working principles sensors can be classified into three types; physical, chemical and biosensors. The physical sensors mainly measure physical parameters such as temperature, pressure, acoustic waves, acceleration, strain, position and magnetic field. The chemical sensors detect all chemical species including ions, gases and neutral compounds. The biosensors comprise metabolites, products or reactants of enzymatic reactions and other biomaterials such as antibodies, antigens and even cells.

1.3 Optical Sensors

In most of the optical sensor designs, the interaction of analyte with the receptor part is converted into optical information. Optical parameters which may serve as an analytical signal in optical sensors include;

- a) absorbance,
- b) reflectance,
- c) luminescence, including fluorescence,
- d) refractive index,
- e) light scattering,
- f) polarization and
- g) optothermal effects (IUPAC, 1991).

Optical sensors have shortly been named optrodes (optical electrodes) or optodes. An **optode** or **optrode** is an optical sensor device that optically measures a specific substance usually with the aid of a chemical transducer.

1.3.1 Advantages and Disadvantages of Optical Sensors

The following features of optical sensors are considered to be advantageous (Wolfbeis, 1991);

- 1) They do, in principle, not require a reference signal. In practice, however, a reference detector for compensating intensity drifts of the light source is sometimes required.
- 2) Electric and magnetic fields do not interfere with optical signals.
- 3) Most optical sensor spots are cheap and simple, and the reagent phase can be easily exchanged.

Especially for fiber optic sensors it can be stated that;

- 1) The ease of miniaturization allows the development of very small, light and flexible sensors.

- 2) Low-loss optical fibers allow transmittance of optical signals over wide distances and remote sensing in hazardous or inaccessible environments.
- 3) Distributed multiplexed sensing is possible.

Notwithstanding the advantages, optical sensors may exhibit one or more of the following disadvantages;

- 1) Ambient light can interfere.
- 2) Sensors with indicator phases are likely to have limited long-term stability because of photobleaching or wash-out.
- 3) Sensors with immobilized pH indicators as well as chelating reagents have limited dynamic ranges as compared to electrodes since the respective association equilibria obey the mass action law.
- 4) Response time is determined by the mass transfer of the analyte into the indicator phase.
- 5) In the water analysis it is often mandatory to control the pH and to correct the signal for pH effects.

1.4 Fiber Optic Sensors

The alternative use of optical fibers in various applications has grown, especially during the past 10-15 years. Optical fibers can be used as sensors to measure temperature, pressure and other physical quantities by modifying a fiber so that the quantity to be measured modulates a light related parameter such as intensity, phase, polarization, and wavelength or transit time of light throughout the fiber. With the development of optical fibers, which are a component of the communication industry, an ideal media for the transport of optical information was found. They are particularly important for remote sensing.

Fiber optic sensors which rely on a change in the light transmission characteristics of the fiber, caused by an alteration in a specific physical property of a medium being sensed are classified as intrinsic sensors. Such physical properties are temperature, acoustic wave, acceleration, strain position and magnetic field (Oehme, 1995).

In extrinsic fiber optic sensors, in contrast, any kind of optical spectroscopy is coupled with the fiber optic technique. They may be further subdivided into first, second and third generation sensors, respectively. In the first group, the fiber simply acts as a light guide. It allows remote spectrometric analysis of any analyte having an intrinsic optical property. These sensors are also called bare-ended fiber sensors or plain fiber sensors.

Because a variety of chemical species does not have an analytically useful intrinsic optical property, in a second group the analytical information of interest is mediated by some sort of indicator chemistry.

Unfortunately, for a variety of analytes there are no indicators known or they do not fulfill certain requirements such as selectivity. This is particularly true for biomolecules. As a result, third order generation sensors have been developed. They make use of a catalytic, mostly biocatalytic process, which result in a species detectable by first or second order generation sensors (Oehme, 1995).

There are two fundamental technologies known for the construction of optical sensors. In the first, the sensor chemistry is manufactured first and then attached to the fiber or fiber bundle. The sensor layers are usually produced on planar supports and then glued or mechanically fixed at the tip of either a bifurcated fiber bundle or a single optical fiber. In the second type, the chemistry is manufactured directly on the fiber, after coating and clad have been removed. The fibers may be coated again at the end of bifurcated fiber bundle or a single optical fiber. Alternatively, the chemistry can be immobilized along a section of the core of the optical fiber to make an evanescent field-type sensor. Planar waveguides covered at one side with the sensing chemistry were utilized as attenuated total reflection elements. In the latter two techniques, the efficiency of the interaction between light and the transducer is increased and thereby even sensitivity (Oehme, 1995).

1.4.1 Theory of Absorption and Florescence

1.4.1.1 Principle of UV/VIS Absorption Spectroscopy

Molecules having proper chromophore groups absorb ultraviolet or visible fraction of light. The absorbance of a solution increases as attenuation of the beam increases. Absorbance is directly proportional to the path length, b , and the concentration, c , of the absorbing species.

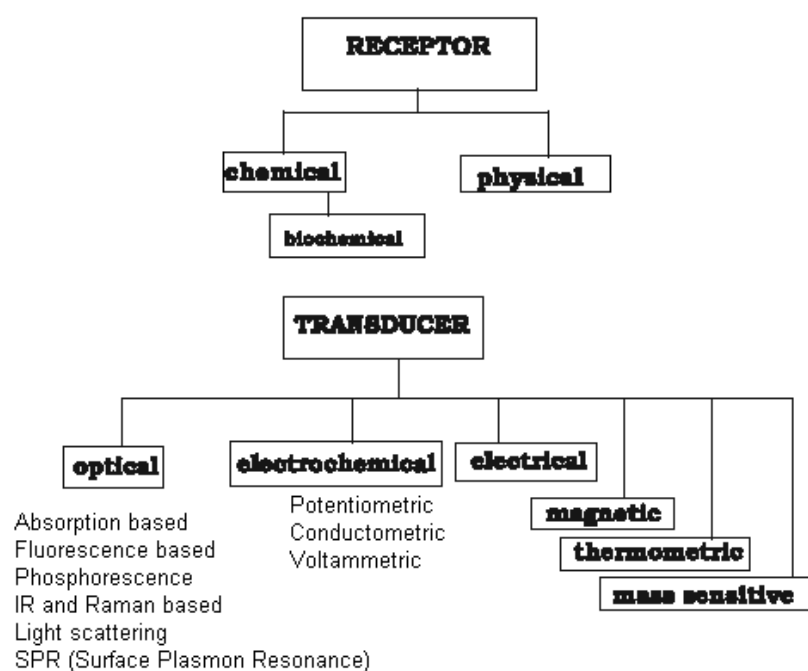


Figure 1.1 Classification of chemical sensors according to the working principle of the receptor and transducer.

Beer's Law states that

$$A = \epsilon bc \text{ (Eq.1.1)}$$

where ϵ is a constant of proportionality, called the molar absorptivity coefficient. Different molecules absorb radiation of different wavelengths. An absorption spectrum will show a number of absorption bands corresponding to certain chromophore groups within the molecule. For example, the absorption that is observed in the UV region for the carbonyl group in acetone is of the same wavelength as the absorption from the carbonyl group in diethyl ketone (Baldini,

Chester, Homola & Martellucci, 2004). Ultraviolet-visible spectroscopy (UV = 200 - 400 nm, visible = 400 – 800 nm) corresponds to electronic excitations between the energy levels that correspond to the molecular orbital of the systems. In particular, transitions involving π orbital and ion pairs (n = non-bonding) are important and so UV/VIS spectroscopy is of most use for identifying conjugated systems which tend to have stronger absorptions (Wolfbeis, 1991; Göpel, Hesse & Zemel, 1991-1993; Janata, 1989; Seitz, 1991; MacCraith and et al. 1977; Skoog, West & Holler, 1994).

1.4.1.2 Principle of Fluorescence Spectroscopy

Luminescence is light that can be emitted at normal and lower temperatures and is observed when the energy of an electronically excited state is released in the form of light. Depending on whether the excited state is singlet or triplet, the emission is called fluorescence or phosphorescence.

In excited singlet states, the electron in the excited orbital is paired (of opposite spin) to the second electron in the ground-state orbital. Consequently, return to the ground state is spin-allowed and occurs rapidly by emission of a photon. The emission rates of fluorescence are typically 10^8 s^{-1} , so that typical fluorescence lifetime is near 10 ns ($10 \times 10^{-9} \text{ s}$) (Lakowicz, 1993; Parker, 1968; Schmidt, 1994). The lifetime (τ) of a fluorophore is the average time between its excitation and its return to the ground state. It is valuable to consider a 1-ns lifetime within the context of the speed of light. Light travels 30 cm or about one foot in one nanosecond. Many fluorophore display subnanosecond lifetimes. Because of the short timescale of fluorescence, measurement of the time-resolved emission requires sophisticated optics and electronics. In spite of the experimental difficulties, time-resolved fluorescence is widely practiced because of the increased information available from the data, as compared with stationary or steady-state measurements (Lakowicz, 1993; Parker, 1968; Schmidt, 1994).

Phosphorescence is emission of light from triplet excited states, in which the electron in the excited orbital has the same spin orientation as the ground-state

electron. Transitions to the ground state are forbidden and the emission rates are slow ($10^3 - 10^0 \text{ s}^{-1}$), so that phosphorescence lifetimes are typically milliseconds to seconds. Even longer lifetimes are possible, as is seen from “glow-in-the-dark” toys: following exposures to light, the phosphorescent substances glow for several minutes while the excited phosphors slowly return to the ground state.

1.5 Luminescence

1.5.1 Mechanism of Luminescence

As mentioned earlier luminescence means emission of light by electronically excited atoms or molecules. Electronic excitation requires the supply of energy. Various kinds of luminescence, such as electroluminescence, chemiluminescences, thermoluminescence and photoluminescence, are known and called by the source from which energy is derived. In the case of photoluminescence (fluorescence and phosphorescence) the energy is provided by the absorption of infra-red, visible or ultra-violet light (Lakowicz, 1993; Parker, 1968; Schmidt, 1994). Two models are necessary to describe the interaction of light with matter: In the one light is regarded as a succession of waves, in the other as a collection of particles. The latter was introduced by Planck, who showed that radiant energy can only be absorbed in definite unites or quanta (Lakowicz, 1993; Parker, 1968; Schmidt, 1994). The energy quantum E , is defined as;

$$E = h \nu = h \frac{c}{\lambda} \quad (\text{Eq. 1.2})$$

where ν is the frequency, h is Planck's constant ($6.626 \times 10^{-34} \text{ Js}$), λ the wavelength, and c the constant velocity of light in vacuum ($2.998 \times 10^8 \text{ ms}^{-1}$). The absorption and emission of light is illustrated by Jablonski level diagram, shown in Figure 1.2. According to the Boltzmann distribution, at room temperature the valance electrons are in the lowest vibration level ($\nu=0$) of the ground electronic state. A transition of these electrons from the ground state (level 0 of S_0) to higher energy levels takes place on absorption (a) of light. The Franck-Condon principle states that there is approximately no change in nuclear position and spin orientation, because absorption of light occurs in about 10^{-15} s . Therefore, the electronic transition is represented by a

vertical line. Molecules excited to an upper vibrational level of any excited state rapidly lose their excess of vibrational energy by collision with solvent molecules, and falls to the lowest vibrational level. Molecules in the upper excited states (S_2, S_3, \dots) relax by internal conversion (IC), radiationless to the lowest excited singlet state (S_1) within 10^{-12} s. Transition from this level to the vibration levels of the ground state can take place by emitting photons (f). A portion of the excited molecules may return to the ground state by other mechanisms, such as electron transfer, collision, intersystemcrossing (ICS), internal conversion or chemical reaction. Fluorescence emission occurs spontaneously, again in accordance with the Franck-Condon principle, if the radiationless transition lifetime is sufficiently long. The radiative lifetime of fluorescence lies between 10^{-9} s for spin allowed transitions ($\pi^* \rightarrow \pi$) to 10^{-6} for less probable transitions ($\pi^* \rightarrow \pi$). Molecules in the lowest excited state (S_1) can also undergo conversion to the first triplet state (T_1) by intersystem crossing (ISC). This process requires a time of the same order of magnitude as fluorescence radiation lifetime and therefore competes with fluorescence. Although radiative transitions between states of different multiplicity are spin forbidden, these transitions do take place with low probability compared with singlet-singlet, or triplet-triplet transitions. Emission from the first triplet state (T_1) to the ground state is termed phosphorescence, and usually shifted to higher wavelengths than fluorescence. The radiation lifetime for this transition is about 10^{-2} to 10^{+2} s (Lakowicz, 1993; Parker, 1968; Schmidt, 1994).

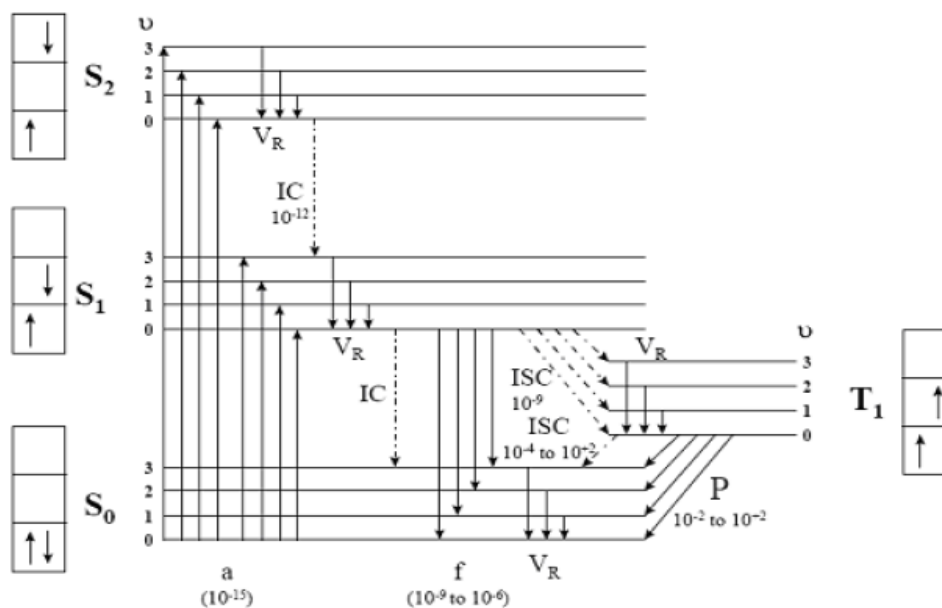


Figure 1.2 Jablonski diagram with the reciprocal rates of transition in [s] (retrieved from Mayr, 1999)

1.5.2 Stoke's Shift

The law of Stokes states that the fluorescence and phosphorescence is shifted to higher wavelengths relatively to absorption (Stoke's Shift). The explanation is provided by the Jablonski diagram. As already mentioned, emission usually occurs from the lowest excited state, but higher excited state are reached by absorption. The radiationless vibrational relaxation (VR) and internal conversion (IC) involves a loss of energy which is reflected in a shift to emission bands of lower energy. Furthermore, molecules generally decay to excited vibrational levels of S_0 (Lakowicz, 1993; Parker, 1968; Schmidt, 1994).

1.5.3 Quantum Yield

A molecule in the relaxed state S_1 (the lowest excited state) can return to the ground state, radiationless or by the emission of fluorescence. The fluorescence quantum yield is the ratio of the number of photons emitted to the number absorbed expressed by the rate constants Γ and k , respectively. Hence, the quantum yield can be written as

$$\Phi = \frac{\Gamma}{\Gamma + k} \quad (\text{Eq. 1.3})$$

The quantum yield can be close to unity if the radiationless rate of deactivation (k) is much smaller than the rate of radiative emission ($k \ll \Gamma$) (Lakowicz, 1993; Parker, 1968; Schmidt, 1994).

1.5.4 Solvatochromism

The excitation and emission spectra of many chromophores are sensitive to the polarity of their surrounding environment. A hypsochromic (or blue) shift of the absorption band, with increasing solvent polarity is called negative solvatochromism. The corresponding bathochromic (or red shift) is entitled positive solvatochromism. Obviously, solvatochromism depends on the solvation of the ground and first excited state of the chromophore. If the ground state is better stabilized by increasing solvent polarity than the excited state, negative solvatochromism is observed. Better stabilization of the excited molecule relative to that in the ground state, with increasing polarity, leads to positive solvatochromism. The solvent polarity does not only affect the absorption spectra, but also the emission spectra. The mechanism is illustrated in Figure 1.3. According to the Franck-Condon principle nuclei do not move during the timespan of an electronic transition (10^{-15} s). Therefore, the excited molecule (B) has the same solvation pattern as the molecule in the ground state. Excited molecules have a lifetime in order of about 10^{-8} s. The solvent molecules reorientate within 10^{-10} s resulting in relaxed excited state, with a solvation shell in equilibrium to this state. From this relaxed excited state (C) light is emitted. By analogy, the orientation of the solvent molecules does not change during the emission (D), due to Franck-Condon principle. Re-orientation of the solvent molecules follows, resulting in an equilibrium ground state (A). The interaction of a molecule with solvent upon excitation and emission, can be described by a change of the molecule's dipole moment in the ground (μ) and excited state (μ^*). A positive solvatochromism is observed if the dipole moment is increased during excitation, while decreasing dipole moment results in negative solvatochromism (Lakowicz, 1993; Schmidt, 1994; Reichardt, 1988).

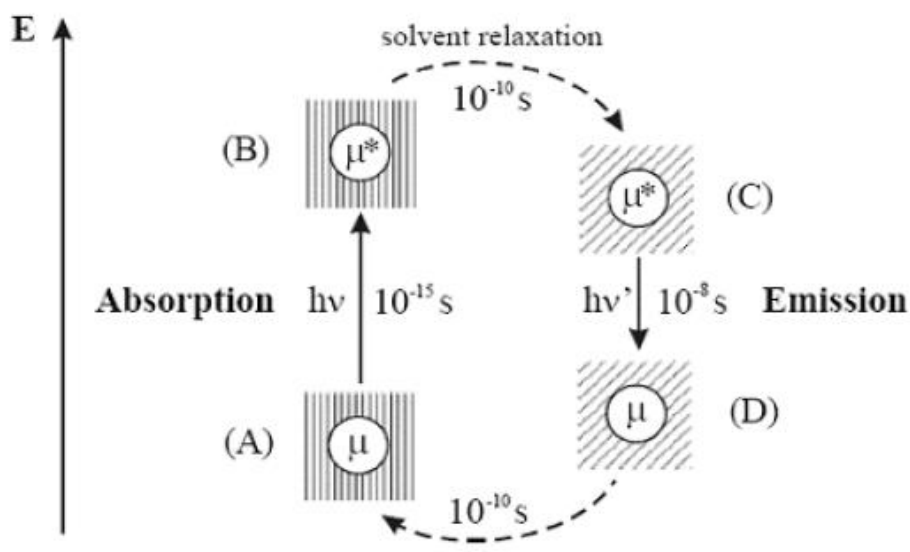


Figure 1.3 Effect of the solvent on the energy of a dipole (μ) upon excitation and emission. Different solvation shells are illustrated by squares filled with different patterns (retrieved from Mayr, 1999).

1.6 Absorption-Based Sensors

An absorption spectrum is the absorption of light as a function of wavelength. Light absorption is a function of the concentration of the absorbing molecules. The absorption of UV or visible radiation corresponds to the excitation of outer electrons. There are three types of electronic transition which can be considered:

1. Transitions involving π , σ , and n electrons
2. Transitions involving charge-transfer electrons
3. Transitions involving d and f electrons (not covered in this Unit)

When an atom or molecule absorbs energy, electrons are promoted from their ground state to an excited state. In a molecule, the atoms can rotate and vibrate with respect to each other. These vibrations and rotations also have discrete energy levels, which can be considered as being packed on top of each electronic level (Figure 1.4). (Baldini, Chester, Homola & Martellucci, 2004).

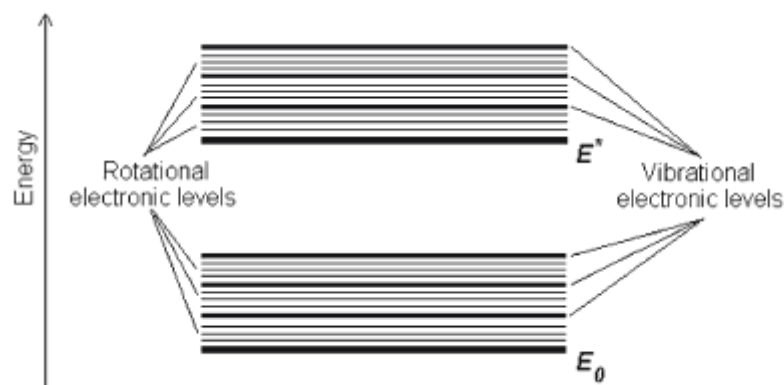


Figure 1.4 Energy Levels (retrieved from Baldini, Chester, Homola & Martellucci, 2004).

1.6.1 Lambert – Beer Law

The Beer-Lambert law reveals the linear relationship between absorbance and concentration of an absorber of electromagnetic radiation (Baldini, Chester, Homola & Martellucci, 2004). The general Beer- Lambert law is usually written as (Wolfbeis, 1991; Göpel, Hesse & Zemel, 1991-1993; Janata, 1989; Skoog, West & Holler, 1994).

$$A = a_{\lambda} \cdot b \cdot c \quad (\text{Eq. 1.4})$$

where A is the measured absorbance, a_{λ} is a wavelength-dependent absorptivity coefficient, b is the path length, and c is the analyte concentration. When working in concentration units of molarities, the Beer-Lambert law is written as:

$$A = \varepsilon_{\lambda} \cdot b \cdot c \quad (\text{Eq. 1.5})$$

where ε_{λ} is the wavelength-dependent molar absorptivity coefficient with units of $\text{M}^{-1} \text{cm}^{-1}$. The λ subscript is often dropped with the understanding that a value for ε is for a specific wavelength. If multiple species that absorb light at a given wavelength are present in a sample, the total absorbance at that wavelength is the sum due to all absorbers:

$$(\text{Eq. 1.6})$$

$$A = (\varepsilon_1 \cdot b \cdot c_1) + (\varepsilon_2 \cdot b \cdot c_2) + \dots$$

where the subscripts refer to the molar absorptivity and concentration of the different absorbing species that are present. Experimental measurements are usually made in terms of transmittance (T), which is defined as:

$$T = \frac{P}{P_0} \quad (\text{Eq. 1.7})$$

where P is the power of light after it passes through the sample and P_0 is the initial light power. The relation between A and T are:

$$A = -\log(T) = -\log\left(\frac{P}{P_0}\right) \quad (\text{Eq. 1.8})$$

The Figure 1.5 shows the case of absorption of light through an optical filter and includes other processes that decrease the transmittance such as surface reflectance and scattering (Baldini, Chester, Homola & Martellucci, 2004).

In analytical applications we often want to measure the concentration of an analyte independent of the effects of reflection, solvent absorption, or other interferences. The next figure shows the two transmittance measurements that are necessary to use absorption to determine the concentration of an analyte in solution (Figure 1.6). The top diagram is for solvent only and the bottom is for an absorbing sample in the same solvent. In this example, P_s is the source light power that is incident on a sample, P is the measured light power after passing through the analyte, solvent, and sample holder, and P_0 is the measured light power after passing through only the solvent and sample holder. The measured transmittance in this case is attributed to only the analyte. Depending on the type of instrument, the reference measurement (top diagram) might be made simultaneously with the sample measurement (bottom diagram) or a reference measurement might be saved on computer to generate the full spectrum.

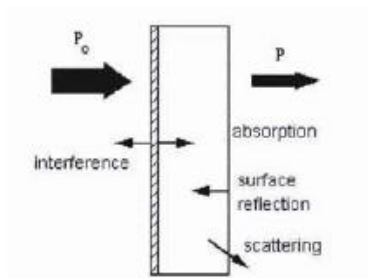


Figure 1.5 Absorption of light by and optical filter (retrieved from Baldini, Chester, Homola & Martellucci, 2004).

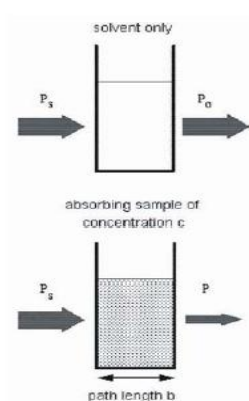


Figure 1.6 The relationship between transmittance and concentration of an analyte in solution (retrieved from Baldini, Chester, Homola & Martellucci., 2004).

Modern absorption instruments can usually display the data as transmittance, %-transmittance, or absorbance. An unknown concentration of an analyte can be determined by measuring the amount of light that a sample absorbs and applying Beer's law. If the absorbtivity coefficient is not known, the unknown concentration can be determined using a working curve of absorbance versus concentration derived from standards.

1.6.2 Instrumentation

The light source is usually a hydrogen or deuterium lamp for UV measurements and a tungsten lamp for visible measurements. The wavelengths of these continuous light sources are selected with a wavelength separator such as a prism or grating monochromator. Spectra are obtained by scanning the wavelength separator and quantitative measurements can be made from a spectrum or at a single wavelength (Skoog, West & Holler, 1994).

1.7 Fluorescence-Based Sensors

Ultraviolet and visible emission of light originates from a competitive deactivation pathway of the lowest electronic excited state of atoms and molecules that produces the so called *luminescence* (the sub-terms *fluorescence* and *phosphorescence* just designate whether the return of the excited to the ground state is an “allowed” or “forbidden” process, namely it is fast or slow, the loosely-defined border between them being a $1\text{-}\mu\text{s}^{-1}$ rate constant) (Lakowicz, 1999). The most widely used basic measuring techniques for luminescence are classical, steady-state spectrofluorimetry and time-based techniques (Baldini et. al., 2006).

The introduction of optical fibers and integrated optics has added more value to such sensing since now light can be confined and readily carried to difficult-to-reach locations, higher information density can be transported, indicator dyes can be immobilized at the distal end for unique chemical and biochemical sensing optical sensors can be subject to mass production and novel optosensing schemes have been established (interferometric, surface plasmon resonance, energy transfer, supramolecular recognition...).

1.7.1 Fluorescence Based Gas Sensors

Current investigations include the detection of traces of toxic gases such as NH_3 , H_2S , Cl_2 , SO_2 , HCHO , HCl , etc. and also other gases such as CO_2 and O_2 using chemically sensitive matrices. They can be interfaced to the optical fibres to produce devices that will have probe configurations and employ reflectance or fluorescence

detection techniques at the chemical transducers for gas sensors. These optical gas sensing systems have their own characteristics in sensor structure and application. Various types of optical gas sensing devices are reviewed here.

1.7.1.1 Optical Oxygen Sensors

Optical sensors for oxygen based on dynamic quenching of luminescence have had particular success in the past years, and they are now being improved and adapted to specific problems. A plastic fiber-based optical sensor array has been introduced for the in situ measurement of ground air oxygen concentrations in a lignite mine tailing affected by acid mine drainage formation (Koelling, Hecht & Holst, 2002). The instrument evaluates the oxygen dependent change of the luminescence lifetime of an oxygen indicator using a phase modulation technique. Optical oxygen sensors generally are based on the fluorescence of a ruthenium complex in a polymer matrix to measure the partial pressure of oxygen. This kind of sensors generally uses the below working mechanism:

1. The pulsed LED lamp sends light to an optical fiber.
2. The optical fiber carries the light to the probe. The distal end of the probe tip consists of a thin layer of a hydrophobic polymer material. A ruthenium complex is trapped in the matrix, effectively immobilized and protected from water.
3. The light from the LED excites the ruthenium complex at the probe tip.
4. The excited ruthenium complex fluoresces, emitting energy.
5. If the excited ruthenium complex encounters an oxygen molecule, the excess energy is transferred to the oxygen molecule in a non-radiative transfer, decreasing or quenching the fluorescence signal. The degree of quenching correlates to the level of oxygen concentration or to oxygen partial pressure in the film, which is in dynamic equilibrium with oxygen in the sample.
6. The energy is collected by the probe and carried through the optical fiber to the spectrometer. The analog data will be converted to digital data that the PC can understand.

1.7.1.2 Optical NO_x Sensors

Current NO_x sensor research and development is centered on either optical or electronic methods for detection. In general, optical sensors exhibit better selectivity based upon the uniqueness of atomic absorption and emission lines, however, they suffer from low signal to noise ratios. These sensors integrate a fluorescence emission method with an electronic detection system in a thin film geometry. These sensors consist of a thin film adjacent to the species being detected; a solid, liquid or gas. The thin films comprising the sensor contain fluorescent material in a proper matrix material. The excited molecules/atoms can decay and excite optical modes in the thin film stack.

1.7.1.3 Optical CO₂ Sensors

The present CO₂ sensing techniques are based on infrared (IR) absorptiometry, electrochemical Severinghouse electrode and optical sensors. However, in spite of the sensitiveness of the IR absorptiometry sensor, it is subject to strong interference from water vapor and is an expensive, bulky and not particularly robust system. On the other hand, Severinghouse electrode detects CO₂ due to the changes in the pH of the solution and is markedly affected from electromagnetic disturbances, from interferent acidic and basic gases and from osmotic pressure in the sample. Recently, the optical CO₂ sensors based on the absorbance or fluorescence change of pH indicator have been developed. They offer several attractive features which include electrical isolation, reduced noise interference, ability of miniaturization and remote sensing. Amai & Nakamura (2004) designed an optical CO₂ sensor based on the overlay of the CO₂ induced absorbance change of pH indicator dye α -naphtholphytaein with the fluorescence of tetraphenylporphyrin using ethyl cellulose and polystyrene membrane and obtained 53.9 % signal change from 100 % N₂ to 100 % CO₂. Müller & Hauser (1996) performed an optode for measurements of low concentrations of dissolved CO₂. The useful measuring range was found from 10⁻⁵ up to 10⁻³ M H₂CO₃ which contributes to 10⁻³-10⁻¹ M NaHCO₃ concentration and the response and recovery times were found as 6 and 20 minutes respectively. Neurauter,

Klimant & Wolfbeis (1999) measured dissolved and gaseous CO₂ with ethyl cellulose made sensor films and found the detectable CO₂ level between 0-30 hPa. The cross sensitivity to oxygen was the most crucial factor in this sensors performance. If stored in air and exposed to sunlight the sensors were destroyed within a few days.

Water-dissolved carbon dioxide was quantified with a reservoir type capillary microsensor (Ertekin, Klimant, Neurauder & Wolfbeis, 2003). A pH indicator in the form of its ion pair with a quaternary ammonium base and a buffer in an ethyl cellulose matrix, all placed at the tip of an optical fiber, served as the sensing chemistry. The dynamic range was between 1 and 20 hPa pCO₂. The response time is 15 s, and the detection limit is 1 hPa pCO₂. The sensitivity of fiber-optic CO₂ sensors utilizing indicator dyes was studied once more. Gastric CO₂ can be monitored with optical fibers of similar design (Baldini et al., 2003) and the results compare favorably with those obtained with a commercial (non-fiber-optic) instrument. A solgel-based optical carbon dioxide sensor that employs dual luminophore internal referencing and is intended for application in food packaging technology was described (Buelzingsloewen et al., 2002). A fluorescent pH indicator was immobilized in a hydrophobic organically modified silica matrix, along with cetyltrimethylammonium hydroxide as an internal buffer. Fluorescence is measured in the phase domain by means of the dual luminophore referencing scheme. The resolution is <1%, and the limit of detection is 0.08% CO₂. Oxygen cross-sensitivity is minimized by immobilizing the reference luminophore in polymer nanobeads.

1.7.1.3.1 Gas Phase CO₂ Measurements. Global climate change has triggered intensive studies on bio-geochemical cycles of CO₂, the primary anthropogenic greenhouse gas in the atmosphere. Accurate, in situ, long-term and inexpensive pCO₂ monitoring equipment would be invaluable for determining land-sea and air-sea CO₂ exchange on global and local scales (Wang, Cai, Liu, 2002). An ultimate goal of reaching an accuracy of better than ±1 µatm in the range 100–1000 µatm is highly desirable. In many environments, such as coastal oceans, estuaries, rivers, etc. a sensor with a fast response is also needed for studying the dynamics of the carbon

dioxide system. Optical methods for determining CO₂ partial pressures have been extensively studied and tested in many research areas since the 1980s due to their stability and operational convenience (Munkholm, Walt & Milanovich, 1988; Wolfbeis, 1988). Direct measurements of CO₂ partial pressures using optical sensors have a fundamental similarity with the spectrophotometric pH measurement (Robert-Baldo, Morris & Byrne, 1985), because the changes of $p\text{CO}_2$ are directly related to pH changes in a solution. Fiber optic CO₂ sensors typically contain a CO₂-permeable membrane filled with a pH-sensitive dye (colorimetric or fluorometric acid–base indicator) solution (Munkholm, Walt & Milanovich, 1988; Wolfbeis, 1988; Zhang & Seitz, 1984; Mills, Chang & McMurray, 1992; Uttamlal & Walt, 1995; Mills, 1993; Walt & Gabor, 1993; Goyet, Walt & Brewer, 1992; Tabacco, Uttamlal, McAllister & Walt, 1999). By establishing an equilibrium of CO₂ with its surrounding sample outside the membrane, a pH change of the indicator solution is obtained and can be detected optically (e.g. by a spectrophotometer). CO₂ permeable membranes used by previous researchers were made of PTFE or silicone rubber, which also functioned as an optical cell. Alternatively, the equilibrated solution in the CO₂ permeable membrane was pumped into a fiber optic flow cell for optical measurement (DeGrandpre, Hammar, Smith, Sayles & Limnol, 1995). Due to the fact that the refractive index (RI) of PTFE and silicone membranes (or the fiber optic flow cell) is higher than that of the indicator solution (Dasgupta and et al., 1998), a significant amount of source light will be lost through the cell walls. As a result, the length of the gas membranes (the actual optical pathlength) in the PTFE and silicone CO₂ optic sensors has to be fairly short (normally less than 1 cm) in order to collect enough light for detection. Therefore, according to the Lambert–Beer law, the sensitivity of the PTFE and silicone CO₂ optic sensors may be greatly limited by their short optical pathlength. Another shortcoming of previously reported CO₂ optic sensors is their long response time for low-level (<1000 $\mu\text{atm } p\text{CO}_2$) CO₂ measurement (Wang, Cai, Liu, 2002).

1.7.1.3.2 Dissolved CO₂ Measurement. The measurement of dissolved carbon dioxide (dCO₂) is of importance in many different areas, including in aquatic moieties, agriculture, water treatment and biotechnological studies. There are

currently a number of $d\text{CO}_2$ sensors available on the market that employs electrochemical pH detection (Burke, Markey, Nooney, Byrne & McDonagh, 2006). However, such devices are expensive and, in the case of pH electrodes, are not particularly user-friendly, requiring regular renewal for efficient operation.

Optical sensors for $d\text{CO}_2$ are a more attractive option as they do not require regeneration and facilitate the use of low-cost optoelectronic components (Burke, Markey, Nooney, Byrne & McDonagh, 2006). A variety of CO_2 optodes exploiting colorimetric detection techniques have been reported to date (Mills & Chang, 1994; Mills, Lepre & Wild, 1997, Weigl & Wolfbeis, 1995). In recent years however, the majority of work on optical CO_2 sensors has focused on the use of fluorescence detection techniques, employing the pH-sensitive fluorescent indicator, hydroxypyrenetrisulfonic acid (HPTS). Examples of such sensors include both optical fiber-based and planar devices, exploiting sensing techniques such as the analysis of fluorescence intensity (Nivens, Schiza & Angel, 2002; Mills & Chang, 1993; Ge, Kostov & Rao, 2003; Muller & Hauser, 1996), fluorescence resonance energy transfer (Neurauter, Klimant & Wolfbeis, 1999; Bultzingslowen, McEvoy, McDonagh & MacCraith, 2003) and dual luminophore referencing (DLR) (Bultzingslowen and et.al, 2002). A number of these sensors have also been applied to the detection of $d\text{CO}_2$ (Nivens, Schiza & Angel, 2002; Muller & Hauser, 1996; Neurauter, Klimant & Wolfbeis, 1999) and, in principle, all of the aforementioned sensing techniques are suitable for this application, given a compatible host matrix. An alternative route for the detection of $d\text{CO}_2$ was also reported recently, namely that of direct spectroscopic measurement using a mid-infrared quantum cascade laser (Schaden, Haberkorn, Frank, Baena & Lendl, 2004). However, the cost and complexity of this device in its current form would appear to preclude its use outside a laboratory environment. With regard to the fluorescence-based $d\text{CO}_2$ optodes presented to date, they have served to demonstrate the high degree of sensitivity that is achievable by exploiting these techniques, yielding micromolar (Nivens, Schiza & Angel, 2002; Ge, Kostov & Rao, 2003; Muller & Hauser, 1996) and even sub-micromolar limits of detection (Neurauter, Klimant & Wolfbeis, 1999). However, the reported systems are not ideally suited to use outside a laboratory environment due to

the incorporation of elements such as optical fibers and photomultiplier tubes (Muller & Hauser, 1996; Neurauter, Klimant & Wolfbeis, 1999) into the device, which, despite excellent performance characteristics, detract from the robustness and cost effectiveness of the system. Others rely on bench-top apparatus such as fluorimeters for sensor characterization (Nivens, Schiza & Angel, 2002; Mills & Chang, 1993; Ge, Kostov & Rao, 2003), systems that are obviously intended for use solely in a laboratory-based setting (Burke, Markey, Nooney, Byrne & McDonagh, 2006).

1.8 Polymers for Optical Sensors

1.8.1 Polymers as Matrix Materials

Polymer materials are frequently used as matrix materials for the indicator in optical sensor designs. This is necessary for several reasons: first, the indicator has to be immobilized to an optical waveguide or an optical fiber which is then brought into contact with the analyte solution. (Baldini et al., 2006, 297–321).

Next, the indicator dye needs a solvent to interact with the analyte. Pure crystalline indicator dyes might react at the surface but not all indicators would react due to hindered diffusion. Therefore, the indicator is dissolved in a polymer which allows free diffusion of the analyte to and from the indicator molecule. The polymer has the function to retain the indicator in place so that no leaching into e.g. aqueous sample solution occurs. This can be achieved by covalently immobilizing the dye to the matrix but also by simply dissolving a hydrophobic and water-insoluble dye in a hydrophobic polymer (Baldini et al., 2006, 297–321). The polymer can also be used to design the selectivity and sensitivity of the optical sensor due to enrichment of the analyte by the polymer material.

Furthermore, the polymer may be selectively permeable for gases but not by ions. Finally, the polymer can provide optical isolation against ambient light and therefore prevent bleaching and light interference.

1.8.2 Requirements for Polymer Matrix Materials

Polymer materials have to provide various requirements to enable optical sensing. First of all, the indicator dye and all additives have to dissolve well in the polymer without leaching. The analyte also has to be soluble in the polymer and must be able to diffuse fast into the polymer and within the polymer (Baldini et al., 2006, 297–321). The polymer material has to be chemically and physically stable in order to achieve good operational lifetime and shelf-life (important for practical applications). Furthermore, no crystallization/migration/reorientation of the indicator chemistry in the polymer must occur. This can happen even after weeks or months if indicator solubility is not as high as expected. The polymer must be stable even at elevated temperatures (e.g. to be resistant to steam heat sterilization). It should be stable against ambient light, chemicals (acids, bases, oxidants) and it should be non-toxic and biocompatible (especially when used in clinical and biochemical applications). The polymer should not have any intrinsic color/luminescence, and it should be optically transparent in the spectral range where measurements are being performed (Baldini et al., 2006, 297–321). Finally, the material should have good mechanical stability.

1.8.3 Types of Polymers Used in Optical Sensing

1.8.3.1 Lipophilic Polymers and Plasticizers

Polymers that have a high glass transition temperature (T_g) are brittle. They require plasticizers to make them flexible. Furthermore, the high density/rigidity of the polymer chains (without plasticizers) hinders diffusion of ions and gases in the polymer matrix (Baldini et al., 2006, 297–321). Therefore, a plasticizer content of 2:1 is required for the preparation of sensor layers. Structures of some lipophilic polymers are shown in Figure 1.8. The advantage of plasticized polymers is that their polarity and lipophilicity (and thus selectivity and sensitivity) can be tailored by using different plasticizers with different physical properties. Figure 1.9 and 1.10 show chemical structures of lipophilic and mixed (lipophilic and polar) plasticizers.

A significant disadvantage is that plasticizers may leach out into sample solution or may evaporate on storage. If toxic, they must not be used for clinical purposes. Immobilization of the indicator chemistry is usually performed by dissolving hydrophobic dyes and ligands in hydrophobic polymers (Baldini et al., 2006, 297–321). In Fig. 1.11 structures of some non-polar polymers have been shown.

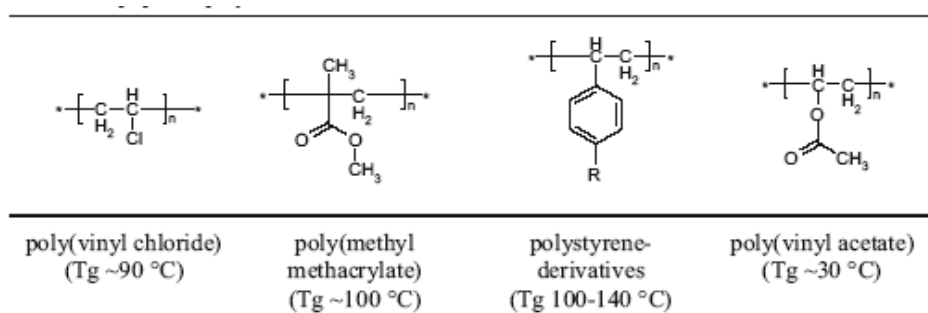


Figure 1.8 Lipophilic polymers (retrieved from <http://www2.uni-jena.de/~c1moge/Mohr/ASCOS2002.pdf>)

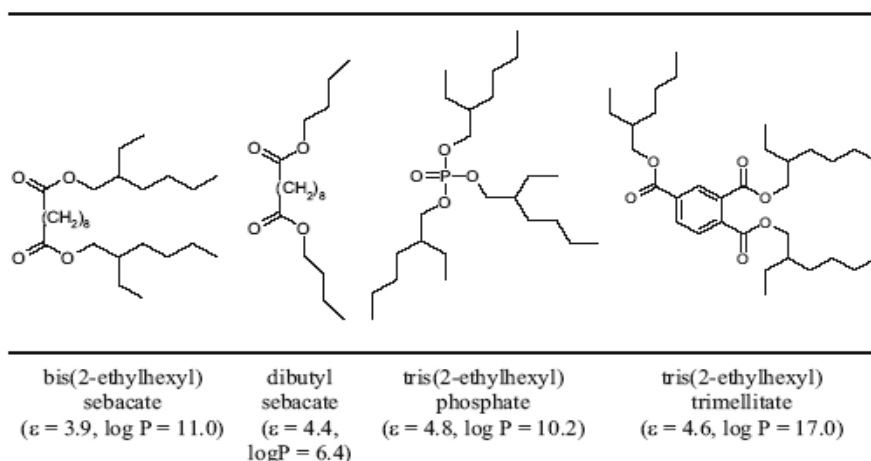


Figure 1.9 Lipophilic plasticizers (retrieved from <http://www2.uni-jena.de/~c1moge/Mohr/ASCOS2002.pdf>)

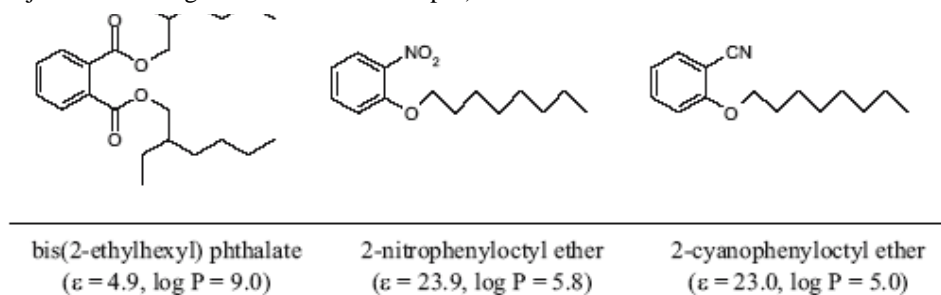


Figure 1.10 Lipophilic and polar plasticizers. (retrieved from <http://www2.uni-jena.de/~c1moge/Mohr/ASCOS2002.pdf>)

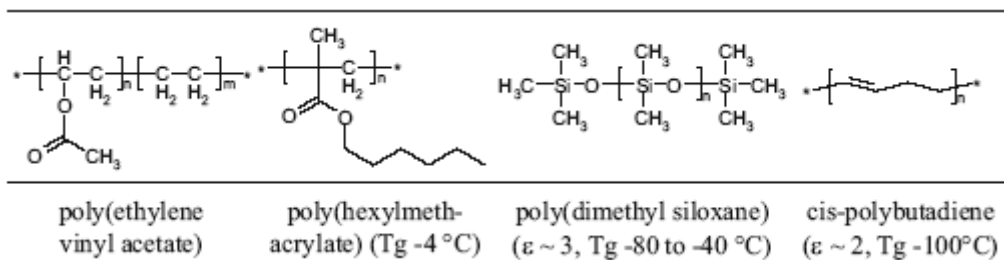


Figure 1.11 Non-polar polymers (retrieved from <http://www2.uni-jena.de/~c1moge/Mohr/ASCOS2002.pdf>)

1.8.3.2 Hydrophilic Polymers

Hydrophilic polymers (Figure 1.12) provide a matrix which is comparable to an aqueous environment. Ions can diffuse quite freely, but the possible water uptake (10-1000%) can cause significant swelling of the polymer. Swelling of the matrix affects the optical properties of the sensors and, consequently, the signal changes. Immobilization of the indicator chemistry usually is achieved via covalent bonding to the polymer (Baldini et al., 2006, 297–321).

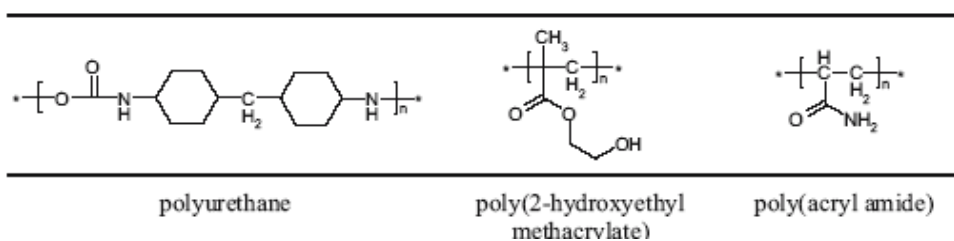


Figure 1.12 Hydrophilic polymers (retrieved from <http://www2.uni-jena.de/~c1moge/Mohr/ASCOS2002.pdf>)

1.8.3.3 Ionic Polymers (Polyelectrolytes)

Polyelectrolytes (Figure 1.13) exhibit a large amount of dissociable groups. These compounds are often used for ion-exchange chromatography. They can also be used to exchange their counter ions with indicator ions (Baldini et al., 2006, 297–321).

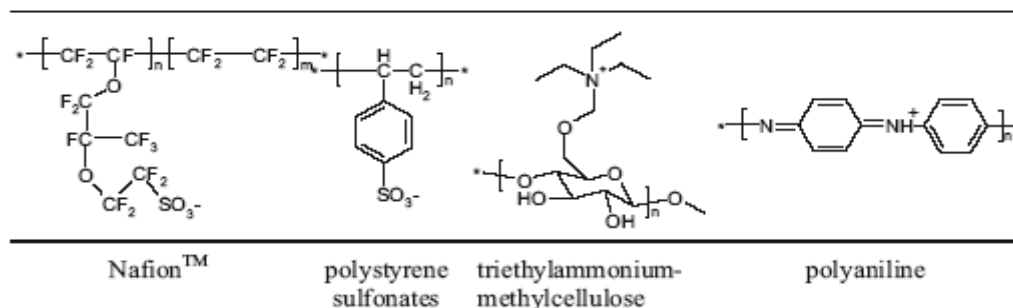
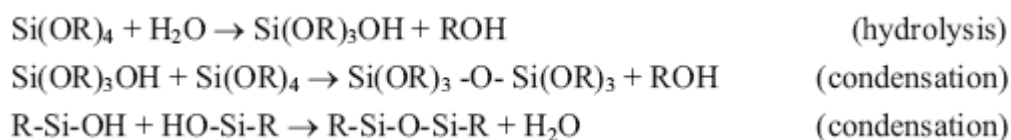


Figure 1.13 Ionic polymers (retrieved from <http://www2.uni-jena.de/~c1moge/Mohr/ASCOS2002.pdf>)

1.8.3.4 Sol-Gel Glass

The sol-gel process allows the preparation of glass films into which indicator chemistry can be incorporated. The production of ceramic materials and glassy networks is based on the polymerization of suitable precursors at low temperature. The increasing popularity of sol-gels in sensor applications results from the processing versatility (Lobnik & Wolfbeis, 1998). At the sol stage, thin glass films can be formed by dip-coating or spin-coating. These films are porous and are used for sensor applications.

The sol-gel process involves the preparation of inorganic matrices via three steps. Components of the sol-gel cocktail are the sol-gel precursor (e.g. tetramethoxysilane), water, a catalyst (acids or bases), the indicator chemistry and a solvent such as ethanol. Mixing these components causes hydrolysis of the ester, silanol-ester condensation, and silanol-silanol condensation of the precursors:



The first phase in the process is the formation of the “sol”. A sol is a colloidal suspension of solid particles in a liquid. Colloids are solid particles with diameters of

1-100 nm. After a certain period, the colloidal particles and condensed silica species link to form a “gel” - an interconnected, rigid network with pores of submicrometer dimensions and polymeric chains whose average length is greater than one micrometer. After the sol-gel transition, the solvent phase is removed from the interconnected pore network. If removed by conventional drying such as evaporation, so-called “xerogels” are obtained, if removed via supercritical evacuation; the product is an “aerogel”. “Ageing” is the process that takes place after mixing precursor, water, solvent and catalyst to form a sol, but before coating, in the case of coating sols (Lobnik & Wolfbeis, 1998). Ageing or pre-polymerization of the sol causes aggregation due to hydrolysis and condensation reactions, and consequently an increase in viscosity.

1.8.3.5 Molecularly Imprinted Polymers (MIPs)

Molecularly imprinted polymers have recently attracted much attention because they are denoted as artificial antibodies which are made from simple chemical components via polymerization and can be used for the preparation of biomimetic sensors, affinity separation matrices, catalysts, etc. (Figure 1.14). Molecular imprinting can be accomplished in two ways: (a), the self assembly approach and (b), the preorganisation approach (Haupt, 2001). The first involves host guest type structures produced from weak intermolecular interactions (such as ionic or hydrophobic interaction, hydrogen bonding) between the analyte molecule and the functional monomers (Baldini et al., 2006, 297–321). The self assembled complexes are spontaneously formed in the liquid phase and are sterically fixed by polymerization. After extraction of the analyte, vacant recognition sites specific for the imprint are established. Monomers used for self assembly are methacrylic acid, vinylpyridine and dimethylamino methacrylate. The preorganisation approach (b) involves formation of strong reversible covalent arrangements (boronate esters, imines, ketals) of the monomers with the print molecule before polymerization. Thus, the print molecule has to be chemically derivatised with the monomers before actual imprinting is performed. After cleaving the covalent bonds and removal of the print molecules, recognition sites complementary to the analyte are obtained again.

Optical sensors based on molecular imprints can be obtained by copolymerising indicator dyes that respond to the analyte by changing their colour (Diaz-Garcia & Badia, 2004) (Figure 1.15). Another approach is to label the analyte with a small dye molecule, perform imprinting, and then measure the competitive release of the labelled molecule when the MIP is exposed to the actual analyte. Recently, indicator dyes that can perform reversible chemical reactions with the analyte and additionally have functional groups for polymerization have been used for the preparation of MIP-based optical sensor layers (Mertz & Zimmerman, 2003). These layers can selectively distinguish between analyte molecules and have detection limits down to the subnanomolar range.

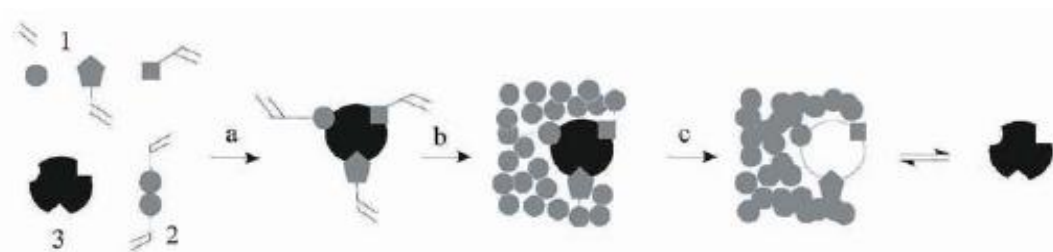


Figure 1.14 1, Functional monomers; 2, Cross-linker; 3, Analyte; a, Self-assembly or Pre-organization; 1, Polymerization; c, Removal of the analyte (retrieved from <http://www2.uni-jena.de/~c1moge/Mohr/ASCOS2002.pdf>).

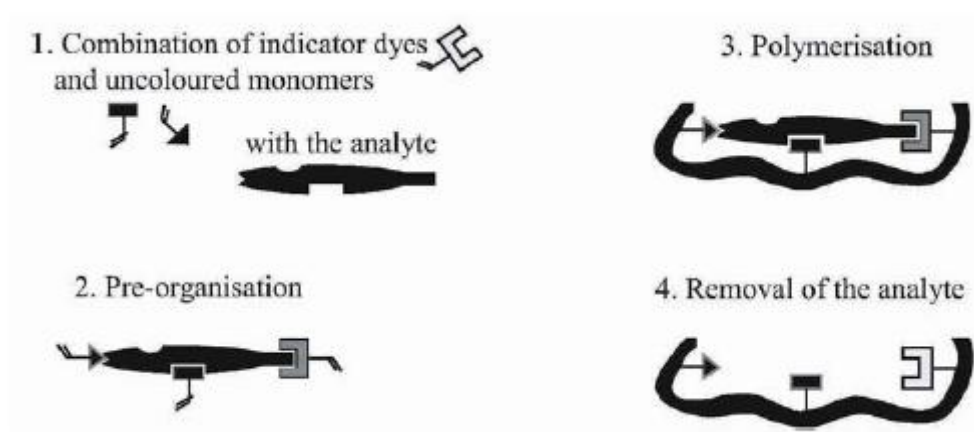


Figure 1.15 Preparation of coloured molecularly imprinted polymers using analyte sensitive indicator dyes (retrieved from <http://www2.uni-jena.de/~c1moge/Mohr/ASCOS2002.pdf>).

1.8.4 Immobilization of Indicator Chemistry in Polymers

1.8.4.1 Hydrophobic Interactions

Most indicator chemistry is adapted to aqueous solution (for titration in water). Therefore, the molecules are water-soluble and if dissolved in lipophilic polymers, they are washed out immediately. In order to make dyes, ionophores and ligands soluble in polymers and to avoid leaching of the components into the sample solution, they have to be made lipophilic (Seiler and et. al, 1991).

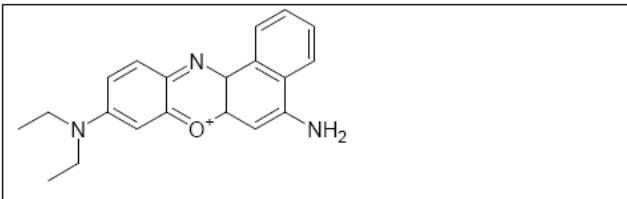
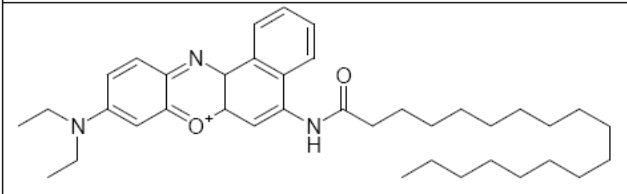
	<p>Nile Blue</p> <p>pH indicator (red to blue upon protonation, pK ~11.6)</p> <p>water-soluble</p>
	<p>Octadecyl Nile Blue</p> <p>pH indicator</p> <p>polymer/plasticizer-soluble</p>

Figure 1.16 Hydrophilic and lipophilic Nile Blue derivatives (retrieved from <http://www2.uni-jena.de/~c1moge/Mohr/ASCOS2002.pdf>).

Lipophilic molecules can be obtained by introduction of long alkyl chains (Figure 1.16). However, the chemical synthesis involved can be tedious. Therefore, another possibility is to obtain lipophilic compounds by ion pairing. Ion pairs are mostly obtained by dissolving both components (water-soluble ionic indicator and water-soluble ionic surfactant of opposite charge) separately in water, pouring both solutions together and filtrating the precipitated product. For example, by mixing aqueous solutions of the sodium salt of bromophenol blue and hexadecyltrimethylammonium chloride a lipophilic polymer-soluble dye is obtained (Mohr and et al, 1997) (Figure 1.19).

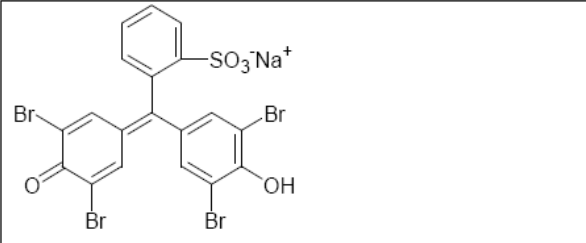
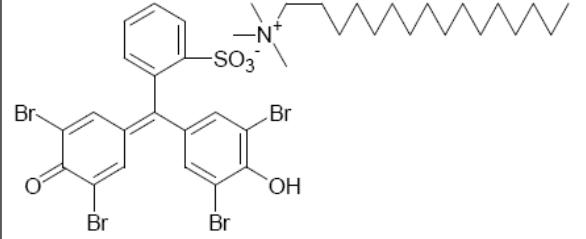
	<p>Bromophenol Blue</p> <p>pH indicator (yellow to blue upon deprotonation, pK ~3.8)</p> <p>water soluble</p>
	<p>Hexadecyltrimethylammonium Bromophenol Blue Ion Pair</p> <p>pH indicator</p> <p>lipophilic and polymer/plasticizer-soluble</p>

Figure 1.19 Hydrophilic and lipophilic triphenylmethane dyes (retrieved from <http://www2.uni-jena.de/~c1moge/Mohr/ASCOS2002.pdf>).

1.8.4.2 Ion-Exchange

Positively or negatively charged indicators can be made lipophilic by ion pairing with surfactants. However, they can also be directly immobilized on the polymer by ion-pairing with ionic polymers (polyelectrolytes) (Figure 1.20). Solutions or suspensions of the polymer are then mixed with aqueous or alcoholic solutions of the dye.

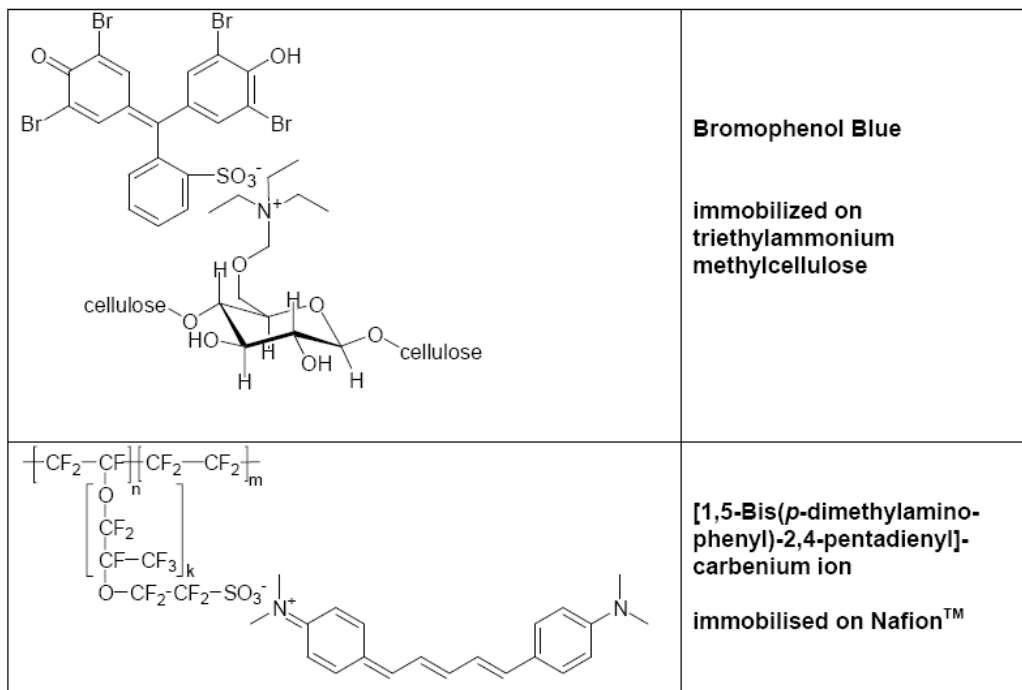


Figure 1.20 Ion pairs of indicator dyes with polyelectrolytes (retrieved from <http://www2.uni-jena.de/~c1moge/Mohr/ASCOS2002.pdf>).

1.8.4.3 Covalent Immobilization

Covalent immobilization of the indicator chemistry to the polymer matrix is the basic and the strongest of all immobilization methods. The operational stability and shelf life is superior. However, to obtain indicator chemistry and polymers with functional groups is inevitably linked with significant synthetic effort (Baldini and et al., 2006, 297–321). Very often, chemical modification of dyes negatively affects their selective and sensitive analyte recognition. In principal two different ways of immobilization are possible, namely (a) to bind a reactive dye (e.g. fluorescein succinimidyl ester) to a reactive polymer matrix (e.g. aminocellulose), or (b) to polymerise a reactive dye (e.g. a dye with a methacrylate group) with monomers such as methyl methacrylate to give a copolymer (Munkholm, Walt, Milanovich & Klainer, 1986) (Figure 1.20).

Several indicator dyes are available in a reactive form (primarily for labelling of peptides, proteins or DNA). These reactive molecules with isothiocyanate groups, sulfonyl chloride groups, vinylsulfonyl groups, or succinimidyl groups (fluorescein

isothiocyanate, dabcyl succinimidyl ester, hydroxypyrene trisulfonyl chloride) can be covalently attached to aminoethylcellulose or amino-PVC. Indicator dyes with amino or hydrazide groups (aminofluorescein, Texas Red hydrazide) can be coupled to carboxy- PVC or carboxymethylcellulose (Figure 1.21).

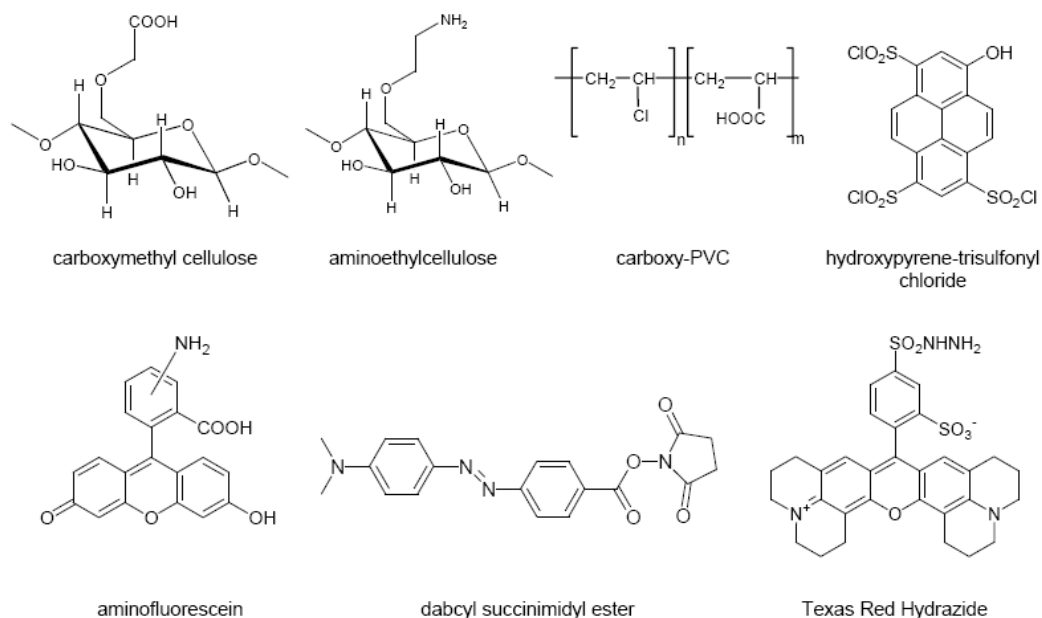


Figure 1.21 Polymers and indicator dyes for covalent immobilization of the sensor chemistry (retrieved from <http://www2.uni-jena.de/~c1moge/Mohr/ASCOS2002.pdf>).

The synthesis of vinylsulfonyl dyes is a good example for a method to obtain pH indicator layers with operational stability of weeks and shelf life of years. Commercial transparencies with a cellulose coating are used as the polymer matrix and the reactive vinylsulfonyl dye is bound to the cellulose directly from aqueous solution (Mohr & Wolfbeis, 1994) (Figure 1.22).

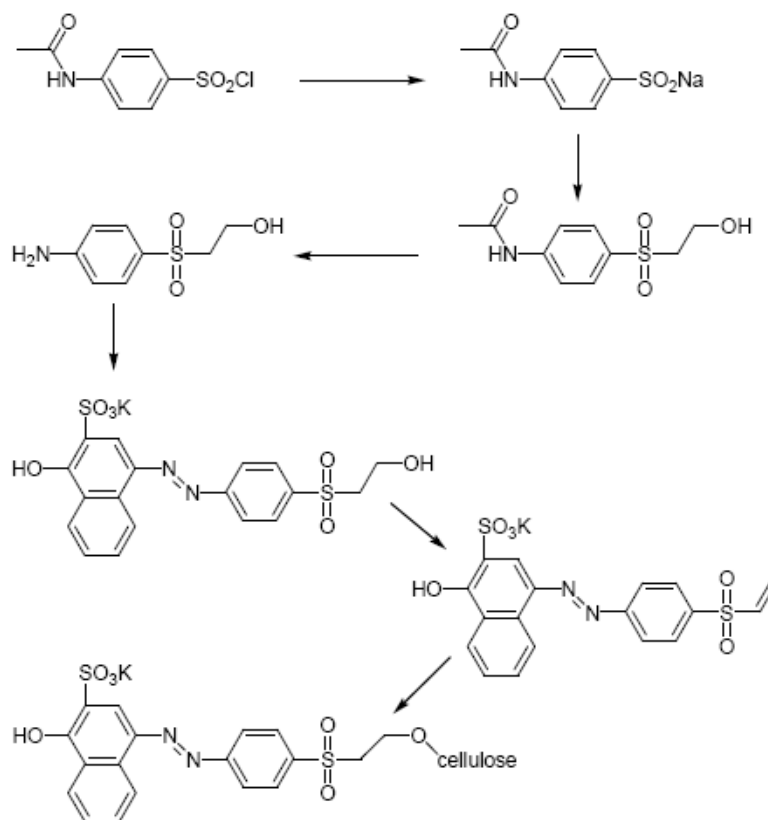


Figure 1.22 Synthesis of vinylsulfonyl indicator dyes for covalent immobilization to the polymer matrix via Michael addition (retrieved from <http://www2.uni-jena.de/~c1moge/Mohr/ASCOS2002.pdf>).

Another way for covalent immobilization is to synthesize indicator chemistry with polymerizable entities such as methacrylate groups (Figure 1.22). These groups can then be copolymerized with monomers such as hydrophobic methyl methacrylate or hydrophilic acryl amide to give sensor copolymers. In order to obtain self-plasticized materials, methacrylate monomers with long alkyl chains (hexyl or dodecyl methacrylate) can be used. Thus, sensor copolymers are obtained which have a T_g below room temperature. Similarly, ionophores and ionic additives (quaternary ammonium ions and borates) can be derivatised to give methacrylate derivatives (Baldini and et al., 2006, 297–321).

1.8.5 Polymer Effect on Indicator Chemistry

The recognition process of the analyte by the indicator chemistry can be completely different, dependent on whether a hydrophilic or a lipophilic polymer matrix is used. In the case of lipophilic polymers, analyte ions can only be transported into a polymer layer, if simultaneously another ion is released or co-extracted (see Fig. 1.23).

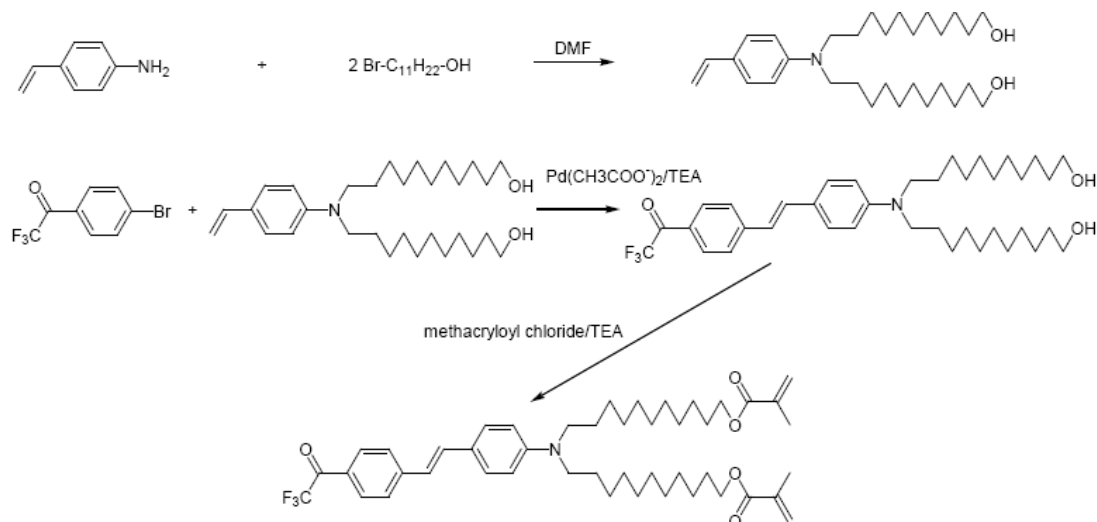


Figure 1.23 Synthesis of an indicator dye for amines which exhibits methacrylate groups for preparation of copolymers. The dye shows a reversible change in fluorescence from green or blue upon interaction with amphetamine. (retrieved from <http://www2.uni-jena.de/~c1moge/Mohr/ASCOS2002.pdf>).

This restriction is not valid for hydrophilic polymers, and clearly not for neutral analytes.

1.8.5.1 Co-Extraction and Ion-Exchange

The optical sensors are generally consisted of ion-selective carriers (ionophores), pH indicator dyes (chromoionophores), and lipophilic ionic additives dissolved in thin layers of plasticized PVC or other proper polymeric matrix materials. Ionophores extract the analyte from the sample solution into the polymer matrix. The extraction process is combined with co-extraction or exchange of a proton in order to maintain electro neutrality within the non-polar polymer matrix. This is optically

transduced by a pH indicator dye which is also called “chromoionophore” (Seiler & Simon, 1992). The preparation of sensor layers requires to dissolve the components (pH-indicator dye, ionophore, ionic additive) together with poly(vinyl chloride) and a plasticizer in tetrahydrofuran (similar to ion-selective electrode membranes). The solutions are then spin coated on transparent support materials and fixed in flow-through cells, or they are applied onto optical fibers as well as planar wave guides by dip coating (Baldini and et al., 2006, 297–321). Since the recognition element (ionophore) and the optical transducer (pH indicator) are different molecules, almost any available ionophore can be combined with one appropriate pH-indicator. Furthermore, it is possible to design the properties of the sensor by using plasticizers of different polarity. The mechanism is mathematically well-defined and allows control of the dynamic range and selectivity ability of the sensor membrane.

1.8.5.1.1 Measurement of Cations. In the case of ion-exchange, a selective carrier (e.g. valinomycin for potassium) extracts the cation into the polymer layer (Figure 1.24 and Figure 1.25). In order to maintain electroneutrality within the polymer layer, a pH indicator dye (also contained in the layer) releases a proton into aqueous solution. Due to this deprotonation of the dye, a colour change is observed that relates to the concentration of the analyte cation (Figure 1.26).

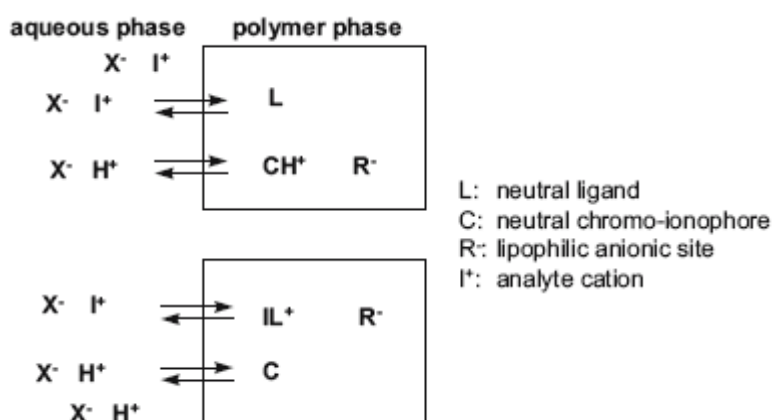
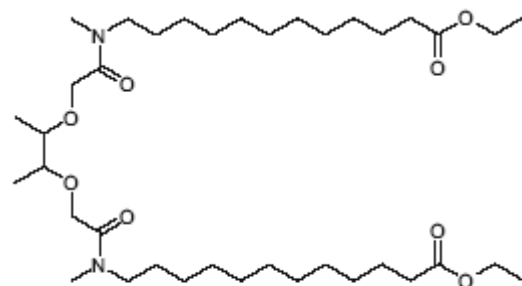
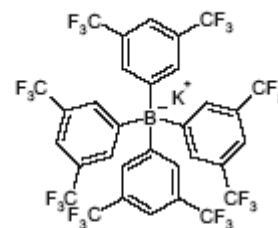


Figure 1.24 Mechanism of ion-exchange of an analyte ion (I^+) and a proton (H^+) between the sensor membrane and the aqueous phase. (retrieved from <http://www2.uni-jena.de/~c1moge/Mohr/ASCOS2002.pdf>).

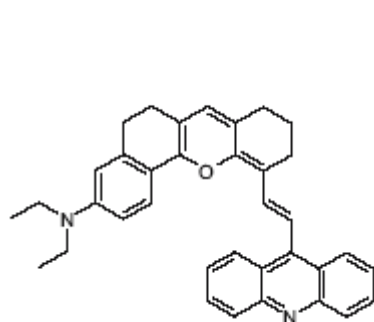


Calcium-selective ionophore ETH 1001

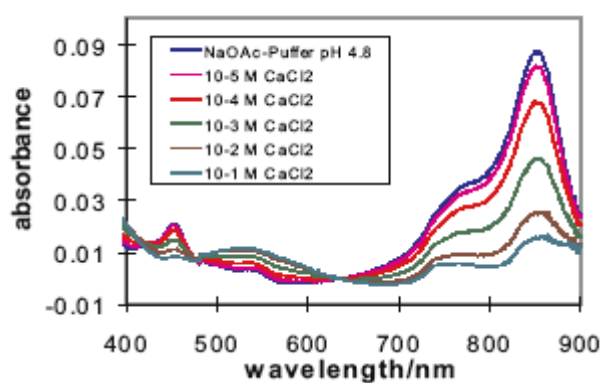


Lipophilic anionic additive potassium tetrakis(3,5-bis(trifluoromethyl)-phenyl) borate (PTTFPB)

Figure 1.25 Selective ligand and ionic additive for ion-exchange sensors. (retrieved from <http://www2.uni-jena.de/~c1moge/Mohr/ASCOS2002.pdf>).



pH indicator dye L 109



Decreasing absorbance of a calcium-sensitive ion-exchange membrane at 850 nm (composed of L109, ETH 1001 and PTTFPB in plasticized PVC) upon exposure to increasing concentrations of calcium ion

Figure 1.26 Sensor for calcium based on ion-exchange. (retrieved from <http://www2.uni-jena.de/~c1moge/Mohr/ASCOS2002.pdf>).

1.8.5.1.2 Measurement of Anions. In the case of co-extraction, a selective anion-carrier (ionophore) extracts the analyte anion into the lipophilic sensor membrane. In order to maintain electroneutrality, a proton is co-extracted into the membrane where it protonates a pH indicator dye contained in the polymer membrane. Due to protonation, the dye undergoes a change in either absorption or fluorescence (Figure 1.27 and Figure 1.28 and 29).

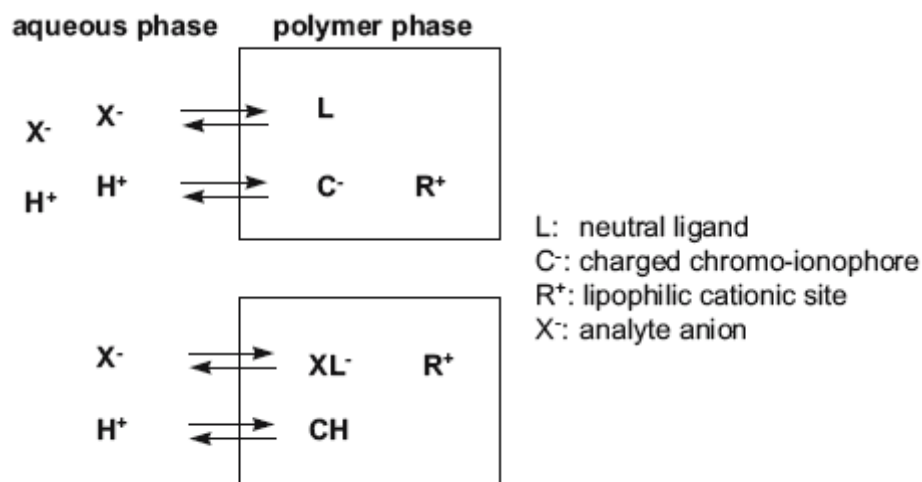


Figure 1.27 Mechanism of co-extraction of the analyte anion (X^-) together with a proton (H^+) into the sensor layer. (retrieved from <http://www2.uni-jena.de/~c1moge/Mohr/ASCOS2002.pdf>).

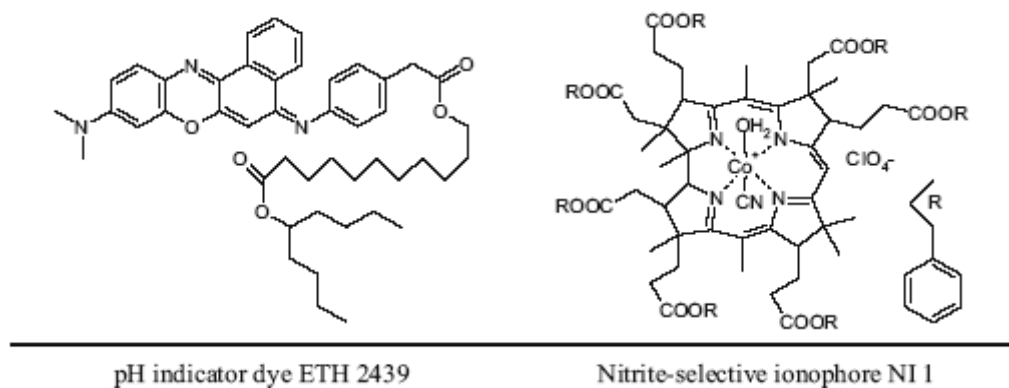
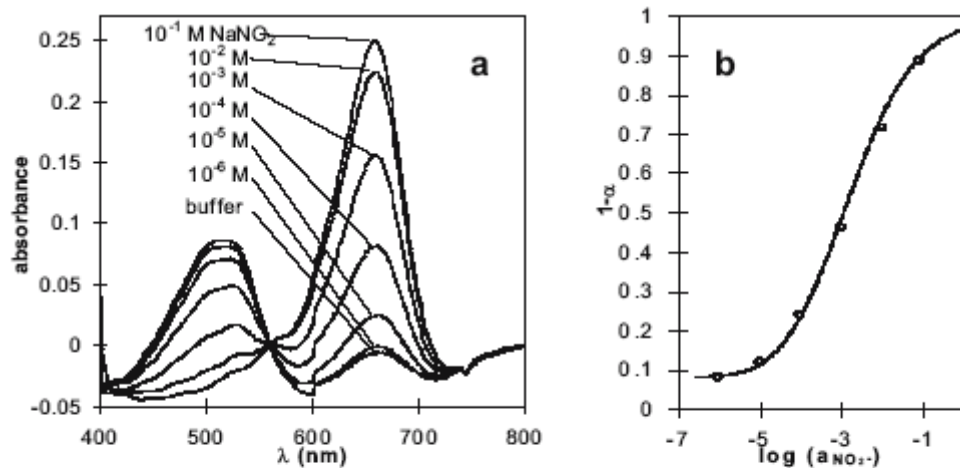


Figure 1.28 pH indicator dye and ligand for sensing nitrite. (retrieved from <http://www2.uni-jena.de/~c1moge/Mohr/ASCOS2002.pdf>).

1.8.5.2 Potential Sensitive Dyes (PSDs)

Potential-sensitive dyes provide an alternative to ionophore based sensing approach (Wolfbeis and et. al., 1991). These dyes are intensively used to measure potential changes across biological membranes.



Absorbance of a nitrite selective sensor membrane (composed of ETH 2439, NI 1, and PTFPB in plasticized PVC) exposed to different concentrations of nitrite

Experimental (o) and theoretical (—) calibration plots

Figure 1.29 Optical response of a nitrite sensor layer (retrieved from Baldini and et al., 2006, 297–321).

In sensor membranes employing PSDs, these changes are induced by selective carriers, which, similar to the mechanisms of co-extraction and ion exchange, extract analyte ions from the sample solution into the polymer membrane. However, the response to the increase of analyte ions in the polymer phase is different. In the case of ion exchange or co-extraction, electroneutrality in the membrane is maintained via protonation/deprotonation of pH indicator dyes. PSDs usually do not possess functional groups that can be protonated or deprotonated. Therefore, electroneutrality can only be established if the PSD moves between the aqueous and the polymer phase. As a consequence of the motion of the PSD between phases of different polarity, optical signal changes are induced which can result from aggregation, but also from solvatochromism (Wolfbeis, 1995). The sensors exhibit significantly lower cross-sensitivity to pH than optical sensors based on the ion-exchange/co-extraction mechanism using pH indicator dyes.

1.8.5.2.1 Measurement of Cations. The sensor layer consists of a cation selective ionophore (e.g. valinomycin for potassium), a lipophilic anionic site (borate) and the cationic PSD. Before interaction with potassium, a lipophilic ion pair between the cationic PSD and borate anion is formed in the polymer layer. When valinomycin

(also contained in the layer) selectively extracts potassium into the layer, then the positively charged valinomycin-potassium complex forms an ion pair with borate. As a consequence, the cationic dye moves into the direction of the aqueous phase to maintain electroneutrality in the layer. Because potential sensitive dyes tend to form weakly fluorescent aggregates and are subject to concentration quenching, their fluorescence is highly concentration dependent (Wolfbeis and et. al., 1991) (Figure 1.30).

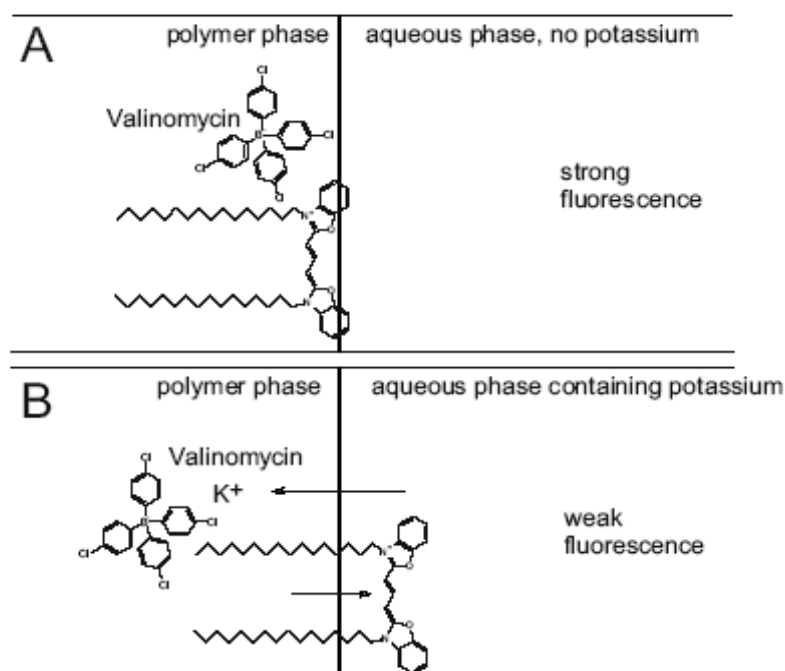


Figure 1.30 Schematic representation of the microenvironment of the cationic PSD diOC16(3) in a potassium sensor before (A) and after (B) extraction of potassium from the aqueous into the lipophilic membrane phase. The sensor membrane is composed of valinomycin, diOC16(3) and a lipophilic borate salt dissolved in plasticized PVC. (retrieved from <http://www2.uni-jena.de/~c1moge/Mohr/ASCOS2002.pdf>).

1.8.5.2.2 Measurement of Anions. Ionophores that selectively bind anions are being developed but this area lags behind the development of cation sensing. Halide ions have been reversibly sensed using fluorescence quenching. Anion sensing may also be performed redox based or ligand exchange based approaches (Wolfbeis et. al., 1991). The indicator may also be a cationic fluorophore covalently immobilized on a glass substrate. The cationic side attracts ions close to the fluorophore

facilitating quenching. Another anion-selective sensor membrane can be obtained by dissolving a cationic PSD (e.g. rhodamine B octadecylester perchlorate) together with an anion-selective carrier in plasticized PVC. Upon exposure to the analyte, the neutral anion carrier forms a negatively charged complex which can form an ion pair with the cationic PSD. The ion pair is more lipophilic than the PSD alone and a fluorescence increase occurs. The fluorescence changes are caused by a change of the counter ion of the PSD which changes the solubility of the PSD in the plasticizer. A different solubility, however, affects the dissociation of dye dimers to monomers. Since the dimers are essentially non-fluorescent, signal changes are observed which correlate with the amount of anion in the sample solution (Baldini and et al., 2006, 297–321) (Figure 1.31).

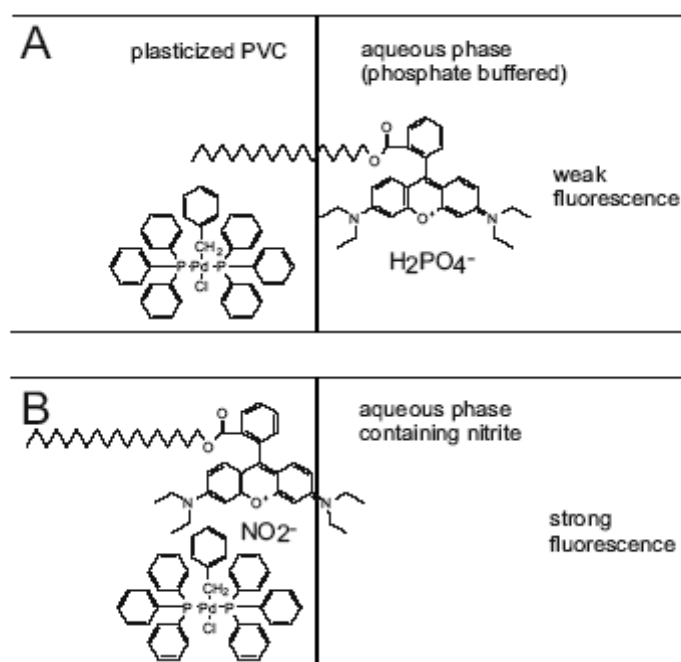
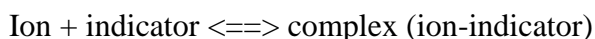


Figure 1.31 Schematic representation of the micro-environment of a PSD (Rhodamine B octadecyl ester) in an anion sensor before (A) and after (B) extraction of nitrite from the aqueous into the lipophilic membrane phase.

1.8.5.3 Chromogenic and Fluorogenic Indicators

1.8.5.3.1 *Measurement of Ions.* The working principle of optical sensors based on chromogenic and fluorogenic indicators is completely different to the sensing mechanisms discussed previously. The above mentioned sensing schemes (ion-exchange, coextraction) employ non-selective pH indicator dyes and selective ionophores together. However, chromogenic and fluorogenic ligands are a combination of selective recognition moiety and optical transduction module in one molecule (<http://www2.uni-jena.de/~c1moge/Mohr/ASCOS2002.pdf>).

Generally, sensors based on chromogenic or fluorogenic indicators are advantageous over sensors based on PSDs or ion-exchange/co-extraction. A specific interaction between a chromophore that already contains the moiety for analyte recognition is simpler than the above mechanisms which require lipophilic ionic sites, specific pH-indicator dyes and selective (uncoloured) ionophores. Furthermore, such ligands are generally less pH-sensitive as long as the recognition process is represented by the equilibrium:



If however, the ion binding process involves the displacement of protons according to:



then the process becomes cross-sensitive to pH. In order to provide a rather aqueous environment for the indicator dyes, they should be embedded in hydrophilic rather than in lipophilic polymers. This, however, demands a significant synthetic effort because the indicator has to be covalently linked to the polymer in order to prevent leaching (<http://www2.uni-jena.de/~c1moge/Mohr/ASCOS2002.pdf>).

1.8.5.3.2 Measurement of Cations. Ionophores have had the greatest impact in the development of ion selective membrane electrodes. The goal of combining ionophore selectively with an optical sensing system can be accomplished in several ways. The most direct approach is to prepare the chromogenic ionophores in which ion binding is accompanied by a change in the optical properties of the chromophore (Wolfbeis and et. al., 1991).

Probably the best optical sensors for pH are based on a pH indicator dye covalently immobilized on transparent cellulose membranes (Figure 1.32). The pKa of the dye is 7.34 and colour changes from yellow to purple are observed upon deprotonation. The cellulose membrane exhibits still more than 50% of the initial colouration after two years of storage in distilled water at ambient light.

Figure 1.32 shows vinylsulfonyl indicator dyes for sensing pH and cations. The pH indicator dye covalently immobilized on a transparent cellulose membrane via the hydroxy groups of cellulose Potassium-sensitive dye immobilized on cellulose This type of sensing chemistry can also be used for determination of cations using a selective ligand (crown ether) linked to the chromophore. The colour change on complexation of potassium is from red to yellow. Another approach for ion-sensing (here: copper and zinc) is based on the water-soluble ligand Zincon.

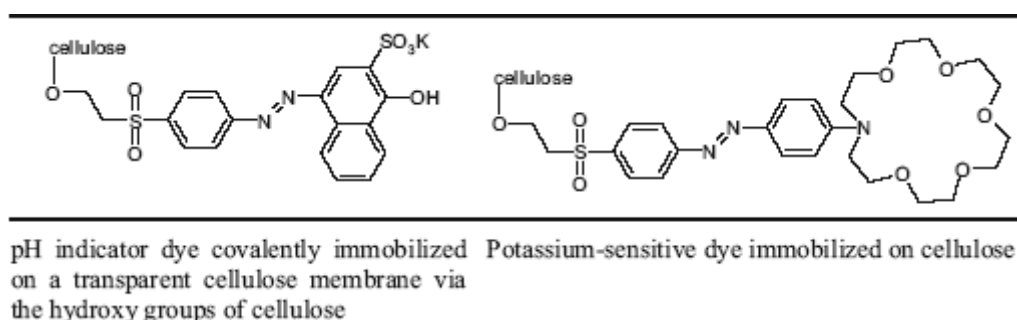
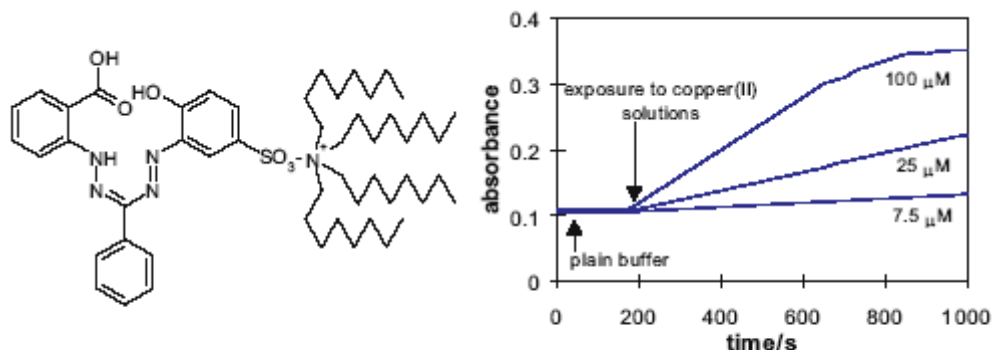


Figure 1.32 Vinylsulfonyl indicator dyes for sensing pH and cations. (retrieved from <http://www2.uni-jena.de/~c1moge/Mohr/ASCOS2002.pdf>).

When the Zincon ion-pair is exposed to an aqueous sample containing the analyte, the latter diffuses into the sensor membrane to react with the indicator, and gives a

colour transition from pink to blue at near neutral pH. The pKa value of Zincon for the color transition from pink to blue is above 13, therefore, the sensor membrane is virtually insensitive to pH changes. However, due to the high complexation constant of Zincon for copper and zinc, the response of sensor membrane is irreversible and must be evaluated kinetically (Oehme and et al, 1994).

1.8.5.3.3 Measurement of Anions. To date, there are only few applications of chromogenic or fluorogenic ligands for anion-sensing. Wolfbeis et al. have presented a sensor for halogenide ions which is based on fluorescence quenching. The indicator is a cationic fluorophore which is covalently immobilized on the polymer matrix (Huber, Krause, Werner & Wolfbeis, 2003). The fluorescence intensity of the fluorophore decreases with increasing halide concentration. The selectivity is governed by the heavy atom effect, therefore, the sensitivity follows the order $I > Br > Cl$. Another approach is the chemical reaction of indicator dyes with anions to yield colour changes, e.g. the reaction of coloured aldehydes with bisulfite to form a bisulfite adduct (Mohr, 2004).



Chemical structure of the Zincon-tetraoctylammonium ion pair

Response of a Zincon-based sensor membrane to different μM concentrations of copper(II) at pH 6.0 (measured at 620 nm)

Figure 1.33 Indicator chemistry for copper ion. (retrieved from <http://www2.uni-jena.de/~c1moge/Mohr/ASCOS2002.pdf>).

1.8.5.3.4 Measurement of Neutral Analytes. The majority of optical sensors for neutral (uncharged) species are based on indicators which selectively interact with the analyte and additionally give optical signal changes. Since the diffusion of neutral analytes is not as strongly affected by the polymer matrix as it is in the case

of ions, all types of polymer matrices can be used. Optical sensors for oxygen are among the few sensors, which have found practical application for process-monitoring and clinical diagnostics. They are generally based on compounds such as platinum porphyrins or ruthenium phenanthroline derivatives (Figure 1.34) which show a decrease in luminescence upon exposure to molecular oxygen (Klimant & Wolfbeis, 1995).

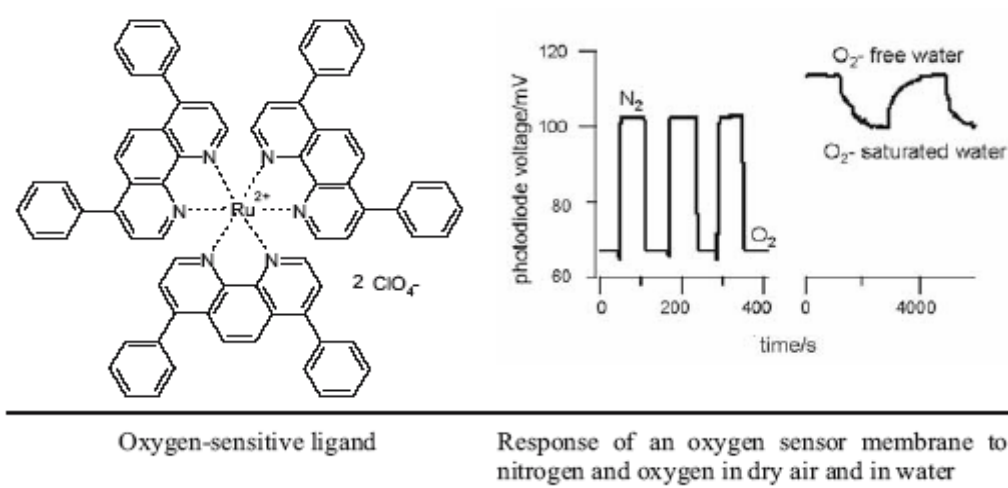


Figure 1.34 Sensor chemistry for gaseous and aqueous oxygen. (retrieved from <http://www2.uni-jena.de/~c1moge/Mohr/ASCOS2002.pdf>).

An alcohol sensor membrane is obtained by dissolving 4-*N,N*-dioctylamino-4'-trifluoroacetylstilbene (ETHHT 4004) and the catalyst tridodecylmethylammonium chloride in plasticized PVC. On exposure to aqueous ethanol, the orange fluorescence of the reactand (so called because it is a combination of a chemical reagent and a ligand) decreases (Figure 1.35). This is due to the chemical reaction of the trifluoroacetyl group of the reactand with ethanol to form a hemiacetal. This conversion results in a change of the electron delocalization within the reactand and, consequently, in a change in fluorescence. Reversible chemical reactions of chromo- or fluororeactands with electrically neutral molecules can also be used to detect analytes such as aldehydes, amines, saccharides, carbon dioxide or sulfur dioxide (Mohr, 2004).

Sensors for acidic (HCl, SO₂, CO₂, acetic acid) or basic gases (NH₃, amines) often make use of pH indicator dyes immobilized in polymers. Lipophilic Bromophenol Blue dissolved in silicone is deprotonated upon exposure to ammonia causing the colour to change from yellow to blue (Figure 1.36).

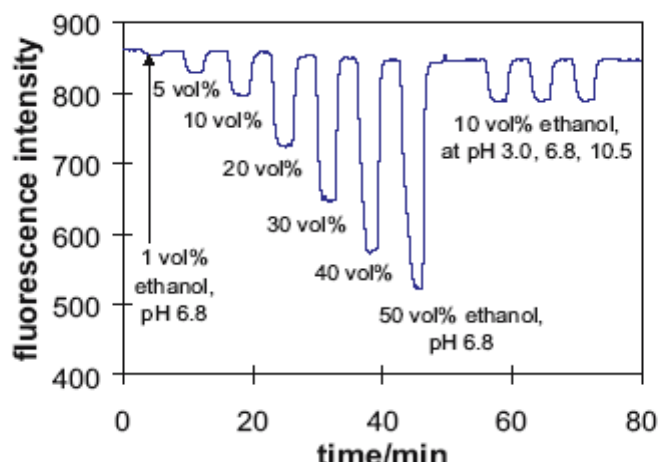


Figure 1.35 Response of the ethanol sensor layer based on ETH^T 4004 on exposure to aqueous ethanol solutions. (retrieved from <http://www2.uni-jena.de/~c1moge/Mohr/ASCOS2002.pdf>).

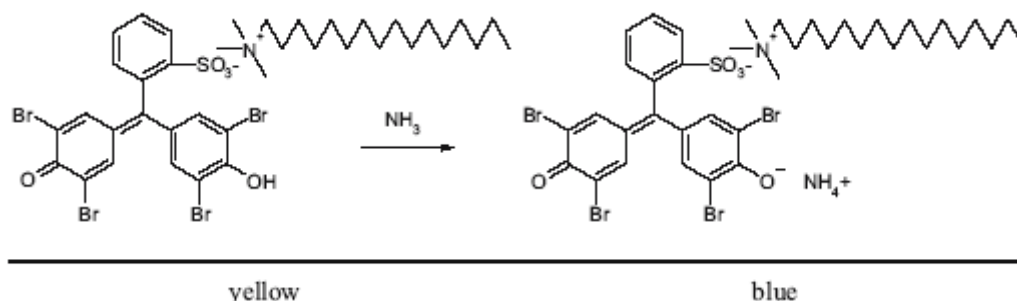


Figure 1.36 Sensor layer for ammonia based on a lipophilic pH indicator dye silicone. (retrieved from <http://www2.uni-jena.de/~c1moge/Mohr/ASCOS2002.pdf>).

1.9 Combination of Sensor Materials with Transducers

Sensor layers are mostly attached to a solid support since their mechanical stability is generally quite low. In most cases, all components (polymer, plasticizer, additives and indicator dyes) are dissolved in a common solvent and spin-coated, spray-coated, dip-coated or simply pipetted onto the support material (Figure 1.37). The solid support can be a glass plate which is mounted in a photometer and exposed

to the analyte in a flow-through cell but it can as well be a surface plasmon resonance (SPR) cell, an attenuated total reflection (ATR) crystal or an optical fiber known from communication technology.

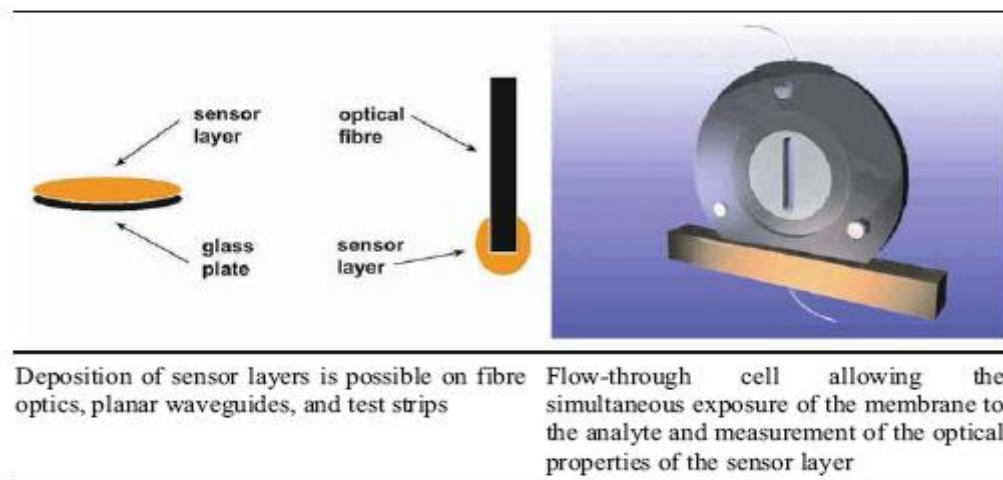


Figure 1.37 Combining sensor chemistry with optical transducer.

Immobilization directly on the light source, e.g. a light emitting diode (LED) is possible as well (Figure 1.37). Recently, the immobilization of indicators in tiny beads rather than in polymer layers has provided nanoparticles which can be inserted into cells and allow the measurement of various analytes (oxygen, sodium, potassium) within a living cell (Shortreed, Kopelman, Kuhn & Hoyland, 1996).

CHAPTER TWO

INTRODUCTION

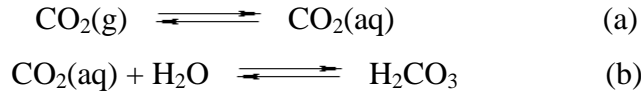
2.1 Carbon Dioxide

The concentration of CO₂, the most potent greenhouse gas, after water vapour, in the atmosphere has increased by more than 30% from the pre-industrial era which increase the average temperature of the earth and result in dramatic changes in climate and the ecosystem. Developed countries are committed to an overall reduction of about 5.2% of all greenhouse gas emissions in the period 2008–2012 compared to 1990 according to Kyoto Protocol. Therefore, the reduce of CO₂ emissions and the continuous and accurate monitoring of CO₂ levels in atmosphere and surface waters such as coastal oceans, deep oceans, estuaries, rivers etc. has a vital importance on global climate and ecosystem and is an exigency for governments. Also the detection of dissolved and gaseous CO₂ is an important feature in industrial applications, in chemical, biochemical, medicine and clinical analysis such as blood gas monitoring, breathe gas analysis, respiration, photosynthesis etc. The continuous and accurate monitoring of CO₂ levels in the atmosphere is of vital importance because of the threat of global warming.

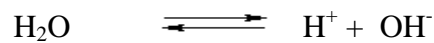
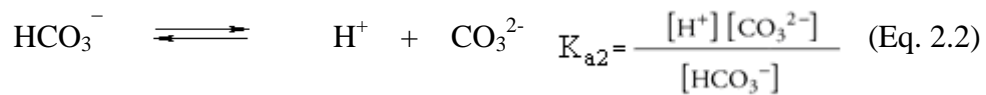
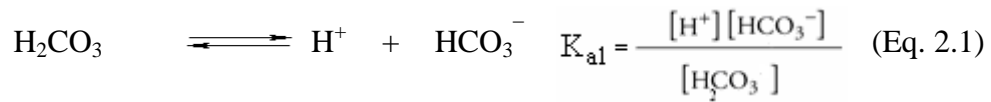
2.2 Dissolved CO₂ Equilibria

In addition to being a component of the atmosphere, carbon dioxide also dissolves in the water of the oceans. At room temperature, the solubility of carbon dioxide is about 90 cm³ of CO₂ per 100 mL of water. In aqueous solution, carbon dioxide exists in many forms. First, it simply dissolves. Then, equilibrium is established between the dissolved CO₂ and H₂CO₃, carbonic acid.

The chemical equilibria are (a) and (b);



where the analytical concentration of H_2CO_3 is $C_{\text{H}_2\text{CO}_3}$ and acidity constants are K_{a1} and K_{a2} , respectively. The equilibrium concentration of $[\text{H}_2\text{CO}_3]$, $[\text{HCO}_3^-]$ and $[\text{CO}_3^{2-}]$ are as follows.



The mass equilibrium is shown in Eq. 2.3.

$$C_{\text{H}_2\text{CO}_3} = [\text{H}_2\text{CO}_3] + [\text{HCO}_3^-] + [\text{CO}_3^{2-}] \quad \text{(Eq. 2.3)}$$

When the equations were arranged $[\text{HCO}_3^-]$ and $[\text{CO}_3^{2-}]$ can be calculated.

$$K_{a1} K_{a2} = \frac{[\text{H}^+]^2 [\text{CO}_3^{2-}]}{[\text{H}_2\text{CO}_3]} \quad \text{(Eq. 2.4)}$$

$$[\text{HCO}_3^-] = K_{a1} \frac{[\text{H}_2\text{CO}_3]}{[\text{H}^+]} \quad [\text{CO}_3^{2-}] = K_{a1} K_{a2} \frac{[\text{H}_2\text{CO}_3]}{[\text{H}^+]^2} \quad \text{(Eq. 2.5)}$$

$$C_{\text{H}_2\text{CO}_3} = [\text{H}_2\text{CO}_3] + K_{a1} \frac{[\text{H}_2\text{CO}_3]}{[\text{H}^+]} + K_{a1} K_{a2} \frac{[\text{H}_2\text{CO}_3]}{[\text{H}^+]^2} \quad (\text{Eq. 2.6})$$

$$C_{\text{H}_2\text{CO}_3} = [\text{H}_2\text{CO}_3] \left[1 + \frac{K_{a1}}{[\text{H}^+]} + \frac{K_{a1} K_{a2}}{[\text{H}^+]^2} \right] \quad (\text{Eq. 2.7})$$

$$[\text{H}_2\text{CO}_3] = C_{\text{H}_2\text{CO}_3} \frac{[\text{H}^+]^2}{[\text{H}^+]^2 + K_{a1} [\text{H}^+] + K_{a1} K_{a2}} \quad (\text{Eq. 2.8})$$

The α functions,

$$\frac{[\text{H}^+]^2}{[\text{H}^+]^2 + K_{a1} [\text{H}^+] + K_{a1} K_{a2}} = \alpha_{\text{H}_2\text{CO}_3} \quad (\text{Eq. 2.9})$$

$$[\text{H}_2\text{CO}_3] = C_{\text{H}_2\text{CO}_3} \alpha_{\text{H}_2\text{CO}_3} \quad (\text{Eq. 2.10})$$

The $\alpha_{\text{H}_2\text{CO}_3}$ is a H_2CO_3 related value; and is equals to

$$\alpha_{\text{H}_2\text{CO}_3} = \frac{[\text{H}_2\text{CO}_3]}{C_{\text{H}_2\text{CO}_3}} \quad (\text{Eq. 2.11})$$

Similar arrangements can also be performed for $[\text{HCO}_3^-]$ calculations.

$$[\text{H}_2\text{CO}_3] = \frac{[\text{H}^+][\text{HCO}_3^-]}{K_{a1}} \quad [\text{CO}_3^{2-}] = K_{a2} \frac{[\text{HCO}_3^-]}{[\text{H}^+]} \quad (\text{Eq. 2.12})$$

$$C_{\text{H}_2\text{CO}_3} = \frac{[\text{H}^+][\text{HCO}_3^-]}{K_{a1}} + [\text{HCO}_3^-] + K_{a2} \frac{[\text{HCO}_3^-]}{[\text{H}^+]} \quad (\text{Eq. 2.13})$$

$$C_{\text{H}_2\text{CO}_3} = [\text{HCO}_3^-] \left[\frac{[\text{H}^+]^2 + K_{a1} [\text{H}^+] + K_{a1} K_{a2}}{K_{a1} [\text{H}^+]} \right] \quad (\text{Eq. 2.14})$$

$$[\text{HCO}_3^-] = C_{\text{H}_2\text{CO}_3} \frac{K_{a1} [\text{H}^+]}{[\text{H}^+]^2 + K_{a1} [\text{H}^+] + K_{a1} K_{a2}} \quad (\text{Eq. 2.15})$$

Similarly the α function for HCO_3^- is as follows.

$$\frac{K_{a1} [\text{H}^+]}{[\text{H}^+]^2 + K_{a1} [\text{H}^+] + K_{a1} K_{a2}} = \alpha_{\text{HCO}_3^-} \quad (\text{Eq. 2.16})$$

$$[\text{HCO}_3^-] = C_{\text{H}_2\text{CO}_3} \alpha_{\text{HCO}_3^-} \quad (\text{Eq. 2.17})$$

When the similar arrangements were performed for $[\text{CO}_3^{2-}]$ the equilibrium concentration of CO_3^{2-} can be calculated as follows.

$$[\text{CO}_3^{2-}] = C_{\text{H}_2\text{CO}_3} \frac{K_{a1} K_{a2}}{[\text{H}^+]^2 + K_{a1} [\text{H}^+] + K_{a1} K_{a2}} = C_{\text{H}_2\text{CO}_3} \alpha_{\text{CO}_3^{2-}} \quad (\text{Eq. 2.18})$$

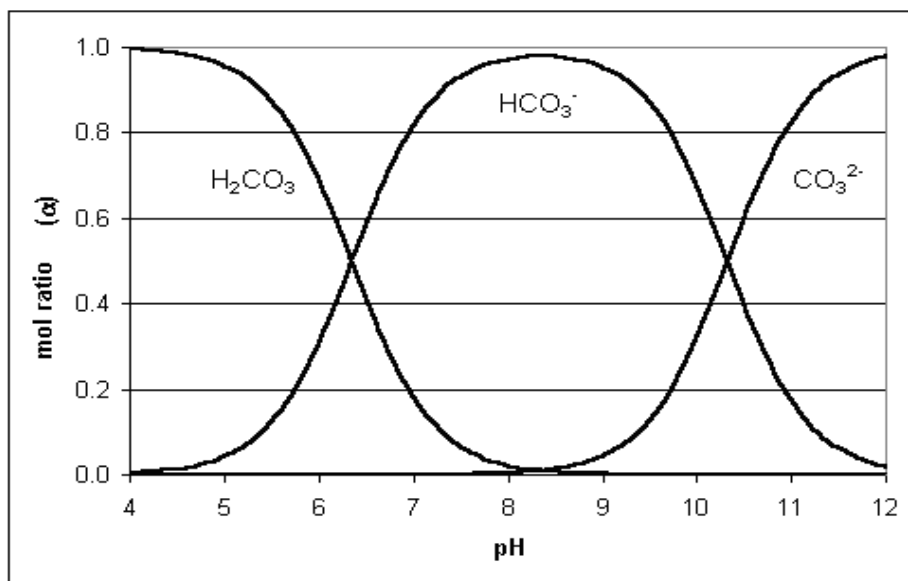


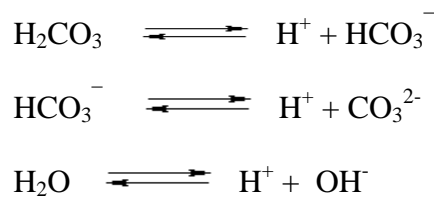
Figure 2.1 pH dependency of $\text{H}_2\text{CO}_3/\text{HCO}_3^-$ and CO_3^{2-} species in terms of α functions.

The equations for α functions of $\text{H}_2\text{CO}_3/\text{HCO}_3^-/\text{CO}_3^{2-}$ are shown below.

$$\begin{aligned}\alpha_{\text{H}_2\text{CO}_3} &= \frac{[\text{H}^+]^2}{[\text{H}^+]^2 + [\text{H}^+]K_{a1} + K_{a1}K_{a2}} = \frac{[\text{H}_2\text{CO}_3]}{\text{top. CO}_2(\text{aq})} \\ \alpha_{\text{HCO}_3^-} &= \frac{[\text{H}^+]K_{a1}}{[\text{H}^+]^2 + [\text{H}^+]K_{a1} + K_{a1}K_{a2}} = \frac{[\text{HCO}_3^-]}{\text{top. CO}_2(\text{aq})} \\ \alpha_{\text{CO}_3^{2-}} &= \frac{K_{a1}K_{a2}}{[\text{H}^+]^2 + [\text{H}^+]K_{a1} + K_{a1}K_{a2}} = \frac{[\text{CO}_3^{2-}]}{\text{top. CO}_2(\text{aq})}\end{aligned}\quad (\text{Eq. 2.19})$$

2.3 pH Calculations in a H_2CO_3 Solution

For a solution of H_2CO_3 the following equations can be written.



The charge balance equation and following steps show the way for pH calculation.

$$[\text{H}^+] = [\text{HCO}_3^-] + 2[\text{CO}_3^{2-}] + [\text{OH}^-] \quad (\text{Eq. 2.20})$$

$$[\text{HCO}_3^-] = C_{\text{H}_2\text{CO}_3} \alpha_{\text{HCO}_3^-} = C_{\text{H}_2\text{CO}_3} \frac{K_{a1} [\text{H}^+]}{[\text{H}^+]^2 + K_{a1} [\text{H}^+] + K_{a1} K_{a2}} \quad (\text{Eq. 2.21})$$

$$[\text{CO}_3^{2-}] = C_{\text{H}_2\text{CO}_3} \frac{K_{a1} K_{a2}}{[\text{H}^+]^2 + K_{a1} [\text{H}^+] + K_{a1} K_{a2}} \quad (\text{Eq. 2.22})$$

$$[\text{OH}^-] = \frac{K_{\text{su}}}{[\text{H}^+]} \quad (\text{Eq. 2.23})$$

$$[\text{H}^+] = C_{\text{H}_2\text{CO}_3} \left(\frac{K_{a1} [\text{H}^+] + 2 K_{a1} K_{a2}}{[\text{H}^+]^2 + K_{a1} [\text{H}^+] + K_{a1} K_{a2}} \right) + \frac{K_{\text{su}}}{[\text{H}^+]} \quad (\text{Eq. 2.24})$$

The equation 2.24 is a quadratic equation and should be simplified,

$$[\text{H}^+] = C_{\text{H}_2\text{CO}_3} \left(\frac{K_{a1} [\text{H}^+] + 2 K_{a1} K_{a2}}{[\text{H}^+]^2 + K_{a1} [\text{H}^+] + K_{a1} K_{a2}} \right) \quad (\text{Eq. 2.25})$$

The equation eq. 2.22 is still a third order equation and should be simplified once more considering

$$[\text{H}^+] \cong [\text{HCO}_3^-] \text{ and}$$

$$[\text{HCO}_3^-] \gg 2 [\text{CO}_3^{2-}]$$

Therefore the equation eq. 2.22 becomes,

$$C_{\text{H}_2\text{CO}_3} \frac{K_{a1} [\text{H}^+]}{[\text{H}^+]^2 + K_{a1} [\text{H}^+] + K_{a1} K_{a2}} \gg 2 C_{\text{H}_2\text{CO}_3} \frac{K_{a1} K_{a2}}{[\text{H}^+]^2 + K_{a1} [\text{H}^+] + K_{a1} K_{a2}} \quad (\text{Eq. 2.26})$$

When the acidity constant of K_{a2} considered as

$$[\text{H}^+] \gg 2 K_{a2}$$

and the assumption shown in eq. 2.27 was accepted the pH can be calculated as follows (Eq. 2.28)

$$\frac{2 K_{a2}}{[\text{H}^+]} < 10^{-2} \quad (\text{Eq. 2.27})$$

$$[\text{H}^+] = \sqrt{K_{a1} C_{\text{H}_2\text{CO}_3}} \quad (\text{Eq. 2.28})$$

CHAPTER THREE

EXPERIMENTAL STUDY AND INSTRUMENTATION

All solvents used in this study were of analytical grade and purchased from Merck, Johnson and Mathey, Acros, Fluka and Riedel. Solvents for the spectroscopic studies were used without further purification. The ionic liquid, 1-ethyl-3-methylimidazolium tetrafluoroborate (RTIL) was obtained from Fluka. Tetrabutylammonium hydroxide for titration (in nonaqueous medium) was standard 0.1 M solution in isopropanol/methanol (0.1 N) from Fluka. The solution was concentrated to 1 M with vacuum evaporator before use for the titrations in ionic liquid media. The sodium bicarbonate in powder form was obtained from Riedel (99-100%). The polymer polyvinyl chloride (PVC) has high molecular weight and obtained from Fluka. The polymer ethyl cellulose was from Organics with an ethoxy content of 8%. Polymethylmethacrylate (PMMA, Mw 120,000) ($-\text{CH}_2\text{C}(\text{CH}_3)\text{CO}_2\text{CH}_3-$) from Aldrich is used to prepare the solutions that are used as working fluid. The plasticizer, dioctyl phthalate (DOP) was 99 % from Aldrich. The additive potassium tetrakis (4-chlorophenyl) borate was selectophore, 98 % from Fluka. Teflon AF (type 1600) was purchased from Du Pont polymers (Switzerland). The standard metal solutions were prepared from their 0.1 M stock solutions by using the metal salts of $\text{Cu}(\text{NO}_3)_2$, $\text{Co}(\text{NO}_3)_2$, $\text{NiCl}_2 \cdot 6\text{H}_2\text{O}$, $\text{Pb}(\text{NO}_3)_2$, $\text{Hg}_2(\text{NO}_3)_2$, $\text{Hg}(\text{NO}_3)_2$, CrCl_3 , CdCl_2 , $\text{Fe}(\text{NO}_3)_3$, ammonium-iron(II) sulphate.hexahydrate, $\text{Al}(\text{SO}_4)_3 \cdot 16\text{H}_2\text{O}$.

Absorption spectra were recorded using a Shimadzu 1601 UV-Visible spectrophotometer. Steady state fluorescence emission and excitation spectra were measured using Varian Cary Eclipse Spectrofluorometer with a Xenon flash lamp as the light source. The fiber optic components were obtained from Varian and explained in detail in Section 1. The emission spectra were corrected using a piece of silica ground on both faces held in a triangular cuvette configuration called the

diffuser. The pH and CO₂ analysis studies were executed by fiber optical and flow system. The flow cell is made from polytetrafluoroethylene (PTFE) in the atelier of University of Ege.

pH measurements were recorded with a WTW pH meter. All of the experiments were carried out at room temperature; 25 ± 1 °C. Rose Bengal, 8-hydroxypyrene-1,3,6-trisulfonic acid (HPTS) and fluorescein were used as reference standards for fluorescence quantum yield calculations

In all of the studies ultra pure water of Millipore was used. Cylinders of carbon dioxide, oxygen and nitrogen gases of 99.99% purity were obtained from Gunes or Karbogaz, Izmir, Turkey. The gas mixtures were prepared with a Sonimix 7000 Gas Diluter instrument.

3.1 Construction of Fiber Optic Measurement System

The fiber optical sensor was constructed with the commercial accessories of Varian Cary Eclipse Spectrofluorometer (Figure 3.1): Eclipse Fiber optic coupler, fluorescence remote read probe (2 meters), Probe tip for solid measurements and Probe tips for liquid measurements (10 mm and 20 mm length tips). This method also allows the remote sensing of the samples. The installation steps are:

- ***The fiber optic coupler*** is an accessory that enables the use of a fiber optic probe with Carry Eclipse spectrofluorometer. After the removal of the sample compartment of the Carry Eclipse, the fiber optic coupler was stabilized to the same position by the help of the screws.

- ***The fiber optic probe*** was connected to the coupler accessory by inserting the two connector ends into the two key holds.

- *The probe tips* were screwed onto the end of the probe. Based on the phase of the sample (solid or liquid), either a solid sample probe tip or a liquid sample probe tip was used.

- To ensure that the fiber optic system will operate at maximum performance, it is necessary to optimize the efficiency with which light passes through the coupling device before the sample measurement. The alignment was done by using the software of the instrument.



Fluorescence
remote read probe



Fibre optic
coupler accessory



probe tips



Figure 3.1 Varian Cary Eclipse Spectrofluorometer and fiber optical system accessories.

3.2 Combination of the Flow System with Fiber Optic System

pH response measurements were carried out with fiber optic probe (2m long) and solid sample tip accessories constructed on the spectrofluorometer. For instrumental control, data acquisition and processing the software package of the

spectrofluorometer was used. The tip of the bifurcated fiber optic probe was interfaced with a sensing film in a buffer containing 300 μL flow cell (Figure 3.3). The flow cell was equipped with a four channel Ismatec Reglo Analog peristaltic pump. Analyte solutions or buffers were transported by the peristaltic pump via tygon tubing of 2.06 mm i.d. (Figure 3.2)



Figure 3.2 Ismatec Reglo Analog peristaltic pump.

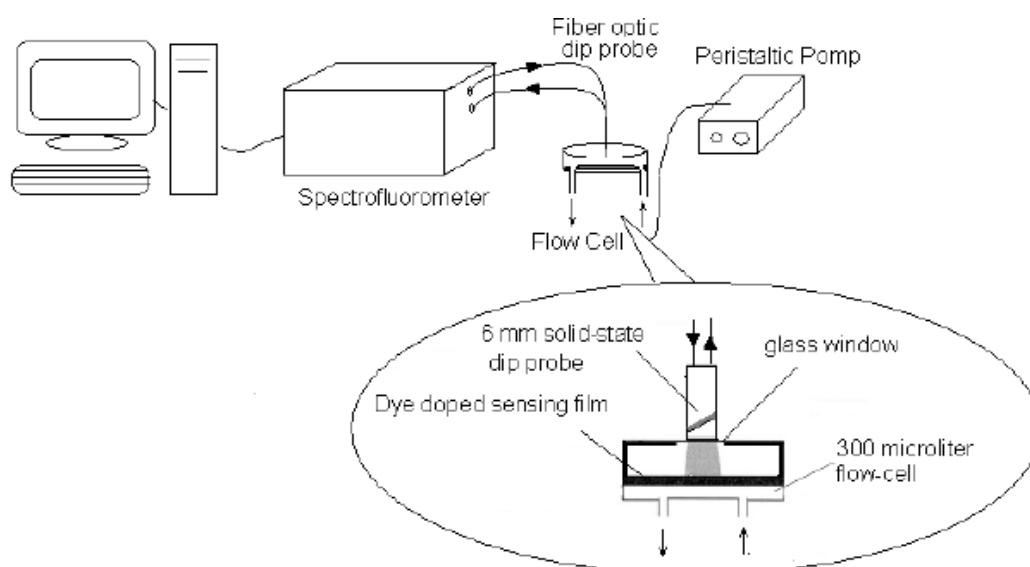


Figure 3.3 Instrumental set-up used for dye-doped thin film evaluation.

3.3 Mixing of the Gases

Gaseous CO₂ and N₂ were mixed in the concentration range 0–100% either in a gas diluter; Sonimix 7000A gas blending system or in a home made gas mixing chamber by controlling the gas flow rates with sensitive flow-meters (Figure 3.4). Gas mixtures were introduced into the sensor agent containing cuvette via a diffuser needle under ambient conditions either directly or after humidification of the gas by bubbling through water at 25 °C.



Figure 3.4 Sonimix 7000 Gas Diluter.

3.4 Construction of the Sensing Films

The sensing cocktails were prepared due to the analyte type either with PVC, ethyl cellulose, PMMA or ionic liquid.

3.4.1 PVC Cocktail Preparation

The membranes were prepared to contain the dye, 33% PVC (High molecular weight), 66% plasticizer (Dioctyl phthalate, DOP) by weight and the additive potassium tetrakis-(4-chlorophenyl) borate (PTCPB). The chemical structures of

PVC, DOP and PTCPB were shown in Figure 3.6. The mixture was dissolved in the solvent of tetrahydrofuran (THF) and mixed by several hours by the help of a magnetic stirrer. The resulting cocktail was spread on a 125 μm polyester support (Mylar from Du Pont) and dried in a desiccator which was saturated with the solvent vapor. The dried films were covered with the non-viscous Teflon solution by spraying technique. The Teflon membrane is permeable for non-polar gaseous but impermeable for polar molecules and ionic species. Since the Teflon membrane would reject the acidic protons, some of the films are separated without Teflon coating for $\text{p}K_a$ determination studies (Seiler & Simon, 1992; Bakker & Simon, 1992; Lerchi, Bakker, Rusterholz & Simon, 1992).

The polyester support was optically fully transparent, ion impermeable and exhibited good adhesion to PVC. The most important function of the polyester was to act as a mechanical support because the thin silicon films were impossible to handle. Once dried, the film was insoluble in water and could be cut into pieces of appropriate size. The approximate thickness of the film was 5 μm . Film thicknesses were measured using Tencor Alpha Step 500 Profilometer. The films were kept in a desiccator in the dark. This way, the photostability of the membrane was ensured and the damage from the ambient air of the laboratory was avoided. For absorbance and steady state fluorescence measurements each sensing film was cut to 1.2 cm width and 2.5 cm length and fixed diagonally into the sample cuvette (Figure 3.5) and the absorption or emission spectra were recorded. For fiber optical and flow system measurements, each sensing film was cut to 1 cm width and 1 cm length and fixed into the flow cell shown in Figure 3.3.

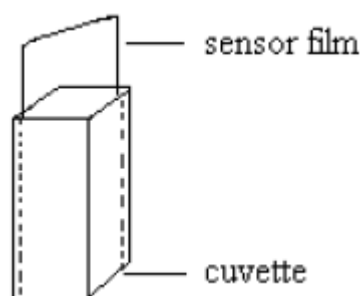


Figure 3.5 The placement of the sensor film in the sample cuvette.

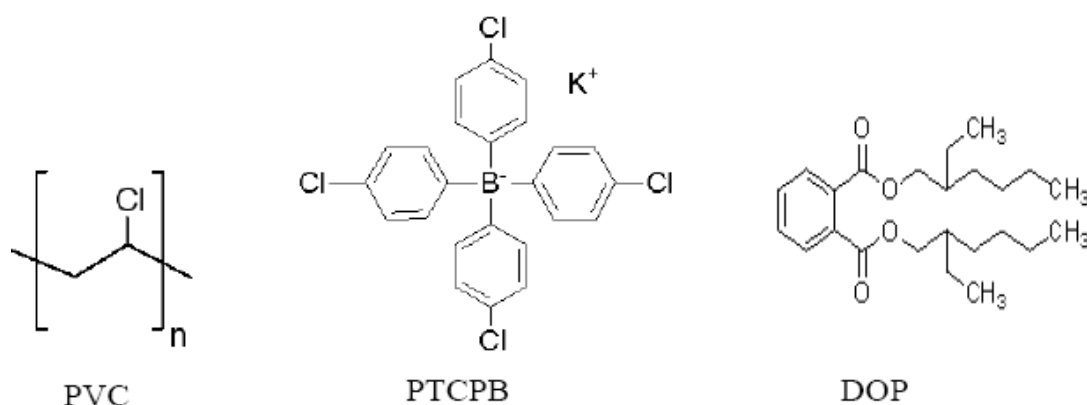


Figure 3.6 Structures of PVC, PTCPB and DOP

3.4.2 Ethyl Cellulose Cocktail Preparation

The membranes were prepared to contain the dye, 33% ethyl cellulose (48-49.5% ethoxy content, ec) and 66% plasticizer (DOP) by weight. The mixture was dissolved in the solvent of tetrahydrofuran and was mixed by several minutes by the help of a magnetic stirrer. After that the same procedure with the PVC matrix was employed. Structure of the ethyl cellulose is shown in Figure 3.7.

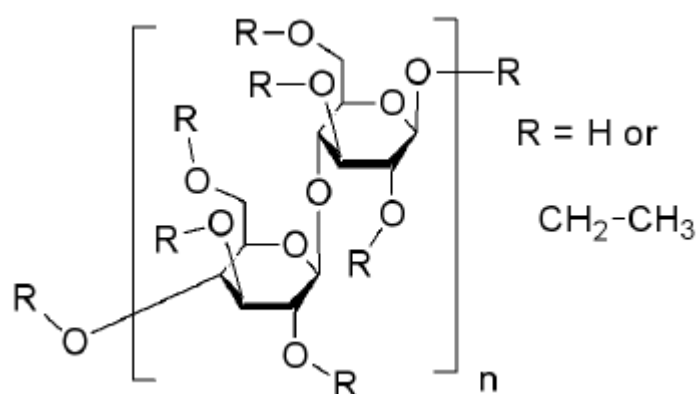


Figure 3.7 Structure of ethyl cellulose

3.4.3 PMMA Cocktail Preparation

PMMA based nano fibers were prepared in three different composition.

(C-1) contains 240 mg of PMMA, 72 mg of ionic liquid (**RTIL**; 1-ethyl-3-methylimidazolium tetrafluoroborate), 168 mg of plasticizer (DOP), 1.0 mg of AZM-I or AZM-II (2.5 mmol dye/kg polymer), stoichiometric amount of potassium tetrakis (4- chlorophenyl) borate and 1.5mL of THF.

(C-2) contains 240 mg of PMMA, 96 mg of ionic liquid 1-ethyl-3-methylimidazolium tetrafluoroborate (**RTIL**; 1-ethyl-3-methylimidazolium tetrafluoroborate), 144 mg of plasticizer (DOP), 1.0 mg of AZM-I or AZM-II (2.5 mmol dye/kg polymer), stoichiometric amount of potassium tetrakis (4- chlorophenyl) borate and 1.5mL of THF.

(C-3) contains 240 mg of PMMA, 120 mg of ionic liquid (**RTIL**; 1-ethyl-3-methylimidazolium tetrafluoroborate), 120 mg of plasticizer (DOP), 1.0 mg of AZM-I or AZM-II (2.5 mmol dye/kg polymer), stoichiometric amount of potassium tetrakis (4- chlorophenyl) borate and 1.5mL of THF.

3.5 Quantum Yield Calculations

Fluorescence quantum yield values (Φ_F) of the employed dyes were calculated by using the comparative William's method (Williams, Winfield & Miller, 1983). This is a reliable method for recording Φ_F and involves the use of well characterized standard samples with known Φ_F values. Essentially, solutions of the standard and test samples with identical absorbance at the same excitation wavelength can be assumed to be absorbing the same number of photons. Hence, a simple ratio of the integrated fluorescence intensities of the two solutions (recorded under identical conditions) will yield the ratio of the quantum yield values. Since Φ_F for the standard sample is known, it is trivial to calculate the Φ_F for the test sample.

According to this method, the standard samples should be chosen to ensure they absorb at the excitation wavelength of choice for the test sample, and, if possible, emit in a similar region to the test sample. In order to minimise re-absorption effects

(Dhami and et al., 1995) absorbances in the 10 mm fluorescence cuvette should never exceed 0.1 at and above the excitation wavelength. Above this level, non-linear effects may be observed due to inner filter effects, and the resulting quantum yield values may be perturbed. This maximum allowable value of the recorded absorbance must be adjusted depending upon the path length of the absorption cuvette being used (for example, 10 mm = 0.1 maximum, 20 mm = 0.2 maximum etc). In this study, standard 10 mm path length fluorescence and absorption cuvettes were used for running the fluorescence and absorbance measurements. The UV-VIS absorption (absorbance ≤ 0.10 at the excitation wavelength) and corrected fluorescence emission spectra were recorded for three or more solutions with increasing concentrations of the sample and the standard. The integrated fluorescence intensities (that is, the area of the fluorescence spectrum) were calculated from the fully corrected fluorescence spectrum. Graphs of integrated fluorescence intensity *vs* absorbance were plotted. The gradient of the plots were later used in the quantum yield calculations according to the following equation.

$$\theta_x = \theta_{st} \left(\frac{Grad_x}{Grad_{st}} \right) \left(\frac{n_x^2}{n_{st}^2} \right) \quad (\text{Eq. 3.1})$$

Where the subscripts *ST* and *X* denote standard and test respectively, Φ is the fluorescence quantum yield, *Grad* the gradient from the plot of integrated fluorescence intensity *vs* absorbance and *n* is the refractive index of the solvent.

3.6. Preparation of the Employed Buffer Solutions

3.6.1 Preparation of 0.005 M Acetic Acid/Acetate Buffer

0.143 mL of acetic acid was dissolved in 950 mL ultra pure water. The solution was titrated to pH 5.0 at the lab temperature of 20°C either with 0.1 M HNO₃ or 0.1 M NaOH as needed. The resulting solution was made up to 1000 mL with ultra pure water in a volumetric flask. The buffer solutions in the range of pH 3.0-7.0 were prepared by the same way by adjusting to the desired pH.

3.6.2 Preparation of 0.005 M NaH₂PO₄·2H₂O and 0.005 M Na₂HPO₄·12H₂O Buffer

0.39 g of NaH₂PO₄·2H₂O was dissolved in 950 mL ultra pure water. The solution was titrated to pH 7.0 at the lab temperature of 20⁰C either with 0.1 M HNO₃ or 0.1 M NaOH as needed. The resulting solution was made up to 1000 mL with ultra pure water in a volumetric flask. The buffer solutions in the range of pH 7.0-9.0 were prepared by the same way by adjusting to the desired pH.

0.895 g of Na₂HPO₄·12H₂O was dissolved in 950 mL ultra pure water. The solution was titrated to pH 7.0 at the lab temperature of 20⁰C either with 0.1 M HNO₃ or 0.1 M NaOH as needed. The resulting solution was made up to 1000 mL with ultra pure water in a volumetric flask. The buffer solutions in the range of pH 10.0-12.0 were prepared by the same way by adjusting to the desired pH

CHAPTER FOUR

SPECTRAL CHARACTERIZATION OF AZOMETINE DYES IN DIFFERENT MATRIX MATERIALS

4.1 Photophysical Characterization of Azometine Dyes

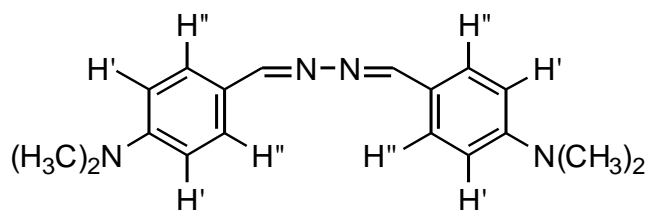
The employed azometine dyes were synthesized in our laboratories according to the literature method and characterized with ^1H NMR and IR based data (Grigoras & Antonoaia, 2005, Méalares & Gandini, 1996, Ambroziak & Szypa, 2007). Schematic structures of the employed molecules AZM-I, AZM-II and AZM-III are shown in Figure 4.1.

4.2 Structural Identification of AZM-I, AZM-II and AZM-III

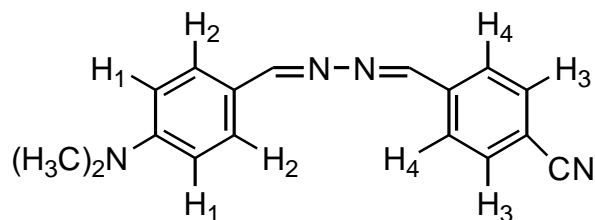
The Schiff bases (4,4'-[hydrazine-1,2-dilidendimethylidene]bis(N,N-dimethylaniline), AZM-I; (4-[(4-(dimethylamino)phenyl)methylidene hidrazono]methyl benzonitrile, AZM-II; and (N,N'-bis-(4-metoxifenyl) methylidene-benzene-1,4-diamine, AZM-III.

AZM-I: IR (KBr): 2909 (C-H), 1598 (C=N) cm^{-1} . ^1H -NMR (400 MHz, d_6 -DMSO): δ 2.97 (s, 12H, 4xCH₃), 6.66 (d, 4H, J=8.4 Hz, 4x ArH), 7.57 (d, 4H, J=8.8 Hz, 4x ArH''), 8.41 (s, 2H, -N=CH), GC-MS [M]⁺ = 294.3, mp=265.2 °C.

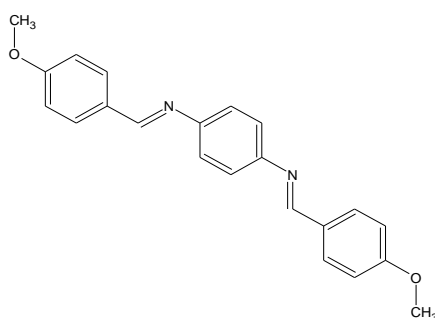
AZM-II: IR (KBr): 2912 (C-H), 2226 (CN), 1604 (C=N) cm^{-1} . ^1H -NMR (400 MHz, d_6 -DMSO): δ 2.95 (s, 6H, 2xCH₃), 6.62 (d, 2H, J=7.6 Hz, 2x ArH₁), 7.56 (d, 2H, J=8.0 Hz, 2x ArH₂), 7.66 (d, 2H, J=8.1 Hz, 2x ArH₃), 8.41 (d, 2H, J=8.2 Hz, 2x ArH₄), 8.47 (s, 1H, -N=CH), 8.54 (s, 1H, -N=CH), GC-MS [M]⁺ = 276.3, mp=269.1 °C.



AZM-I: 4,4'-[hydrazine-1,2-dilidenedimethylidene]bis(N,N-dimethylaniline)



AZM-II: 4-[(4-(dimethylamino)phenyl)methylidene hidrazono] methyl benzonitrile



AZM-III: N,N'-bis-(4-metoxifenyl) methylidene-benzene-1,4-diamine

Figure 4.1 Schematic structure of the employed molecules, AZM-I, AZM-II and AZM-III.

4.3 Thin Film Preparation Protocols

PVC based thin membranes were prepared to contain 120 mg of PVC, 240 mg of plasticizer (DOP), 1.2 mg of AZM-I, AZM-II or AZM-III (2.5 mmol dye/kg polymer), stoichiometric amount of potassium tetrakis (4- chlorophenyl) borate and 1.5mL of THF. The prepared cocktails contained 33% PVC and 66% plasticizer by weight.

Ethyl cellulose based cocktails were prepared from 1.0 g of a 5% ethyl cellulose solution in ethanol/toluene (20/80, v/v) and by addition of 2.0 mg of the AZM-I,

AZM-II or AZM-III dyes. During bicarbonate sensing studies this solution was mixed with 100 μL of the methanolic TOA-hydroxide solution. The TOA-OH solution was previously equilibrated with a CO_2/N_2 gas mixture (CO_2 content 3%) in order to form a lipophilic hydrogen carbonate buffer.

In all cases the resulting cocktails were spread onto a $125\mu\text{m}$ polyester support (MylarTM). The film thicknesses of the dried sensing slides were measured with Tencor Alpha Step 500 profilometer and found to be $5.72 \pm 0.12\mu\text{m}$ ($n = 15$). The employed polyester support was optically fully transparent, ion impermeable and exhibited good adhesion to PVC and EC. Each sensing film was cut to $1.2\text{ cm} \times 3.0\text{ cm}$ size, fixed diagonally into the sample cuvette and the excitation and fluorescence emission spectra were recorded. For flow through measurements, the sensor films of 30mm diameter were cut, placed into the buffer containing 300 μL black-Teflon flow cell and interfaced with the fiber tip (6mm diameter). The contact between the sensor membrane and the buffer provided a constant fluorescence signal. pH determinations were carried out pumping buffer solutions of desired pH.

4.4 Results and Discussion

4.4.1 Absorption Based Spectral Characterization

For spectral characterization of the AZM-I, AZM-II and AZM-III absorption excitation and corrected emission spectra were recorded in the solvents of EtOH, DCM, THF and toluene/ethanol (To: EtOH; 80:20) mixture (see figures 4.2.1, 4.2.2 and 4.2.3). The UV-VIS spectroscopy related data (absorption maxima; λ_{Abs} , and molar extinction coefficient; ϵ), were shown in Table 4.1 and 4.2. AZM-I, AZM-II and AZM-III exhibited very efficient absorbance and high molar extinction coefficients around 400 nm and 500 nm in PVC and EC matrices.

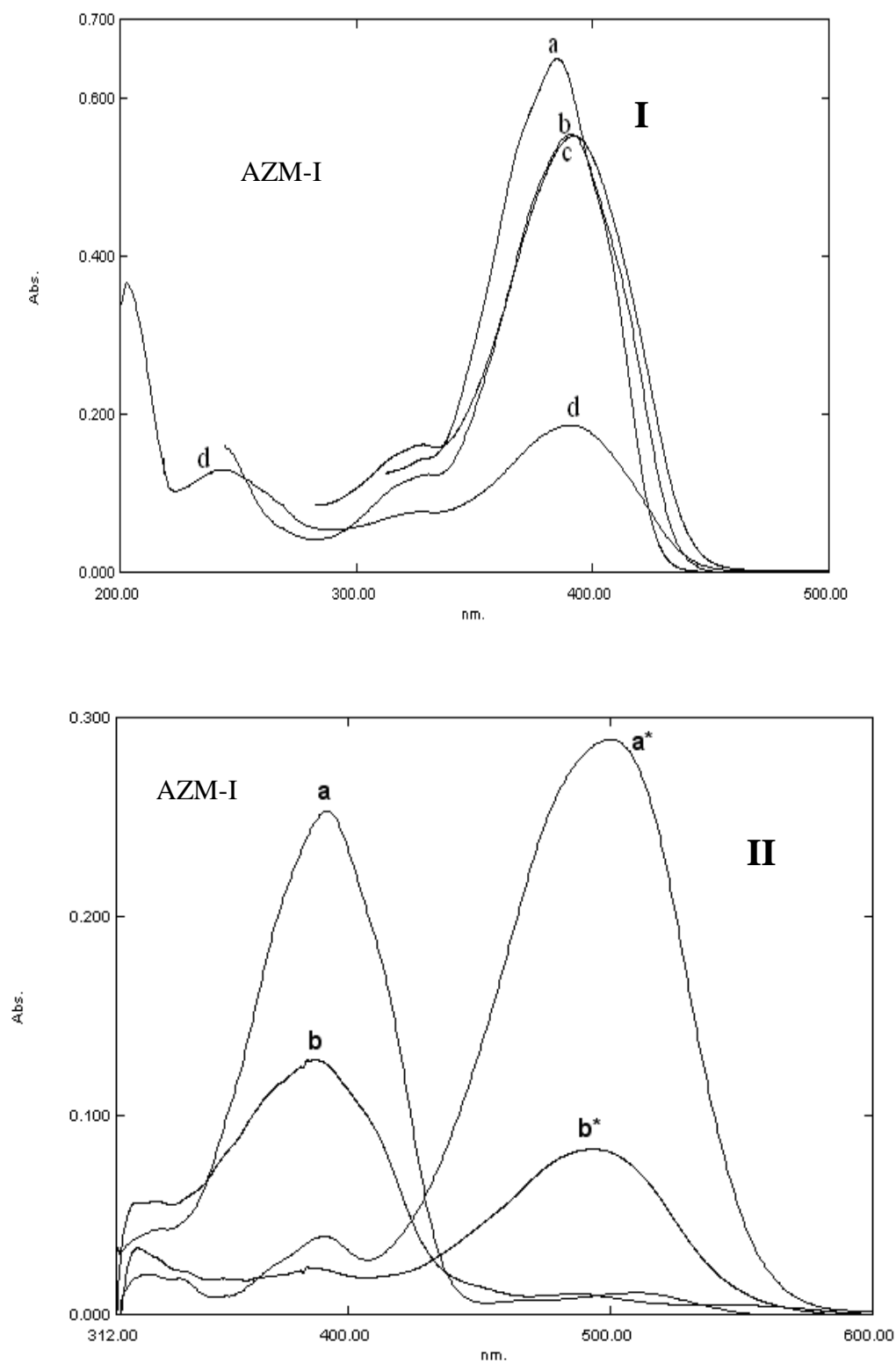


Figure 4.2.1 Absorption spectra of the AZM-I, AZM-II and AZM-III dyes (10^{-6} M dye or 2 mmol dye/kg polymer).

AZM-I: **I:** a) THF b) DCM c) To:EtOH d) EtOH; **II:** a) PVC (basic) a*) PVC (acidic) b) EC (basic) b*) EC (acidic).

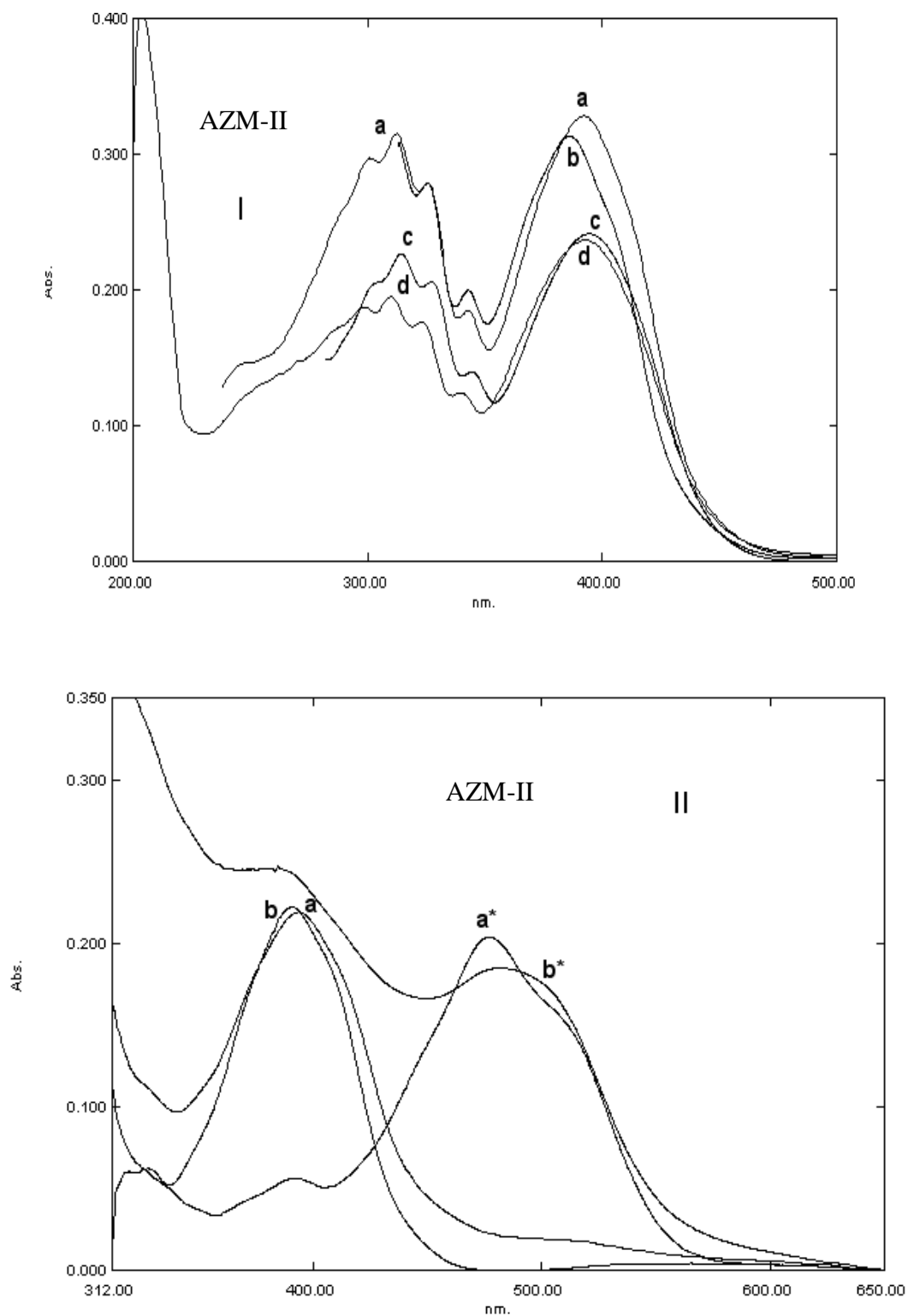


Figure 4.2.2 Absorption spectra of the AZM-I, AZM-II and AZM-III dyes (10^{-6} M dye or 2 mmol dye/kg polymer).

AZM-II: I: a) DCM b) THF c) To:EtOH d) EtOH; **II:** a) PVC (basic) a*) PVC (acidic)
b) EC (basic) b*) EC (acidic)

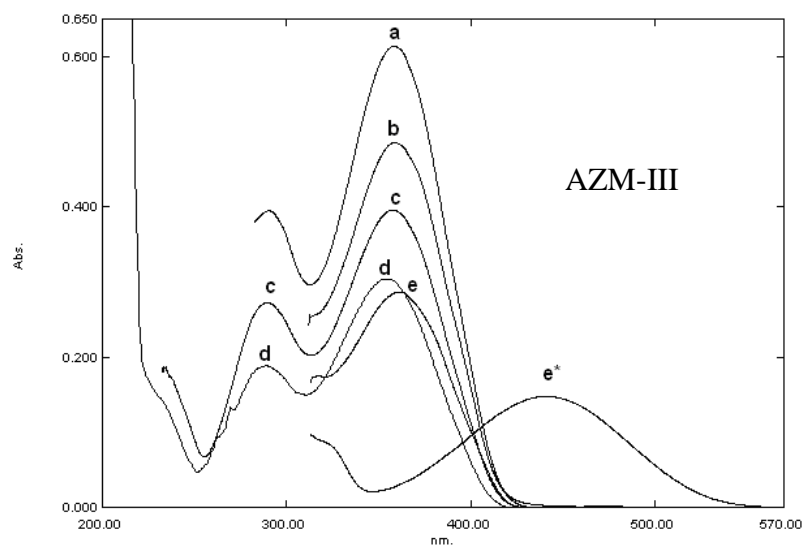


Figure 4.2.3 Absorption spectra of the AZM-I, AZM-II and AZM-III dyes (10^{-6} M dye or 2 mmol dye/kg polymer).

AZM-III: a) To:EtOH b) THF c) DCM d) EtOH e) PVC (basic)
e*) PVC (acidic)

Table 4.1 and 4.2 reveal UV-VIS and fluorescence spectra related characteristics (absorption maxima and molar extinction coefficient) of AZM-I, AZM-II and AZM-III, respectively. In agreement with literature (Ertekin ve diğerleri, 2000) molar extinction coefficients (ϵ_{\max}) of AZM-I, AZM-II and AZM-III were increased in PVC and EC with respect to (ϵ_{\max}) of AZM-I, AZM-II and AZM-III in solution phase (see Table 4.1, Table 4.2). These data can be taken as proofs that AZM-I, AZM-II and AZM-III molecules absorb better in plasticized PVC and EC matrices with respect to solution phase.

Table 4.1. UV-Vis spectra related data of AZM-I and AZM-II in the solvents of EtOH, DCM, THF and toluene/ ethanol mixture (80:20) and in solid matrices of PVC and EC.

Compound	Matrix	λ_{abs}^1	λ_{abs}^2	ϵ_{max} (λ_{abs}^1)	ϵ_{max} (λ_{abs}^2)
AZM-I	EtOH	243	391	12900	18600
AZM-I	DCM	244	391	15800	55200
AZM-I	THF	--	385	--	65000
AZM-I	To: EtOH	--	391	--	55200
AZM-I	PVC	392 (basic)	500 (acidic)	107000	108544
AZM-I	EC	388 (basic)	488 (acidic)	96045	84100
AZM-II	EtOH	310	394	19500	23600
AZM-II	DCM	312	393	31500	32800
AZM-II	THF	--	387	--	38300
AZM-II	To: EtOH	314	395	22600	24100
AZM-II	PVC	394 (basic)	496 (acidic)	41030	40846
AZM-II	EC	390 (basic)	494 (acidic)	32165	26372

Table 4.2 UV-Vis spectra related data of AZM-III in the solvents of EtOH, DCM, THF and toluene/ ethanol mixture (80:20) and in solid matrices of PVC.

Compound	Matrix	λ_{abs}^1	λ_{abs}^2	ϵ_{max} (λ_{abs}^1)	ϵ_{max} (λ_{abs}^2)
AZM-III	EtOH	289	355	4700	7600
AZM-III	DCM	290	358	27200	39600
AZM-III	THF	--	360	--	48600
AZM-III	To: EtOH	291	359	39600	61300
AZM-III	PVC	361	444	65525	33789

4.4.2 Spectral Evaluation, Fluorescence Quantum Yield Calculations and Interpretation of Emission Spectra

The Schiff bases; AZM-I and AZM-II exhibited bright fluorescence in all of the employed solvents and solid matrices. The AZM-I dye was excited around 420 nm and emitted at 470 nm. The AZM-II dye was excited at shorter wavelengths; around 415 nm in solvents (See Table 4.3). The employed dyes AZM-I and AZM-II were excited at 505 / 590 and 510 / 582 nm in PVC and EC respectively (See Figure 4.3,

Table 4.3). The AZM-III dye did not give significant fluorescence emission spectra both in solvents and solid matrices.

Fluorescence quantum yield values (ϕ_F) of the AZM-I and AZM-II were calculated employing the comparative William's method (Williams, Winfield, Miller, 1983), which involves the use of well-characterized standards with known ϕ_F values. For this purpose, the UV-Vis absorbance and corrected emission spectra of different concentrations of reference standard Rose Bengal ($\lambda_{ex} = 525$ nm, quantum yield (ϕ_F) = 0.11 in alkaline ethanol) and the employed molecules were recorded, and, the integrated fluorescence intensities were plotted versus corresponding absorbances.

Quantum yield (ϕ_F) values were calculated according to the following equation where ST and X denote standard and sample, respectively. Grad is the gradient from the plot and n is the refractive index of the solvent or polymer matrix material (Williams, Winfield & Miller, 1983).

$$\phi_F = \phi_{ST} \left(\frac{Grad_X}{Grad_{ST}} \right) \left(\frac{n_x^2}{n_{ST}^2} \right)$$

The AZM-I dye displayed enhanced fluorescence emission quantum yield (ϕ_F); 0.4290 and longer excitation wavelength $\lambda_{ex}=505$ nm in immobilized PVC with respect to (ϕ_F) of 4.2×10^{-3} and $\lambda_{ex} = 422$ nm, in ethanol (see Table 4.3). The comparatively small ϕ_F values reported in ethanol can be attributed to the internal charge transfer (ICT) state by rotation of the central N–N bond and a following radiationless deactivation. The enhancement observed in fluorescence emission quantum yield of AZM-II can be explained in the same way.

In all of the employed matrices, Stokes' shift values were high enough and extended from 47 to 85 nm. Stokes' shift is an important parameter for fluorescence

and optical sensor studies because the high Stokes' shift value allows the emitted fluorescence photons to be easily distinguished from the excitation photons. Stokes' shift exceeding 30 nm is recommended for easy visualization and sensitive detection. The Stokes' shifts of AZM-I and AZM-II which are 85 nm and 72 nm in PVC matrix, respectively, permit the usage of azometine dyes in together with solid-state optic components such as LEDs or fiber optics.

Table 4.3 Spectral characterization of AZM-I and AZM-II dyes. λ_{ex}^{em} : excitation wavelength for emission in nm; λ_{ex}^{ex} : excitation wavelength for excitation in nm; λ_{max}^{em} : maximum emission wavelength in nm; λ_{max}^{ex} : maximum excitation wavelength in nm; $\Delta\lambda_{ST}$: Stoke's shift and ϕ_F : Quantum yield.

Compound	Matrix	λ_{ex}^{em} (excitation wavelength for emission)	λ_{ex}^{ex} (emission wavelength for excitation)	λ_{max}^{em}	λ_{max}^{ex}	$\Delta\lambda_{ST}$ (Stoke's shift)	ϕ_F (Quantum yield)
AZM-I	EtOH	422	473	473	420	53	4.2×10^{-3} in EtOH
AZM-I	DCM	--	--	--	--	--	
AZM-I	THF	422	466	466	422	44	
AZM-I	To:EtOH	422	469	469	422	47	
AZM-I	PVC	505	590	590	505	85	0.4290
AZM-I	EC	505	580	580	505	75	0.2336
AZM-II	EtOH	415	473	473	415	58	1.9×10^{-3} in EtOH
AZM-II	DCM	400	454	454	400	54	
AZM-II	THF	420	480	480	420	60	
AZM-II	To:EtOH	410	468	468	410	58	
AZM-II	PVC	510	582	582	510	72	0.4153
AZM-II	EC	500	572	572	500	72	0.3805

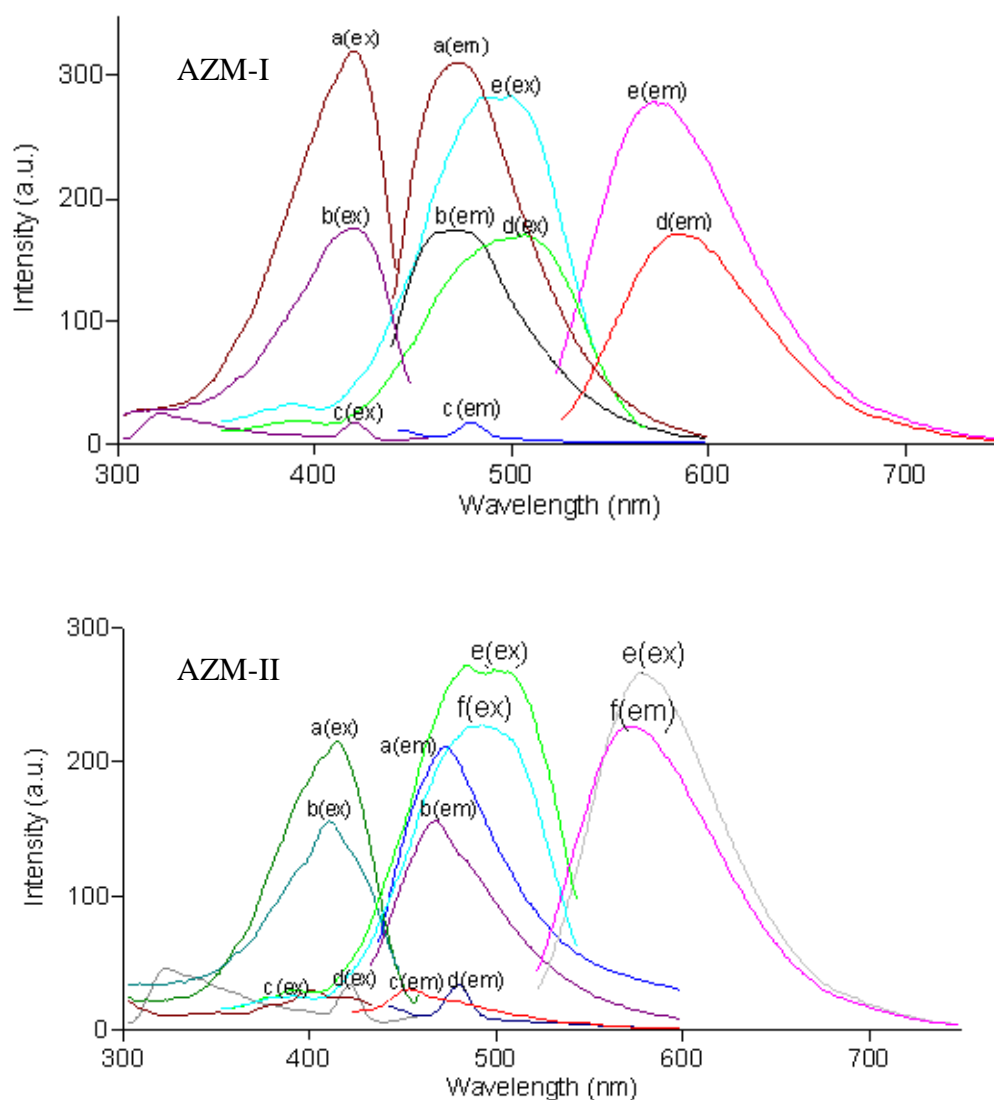


Figure 4.3 Excitation and corrected emission spectra of the AZM-I and AZM-II dyes (10^{-6} M dye or 2 mmol dye/kg polymer).

AZM-I: a) EtOH b) To: EtOH (80:20) c) THF d) PVC e) EC.

AZM-II: a) EtOH b) To: EtOH (80:20) c) DCM d) THF e) PVC f) EC.

The PVC-doped AZM-I and AZM-II displayed an enhancement in quantum yield (AZM-I, $\phi_F = 0.4290$; AZM-II, 0.4153), and a longer excitation wavelength (AZM-I, $\lambda_{ex} = 505$; AZM-II, $\lambda_{ex} = 510$ nm) compared with those measured in EtOH ($\phi_F = 0.0042$, $\lambda_{ex} = 422$ nm (See Table 4.3).

Red shift of absorption and emission of AZM-I and AZM-II is related to enhanced conjugation in immobilized polymer phase by hindrance of vibrational rotational motions. Increase observed in the Stoke's shifts ($\Delta\lambda_{ST}$) values of AZM-I dye is in the order of THF, Toluene: EtOH (80:20), EtOH solutions and PVC film; 44, 47, 53 and 85 nm, respectively. This is evidence of restricted vibrational rotational motions. Similar trends in Stoke's shifts values were also observed for AZM-II dye.

4.4.3 Acid–Base Behavior of the Schiff Bases

4.4.3.1 Acid–Base Behavior of the AZM Derivatives in Ethanol

The AZM derivatives contain available active centers for proton attacks. Possible protonation-deprotonation route and following electronic shifts of the AZM derivatives were shown in Figure 4.4. On the other hand the knowledge of acidity constants (pK_a) of AZM derivatives is of fundamental importance in order to provide information on chemical reactivity range of the dyes. For this reason, the absorption and emission based pH induced response of AZM-I and AZM-II were investigated in ethanol.

The representative fluorescence spectra of **AZM-I** in ethanol between pH 4.7 and 8.9 and related emission based sigmoidal response (pH versus $(I-I_0)/I_0$) were shown in Figure 4.5. pH measurements were performed with commercially available pH electrodes for non-aqueous media.

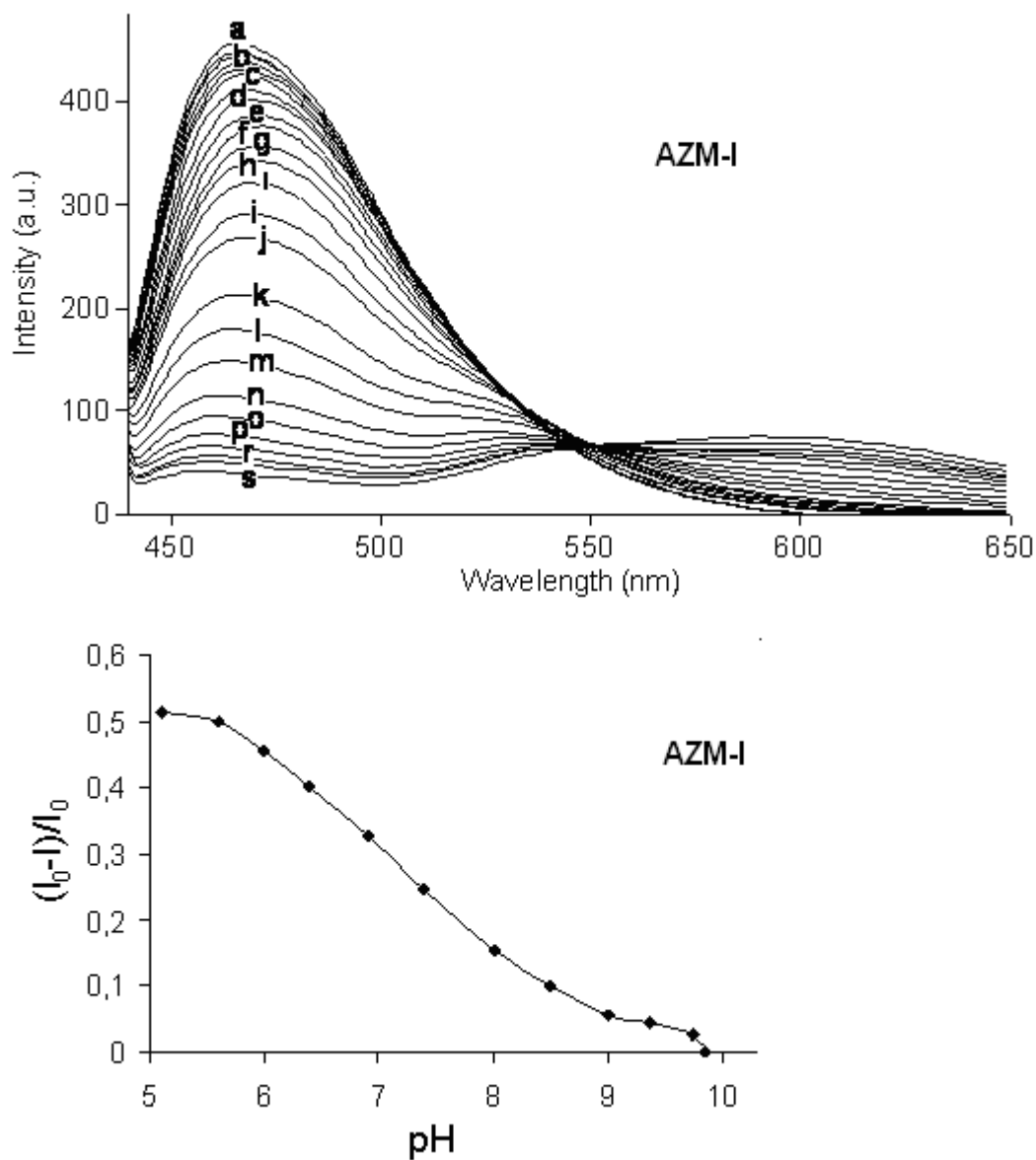


Figure 4.5.1 pH dependent emission spectra of 10^{-5} M AZM-I in EtOH between pH 8.9 and 4.7

a: pH = 8.98, b:8.62, c:8.27, d:8.12, e:7.80, f:7.67, g:7.47, h:7.18, i:7.02, j: 6.75, k: 6.38, l: 6.04, m:5.88, n:5.62, p:5.4 s: 4.7)

Excitation wavelength; 422 nm emission wavelength; 473 nm.

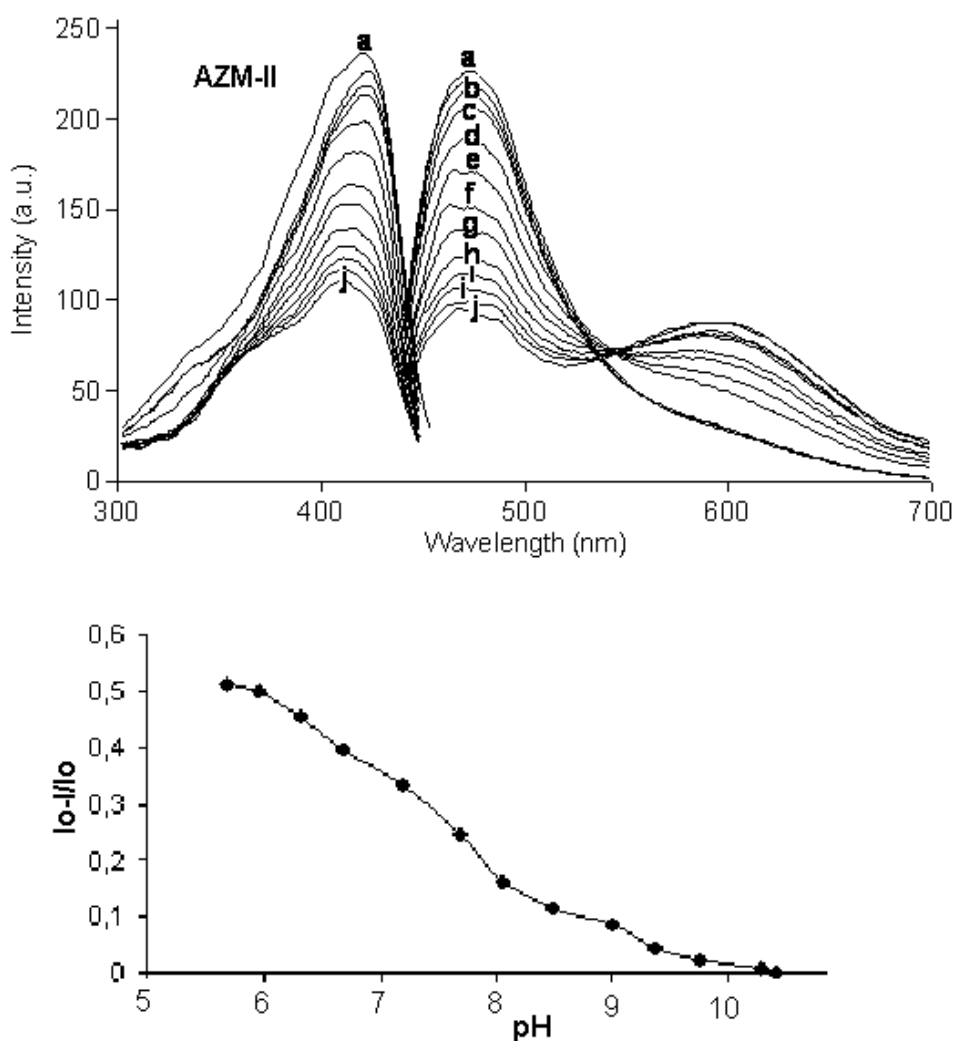


Figure 4.5.2 pH dependent emission spectra of 10^{-5} M AZM-I in EtOH between pH 9.40 and 5.32.

a) 9.40 b) 9.28 c) 8.75 d) 8.36 e) 8.00 f) 7.48 g) 7.06 h) 6.69 i) 6.20 j) 5.68 j) 5.32, at 473 nm.

The acidity constants were calculated via the following equation;

$$pK_a = \text{pH} + \log [(I_x - I_b)/(I_a - I_x)]$$

where I_a and I_b are the signal intensities of the dyes in their acid and conjugate base form respectively (Mills & Chang, 1992). The pK_a values were found to be 7.45 and 7.72 for AZM-I and AZM-II in ethanol, respectively. Since the employed dyes are nonsoluble in water, it is nearly impossible to assess their acid-base characteristics in known water-solvent systems and a known pH scale. It is a well known fact that, the

pH scale in nonaqueous media is governed by the autoprotolysis or autodissociation constant of the solvent.

Ethanol provides a pH scale between 0-20 ($K_0 = 10^{-19.8}$) where a pH less than 10 is acidic and a pH greater than 10 is basic. The calculated pKa values ranging from 7.45 to 7.42 reveal that the AZM dyes can measure the pH with a high resolution in near neutral region in ethanol.

Both of the AZM dyes exhibited a ratiometric but irreversible response to H^+ ions in the ethanol. Due to the observed irreversible response, the potential of AZM molecules as optical switches for the potential realization of artificial functions at the molecular level was not explained in the solution phase.

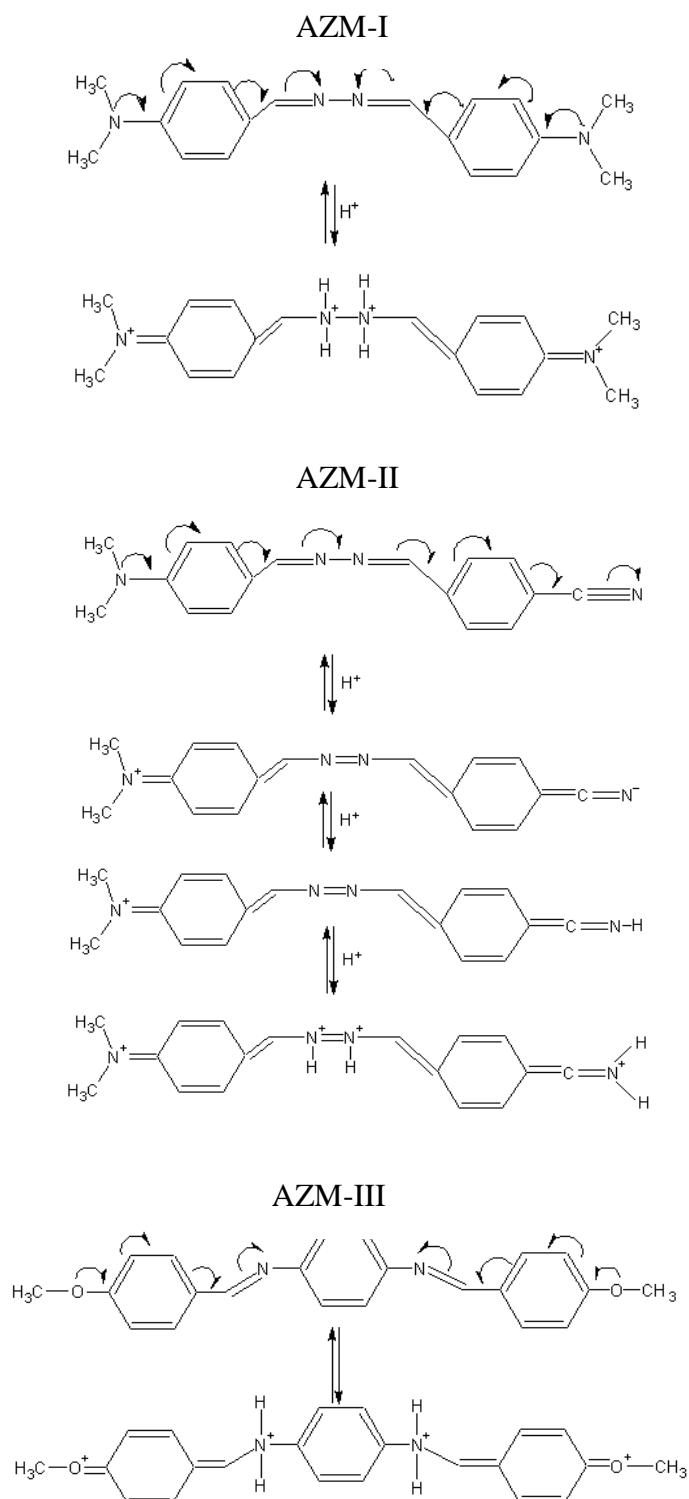
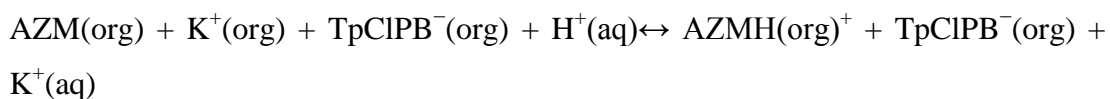


Figure 4.4 Protonation-deprotonation equilibria of Schiff bases;
AZM-I:4,4'-[hydrazine-1,2-dilidene]bis(N,N-dimethylaniline),
AZM-II:4-[(4-(dimethylamino)phenyl)methylidenehydrazono] methyl benzonitrile,
AZM-III:N,N'-bis-(4-metoxifenyl)methylidene-benzene-1,4-diamine

4.4.4 pK_a Calculations of AZM-I, AZM-II and AZM-III in PVC Matrix Acid–Base and Molecular Switch Behavior of The AZM Derivatives in PVC Matrix

Understanding of the switching behavior and indicator chemistry in solid-state is important to transfer the switching mechanisms to miniaturized molecule-based solid-state devices.

The AZM derivatives become reversibly working H⁺ selective molecular probes when doped into plasticized PVC together with the anionic additive; potassium tetrakis-(4-chlorophenyl) borate. In these systems, H⁺ ions are extracted into the optode membrane by the anionic additive, meanwhile, potassium ions diffuse from the membrane into the aqueous phase according to the mechanism of ion-exchange. The first-step of response mechanism of AZM derivatives can be explained by the following ion-exchange pathways. Following this; successive and fast protonation steps occur (See Figure 4.4).



Figures 4.6 and 4.7 reveal pH dependent absorption and emission response of PVC doped AZM-I and AZM-II upon exposure to solutions between pH 6.0-11.0.

Both of the dyes exhibited “S” shaped spectrophotometric titration curves with one inflection point. The pK_a values of AZM-I and AZM-II were found to be 9.08 and 9.11 in PVC, respectively. Stepwise protonation of inner azometine nitrogens are likely very close so one pK_a value found belong to these.

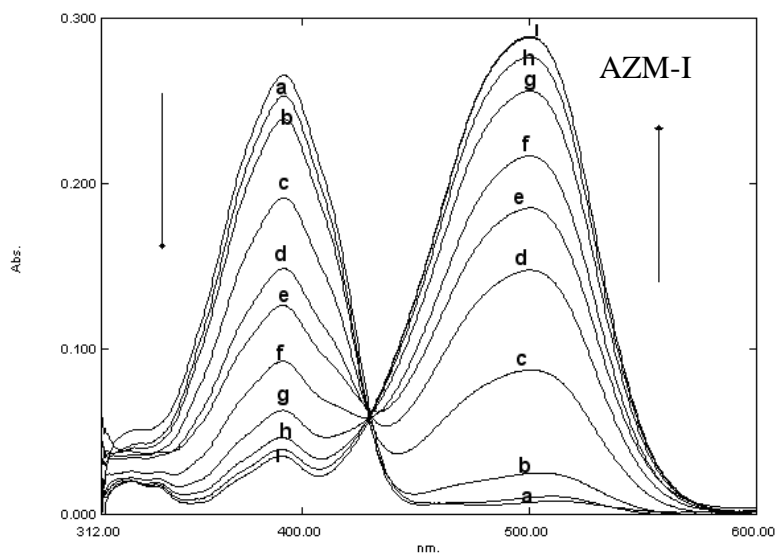


Figure 4.6 Absorption spectra of AZM-I in PVC after addition of acid solutions in the pH range of 6.00-11.00

pH: a) 11.00, 10.50, b) 10.00, c) 9.50, d) 9.00, e) 8.50, f) 8.00, g) 7.50, h) 7.00, i) 6.50, 6.00

Similarly, *competing protonation* of azometine and nitrile nitrogens of AZM-II and AZM-III results with one well shaped distinct inflection point (See Figure 4.7 and 4.8). The lack of a second observable inflection point for AZM dyes is attributable to *rapid protonation*-deprotonation equilibria.

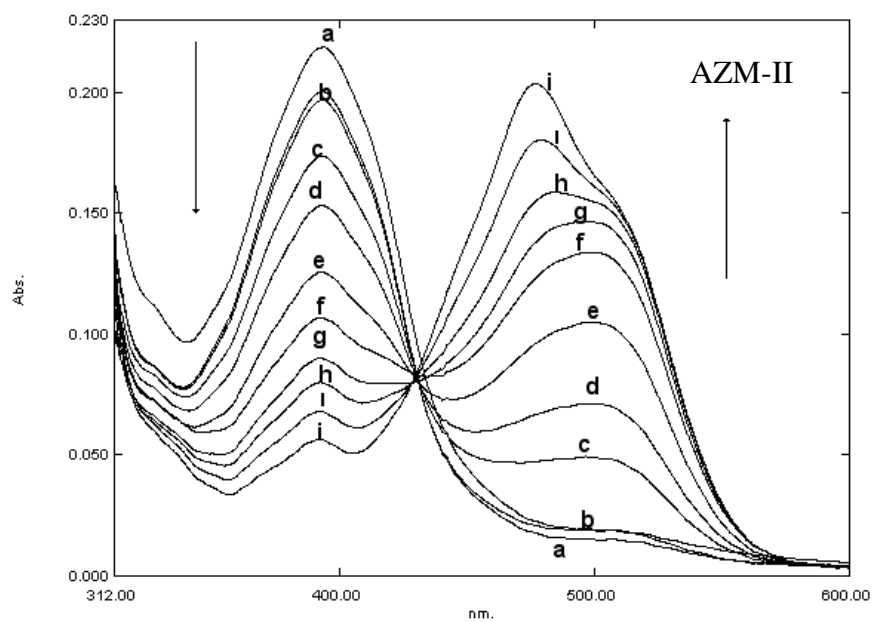


Figure 4.7 Absorption spectra of AZM-II in PVC after addition of acid solutions in the pH range of 6.00-11.00

pH: a) 11.00 b) 10.50, 10.00 c) 9.50 d) 9.00 e) 8.50 f) 8.00 g) 7.50 h) 7.00 i) 6.50 i) 6.00

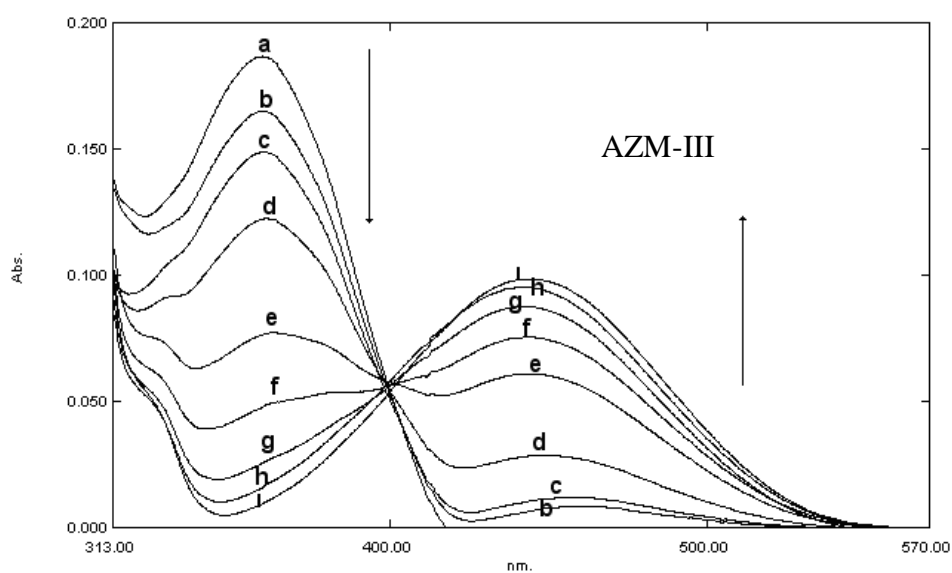


Figure 4.8 Absorption spectra of AZM-III in PVC after addition of acid solutions in the pH range of 6.00-11.00

pH: a) 11.00, b) 10.00, c) 9.50, d) 9.00, e) 8.50, f) 8.00, g) 7.50, h) 7.00, i) 6.00

Figures 4.9 and 4.10 reveal emission based spectral response of AZM dyes in PVC matrix. Due to the observed reversible response, the potential of AZM-I and AZM-II molecules as optical switches at the molecular level was evaluated. The optical and chemical inputs addressing the AZM derivatives modulate the absorption and emission intensities of the molecules. Relying on these operating principles, we have reproduced the functions of regarding logic circuits.

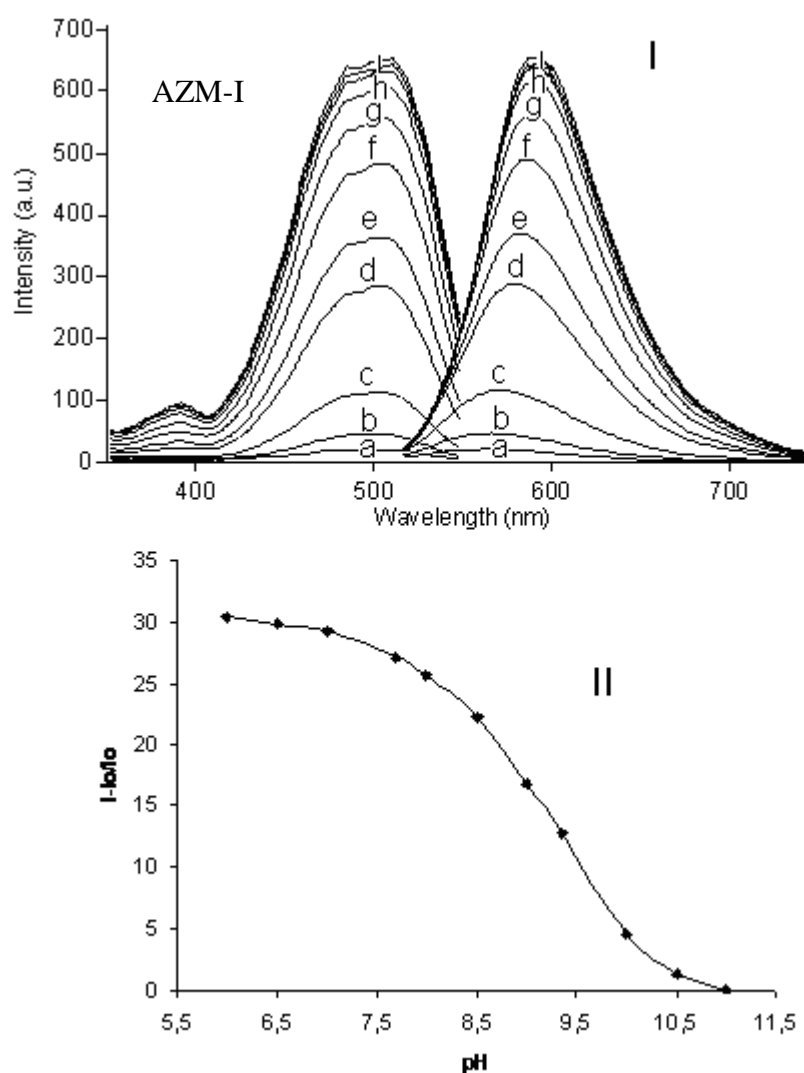


Figure 4. 9 **I**: pH induced emission based spectral response of the PVC doped AZM-I in the pH range of 6.00-11.00. pH: a) 11.00, b) 10.50, c) 10.00, d) 9.50, e) 9.00, f) 8.50, g) 8.00, h) 7.50, i) 7.00, 6.50, 6.00

II: Emission based sigmoidal response of AZM-I to pH.

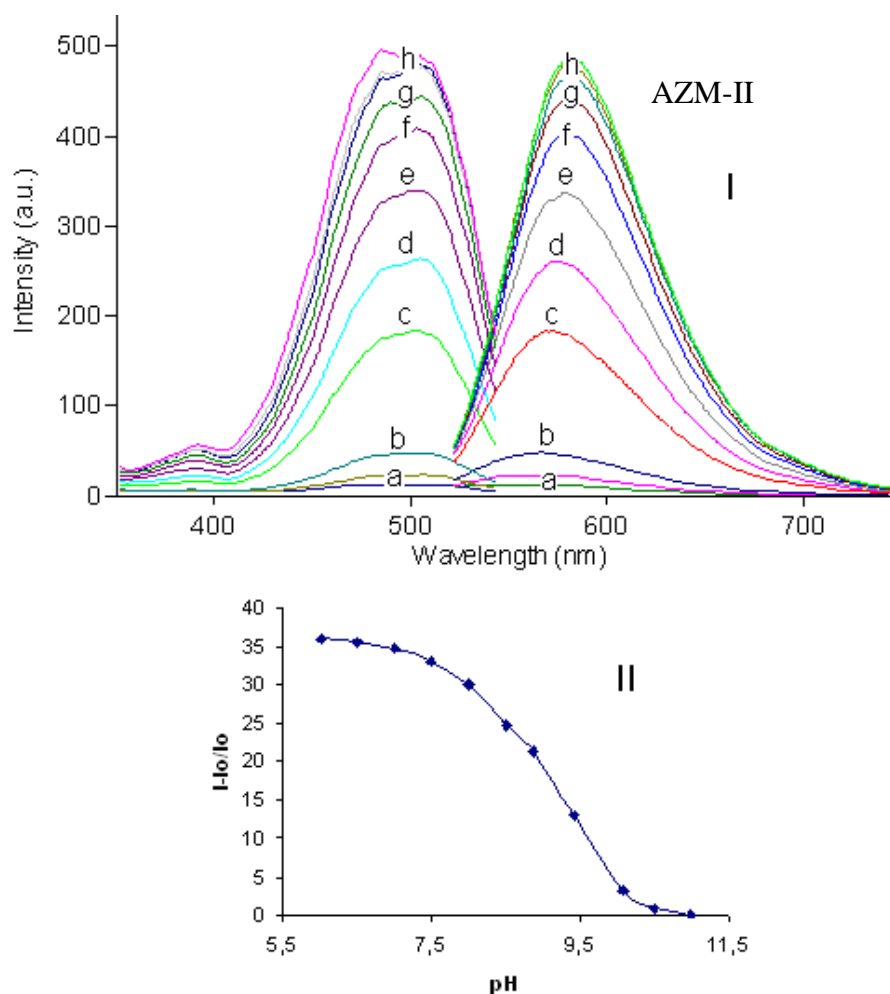


Figure 4.10 **I:** pH induced emission based spectral response of the PVC doped AZM-II in the pH range of 6.00-11.00. pH: a) 11.00, 10.50 b) 10.00 c) 9.50 d) 9.00 e) 8.50 f) 8.00 g) 7.50, h) 7.00, 6.50, 6.00

II: Emission based sigmoidal response of AZM-II to pH.

Figures 4.11 and 4.12 reveal the optical and chemical inputs and absorption/emission based switching principles of PVC doped AZM dyes.

Under the influence of a chemical input (varying pH between 6.0-11.0) AZM-I yielded two different optical outputs; an increasing absorption intensity upon protonation at 500nm and a decreasing absorption intensity at 392 nm. The spectroscopic output at 500 nm switches to a high value when the concentration of H^+ (chemical input) is high (**1**) (See Figure 4.11-a). It reverts to a low value when the concentration of H^+ is low (**0**). In a contrast manner, the spectroscopic output at 392

nm switches to a high value when the concentration of H^+ is low (**1**) and a low value when the H^+ is high (**0**).

Molecular switch behavior of AZM-II is very similar (See Figure 4.12-b) and the both logic gates shown in Figure 4.11 can be concluded as “NOT” gates or “inverter” gates.

Figure 4.12 a and b, reveal excitation-emission based molecular switch behavior of PVC doped AZM-I and AZM-II respectively. Under the influence of two different inputs (a chemical input; varying pH between 6.0-11.0 and an optical input; excitation at 505 nm) AZM-I exhibited two different optical outputs; a varying emission intensity at 590 nm and an excitation intensity at 505 nm (See Fig 4.7 and Fig 4.9). The spectroscopic output at 590 nm switches to a high value when the pH is in the range of 6.0-7.5 (**1**). (See Figure 4.12-a). It reverts to a low value when the pH is in the range of 10.0-11.0 (**0**). The 0 and 1 positions of the spectroscopic output observed at 505 nm were parallel to the responses of the output of 590nm. Except that of slight changes observed in the excitation/ emission wavelengths or relative signal changes, the switch behavior of the AZM-II in PVC was parallel to the AZM-I. Both logic gates shown in Figure 4.12 can be concluded as “NOT AND” gates.

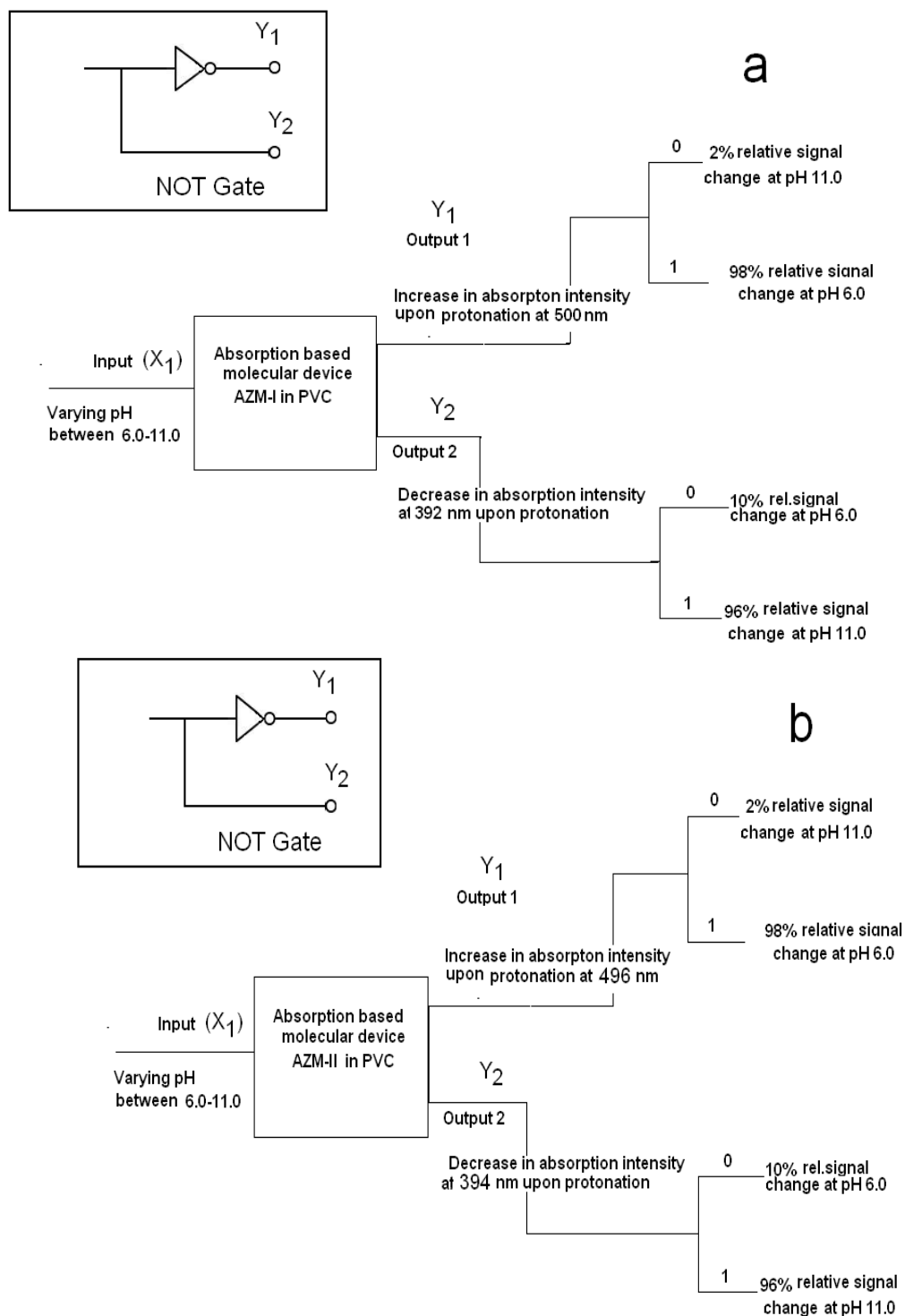


Figure 4.11 Modulation of the absorption intensities of PVC doped molecular devices; AZM-I and AZM-II by chemical inputs and their operating principles.

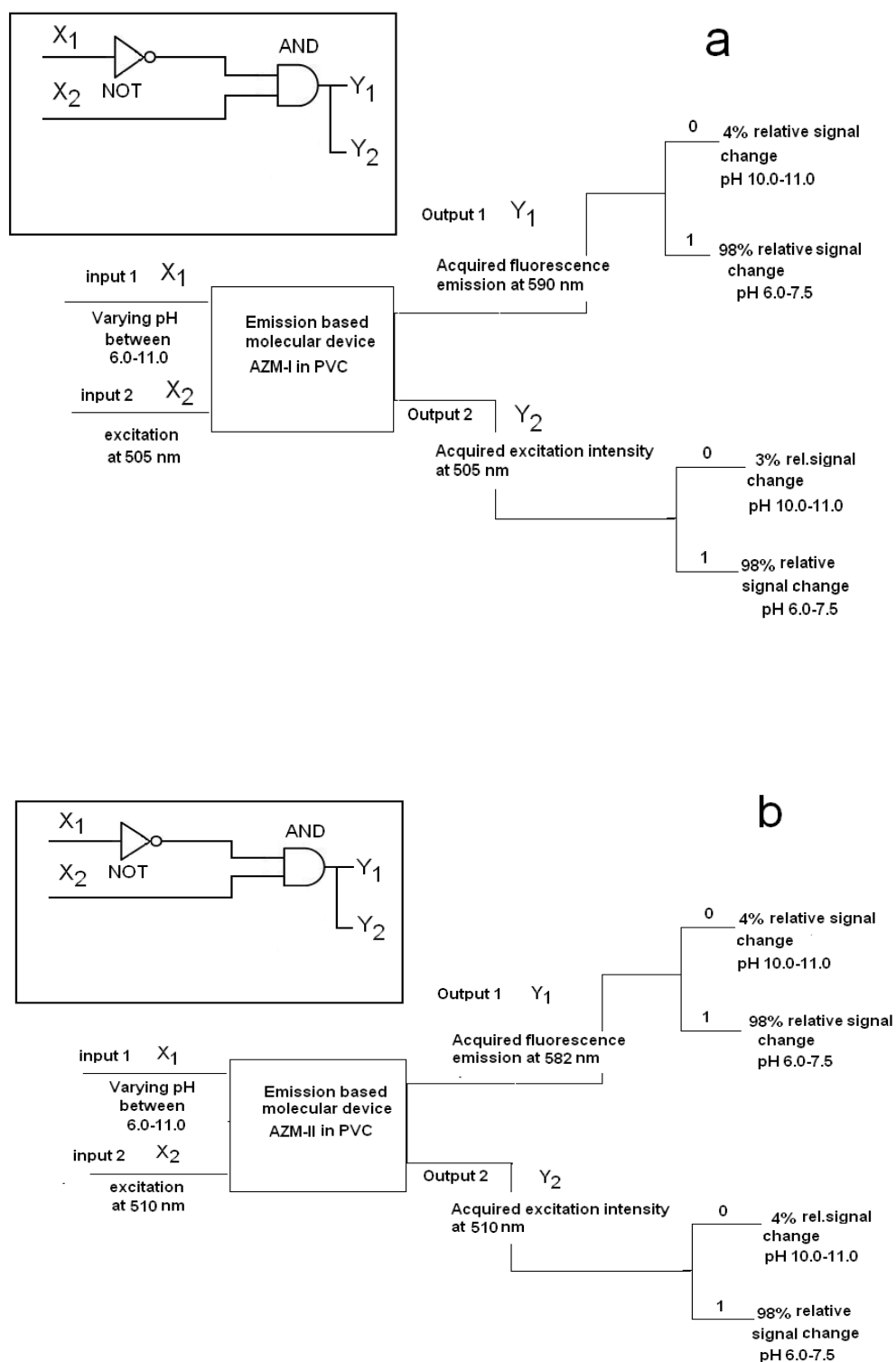


Figure 4.12 Modulation of the emission intensities of PVC doped molecular devices; AZM-I and AZM-II by chemical and optical inputs and their operating principles.

As a result, a chemical input or a combination of chemical and optical inputs can modulate an optical output on the basis of ion exchange dependent protonation-deprotonation equilibrium. These processes can be monitored by visible absorption or emission spectroscopy, following the absorbance/emission changes associated with the bands of the protonated and deprotonated forms. Furthermore, photoinduced protonation –deprotonation reactions, are fast enough and equilibrium state can be established within minutes in the employed solid matrices. These results demonstrate that such simple reactions can be coupled with solid state optics and with microfluidics to transduce incoming chemical inputs to well-defined spectroscopic outputs.

4.4.5 Acid–Base and Molecular Switch Behavior of the AZM Derivatives in EC Matrix

The AZM dyes exhibited very similar absorption and emission based spectral response to proton ions when doped into EC matrix. The EC doped AZM-I and AZM-II exhibited a parallel increase both in emission and excitation intensity after exposure to different concentrations of solutions in the pH range of pH=6.00-11.00. In EC doped films the pK_a values of AZM-I and AZM-II were found to be 7.74 and 7.51, respectively. Figure 4.13 and 4.14 show pH induced emission / excitation based spectral response of the EC doped AZM dyes in the pH range of 6.00-11.00. The similarities of spectral response of AZM dyes to pH in PVC and EC can easily be understood from a comparison of Figure 4.9 and 4.10 with Fig. 4.13 and 4.14. Molecular switch behaviors of AZM-I and AZM-II in EC are very close to the behaviors observed in PVC. Same logic gate schemes were obtained for EC doped AZMs. However, they are not shown in this chapter.

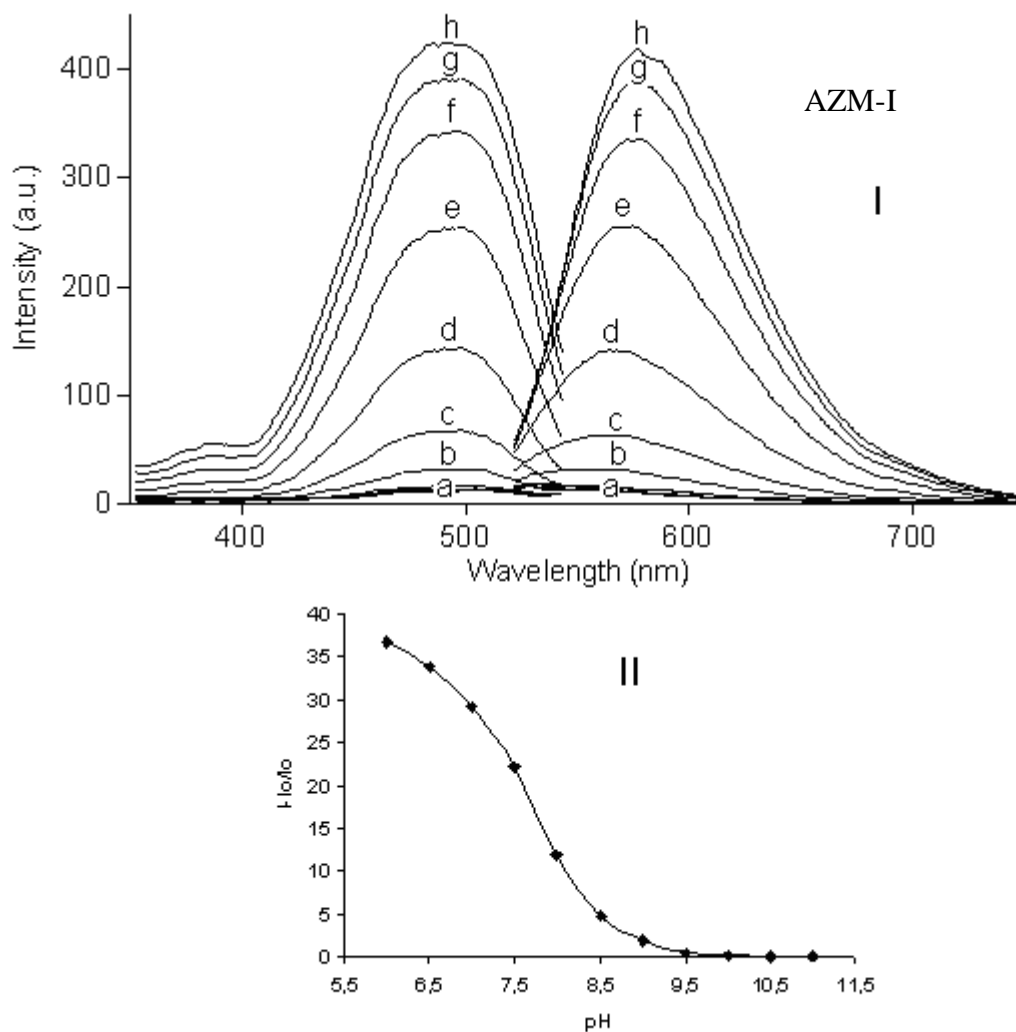


Figure 4.13 **I**: pH induced emission based spectral response of the EC doped AZM-I in the pH range of 6.00-11.00. pH: a) 11.00, 10.50, 10.00, 9.50 b) 9.00 c) 8.50 d) 8.00 e) 7.50 f) 7.00 g) 6.50 h) 6.00

II: Emission based sigmoidal response of AZM-I to pH.

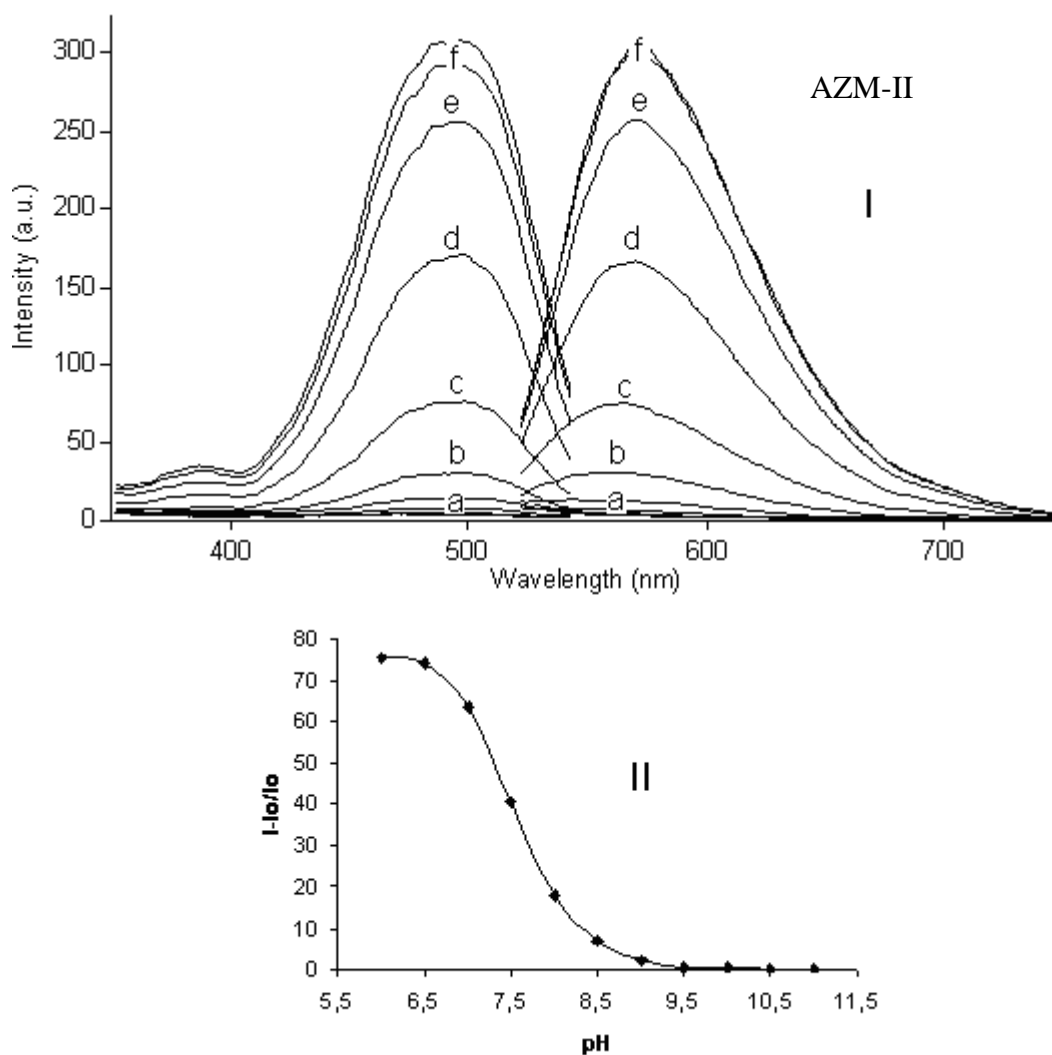


Figure 4.14 **I**: pH induced emission based spectral response of the EC doped AZM-II in the pH range of 6.00-11.00.

pH: a) 11.00, 10.50, 10.00, 9.50, 9.00 b) 8.50 c) 8.00 d) 7.50 e) 7.00 f) 6.50, 6.00

II: Emission based sigmoidal response of AZM-II to pH.

4.4.6 Reproducibility of the Response

The sensing slides were found to give reversible and reproducible results on absorption and fluorescence emission measurements when pH was varied within the dynamic working range. The response of PVC and EC doped AZM-I and AZM-II to pH was investigated in buffered solutions. Regeneration was accomplished with concentrated buffer solutions at opposite pH values. Figure 4.15 shows the relative

signal change, and reversibility performance of the PVC doped AZM-I and AZM-II. The EC doped dyes exhibited very similar response to pH.

The reproducibility of the AZM-I was assessed by repeatedly introducing a sample of pH 11.0 and 6.0. The AZM-I was found to reach 90% of the signal intensity (τ_{90}) within 1.0–3.0 min. between the first and third cycles, the level of reproducibility of the upper signal level was quite good with a S.D. of 280 ± 2 . The reproducibility performance of AZM-II was also quite good except that the relatively longer response times in the alkaline region (See Figure 4.15).

The response time can be improved by adjusting the film thickness of sensing slides and flow rate of buffer solutions. In our case, film thickness was found to be approximately 5 μm . The film thickness can be reduced and shorter response times can be reached.

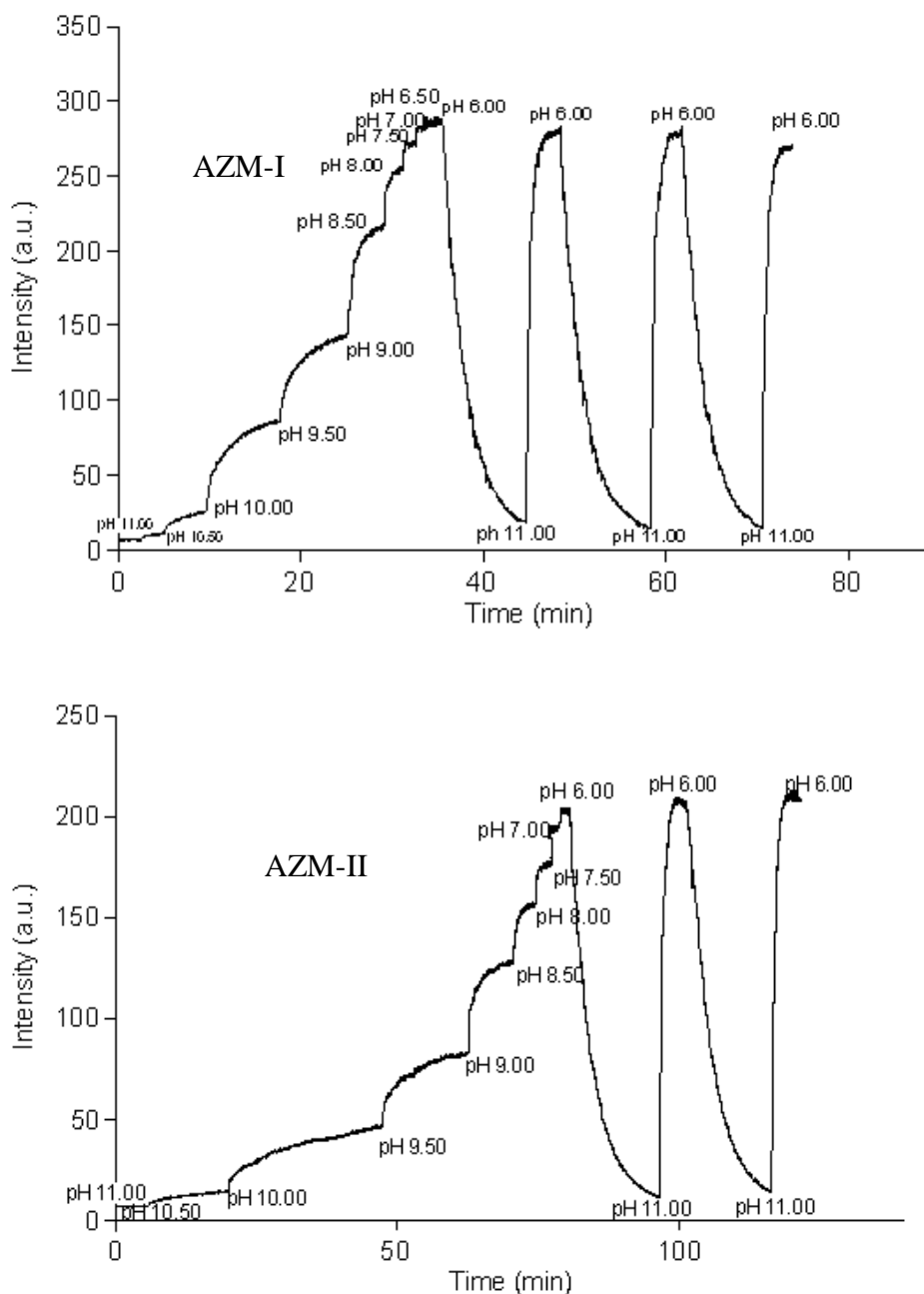


Figure 4.15 Response curve and regeneration performance of PVC doped AZM-I and AZM-II. Data were acquired with fiber optic probe which is in contact with flow system.

4.4.7 Cross Sensitivity to Acidogenic Species, Anions, Metal Cations and Effect of Ionic Strength

The reaction of the indicator with CO_2 is reversible but the reaction with more acidic species such as volatile organic acids is not. Hence the sensor will be poisoned. This is also true for even more acidogenic species such as SO_2 and NO_x .

Here, the advantage of Teflon coating has been used in order to increase the selectivity for carbon dioxide. As mentioned earlier the Teflon membrane is permeable for non-polar gaseous but impermeable for polar molecules and ionic species. During gas sensing studies the teflon coated films were used. However, in pKa calculations and acid titrations the non-coated films were employed.

In order to investigate the interference effects of other anions on fluorescence intensities at 590 and 582 nm in the presence of NO_3^- , ClO_4^- , AcO^- , $\text{C}_2\text{O}_4^{2-}$ and SO_4^{2-} were tested with 10^{-3} M solutions of the anions in separate solutions for both of the dyes. The cross-sensitivities of the AZM dyes to Na^+ , K^+ and many polyvalent metal ions (Zn^{2+} , Hg^+ , Hg^{2+} , Sn^{2+} , Ca^{2+} , Bi^{3+} , Ni^{2+} , Co^{2+} , Cu^{2+} , Pb^{2+} , Al^{3+} , Cr^{3+} , Mn^{2+} , Fe^{2+} and Fe^{3+}) were also investigated in phosphate or acetic acid/acetate buffered solutions at pH 7.0 or pH 5.5.

Results were evaluated in terms of relative signal changes (RSC); $(I - I_0)/I_0$, where I was the fluorescence intensity of the sensing membrane after exposure to ion-containing solutions and I_0 is the fluorescence intensity of the sensing slide in ion-free buffer solution. Only the HCO_3^- , induced fluorescence bands of AZM dyes exhibiting a RSC ratio of 80%.

The fluorescence was dramatically quenched in presence of Hg^{2+} and Ag^+ at 590 nm exhibiting a RSC ratio of 76% and 70%. Other alkali, alkaline earth, and transition metal ions produced insignificant responses where RSCs ranged from 0.02 to 0.28.

The effect of ionic strength on the PVC doped AZM derivatives was tested in 135mM NaCl containing 5.0×10^{-3} M phosphate buffer which covers the physiologically important salinity level. The pKa values of PVC doped AZM-I and AZM-II were found to be 9.35 ± 0.07 and 9.17 ± 0.04 , respectively. In clinically important salinity levels, the pKa of AZM-I exhibited an increase of 0.27 pKa units with respect to its original value but the pKa of AZM-II was not affected.

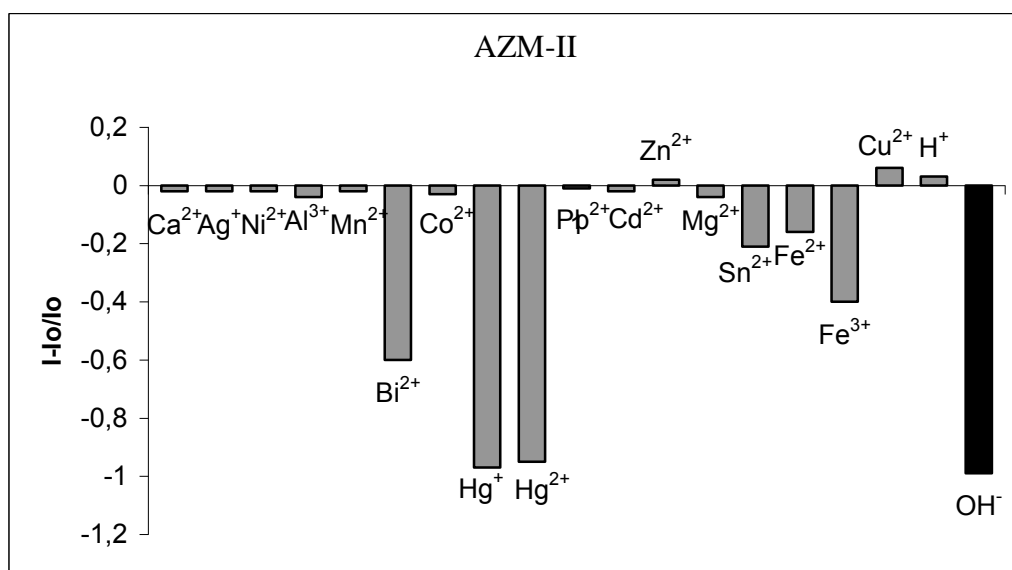
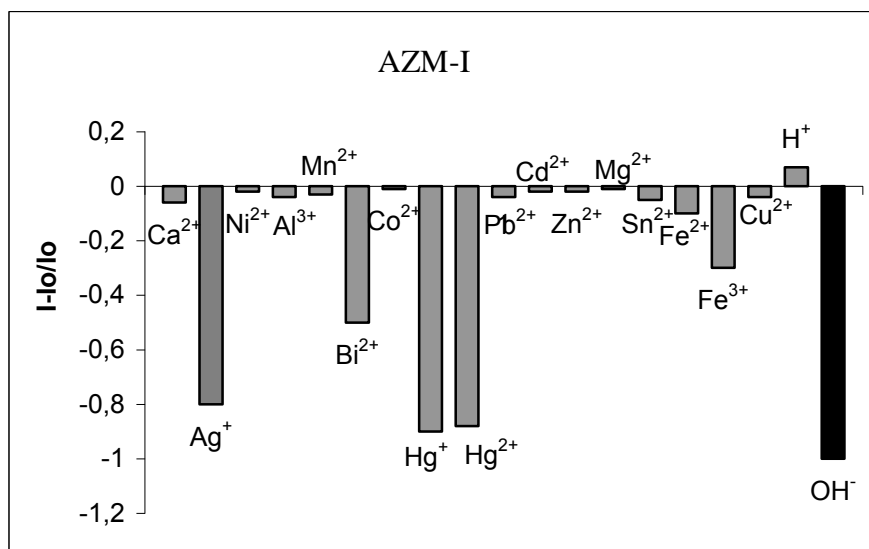


Figure 4.16 Metal-ion response test for AZM-I and AZM-II. Results are plotted as relative fluorescence changes, $(I - I_o)/I_o$, where I is the fluorescence intensity of the sensor membrane after exposure to ion-containing solutions and I_o is the fluorescence intensity of the sensor slide in ion-free buffer solution.

4.5 Conclusion

There are only a limited number of fluorescent “proton driven” molecular switches available covering the neutral-alkaline pH region. We demonstrate that, the AZM derivatives; with fast switching speeds; contain available active centers for proton attacks and are appropriate for use as fluorescent pH probes between pH 6.0–11.0. The pK_a values of 7.74 and 7.51 and large dynamic working range make the EC-doped AZM molecules promising indicators for dissolved CO_2 sensing in environmental and physiological samples. The compatibility of the employed molecules with the solid-state optical components (in particular LED’s emitting in the wavelength range of 500–510 nm) and fiber optics can be useful in construction of inexpensive and miniaturized field available instrumentation. The most notable source of interference to the pH sensitivity of AZM-I and AZM-II is the quenching of the excited state by the cations of Hg^{2+} , Bi^{3+} and Ag^+ at neutral or slightly acidic pHs.

CHAPTER FIVE

DISSOLVED CO₂ STUDIES IN IONIC LIQUID AND ETHYL CELLULOSE MATRIX

5.1 Experimental Studies

In this chapter the schiff bases AZM-I and AZM-II were investigated for dissolved CO₂ (HCO₃⁻) analysis in RTIL.

Sensing cocktails were prepared by dissolving the indicator dye in ionic liquid moiety. Cocktails contain 0.015 mg of indicator dye in 1mL of ionic liquid (1-ethyl-3-methylimidazolium tetrafluoroborate). Responses of indicator dyes (AZM-I and AZM-II) were obtained with and without additives. Cocktail compositions were given in Table 5.1. The AZM-II dye exhibited better response for dissolved CO₂ in RTIL with respect to AZM-I. Therefore, for further studies we focused on AZM-II dye.

Table 5.1 Cocktail compositions for CO₂ analysis.

Compound	Cocktail no	Additive
AZM-I	CC-1	No additive
AZM-II	CC-2	No additive
AZM-II	CC-3	3 µl 1 M TBAOH
AZM-II	CC-4	Perfluoro compound

5.2 Synthesis of the AZM-I, AZM-II

The Schiff bases (4,4'-[hydrazine-1,2-dilidendimethylidene]bis(N,N-dimethylaniline), AZM-I) and (4-[(4-(dimethylamino)phenyl)methylidene hidrazono]methyl benzonitrile, AZM-II) were employed through the studies. Their chemical structures and identification were given in chapter four. Schematic structure of the employed RTIL is shown in Figure 5.1.

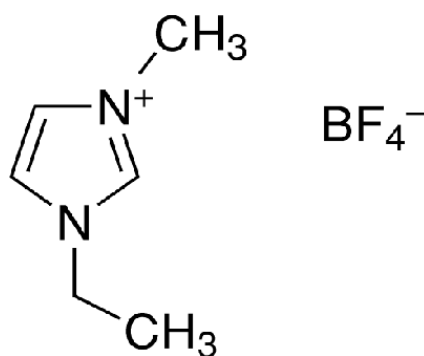
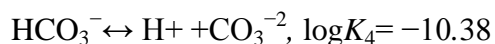
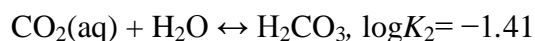
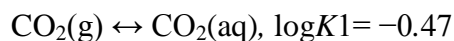


Figure 5.1 Schematic structure of the employed RTIL.
1-ethyl-3-methylimidazolium tetrafluoroborate

5.3 Dissolved CO₂ Sensing Studies

Standard solutions were prepared freshly from a 1M NaHCO₃ stock solution prior to the measurements. Dilute solutions of sodium hydrogen carbonate were used to form dissolved CO₂ calibration graphs. CO₂-free standard solutions were prepared with doubly distilled water after boiling, bubbling with nitrogen, and kept in closed containers. Concentrations were calculated by using the following equations, where K_1 and K_2 are referred to the dissolution equilibrium constant of gaseous CO₂ in water and the equilibrium constant of carbonic acid formation, respectively. K_3 and K_4 are the first and second acid dissociation constants of the carbonic acid (Mills, Chang & McMurray, 1992).



In a HCO₃⁻ solution, the relationship between the partial pressure of dissolved CO₂(g) (P_{CO_2}) and proton concentration is as follows:

$$\alpha P_{CO_2} = [H_2CO_3] = \frac{([H^+]^3 + [H^+]^2[Na^+] - K_w[H^+])}{K_3([H^+] + 2K_4)}$$

where $\alpha = K_1K_2[H_2O]$,

K_w is the water dissociation constant and $[Na^+]$ is the concentration of sodium ions present.

Five microlitre portions of standard solutions of $NaHCO_3$ were added into the sensing agent containing cuvette and sonicated for 10 s. The change in fluorescence due to addition of different concentrations of dissolved CO_2 was measured. The time when 90% equilibrium was reached (τ_{90}) was recorded as the response time. All the experiments were carried out at room temperature of 25 ± 1 °C.

5.4 Results and Discussion

5.4.1 Spectral Evaluation, Interpretation of the Emission Spectra

The effect of the ionic liquid on CO_2 sensitivity was examined for employed dyes. The RTIL provides an increased solubility for CO_2 in the test environment. Gas molecules are believed to occupy ‘molecular cavities’ within ionic liquids. 10 to 20 times higher solubilities were reported for CO_2 in water miscible ionic liquids than that of in conventional solvents, polymer matrices, or water. Hydration of CO_2 and subsequent protolysis is also essential for the functionality of the optical CO_2 sensors (Mills and et al., 1992; Stumm & Morgan, 1981) In the light of the literature information the Schiff bases; AZM-I and AZM-II were excited at 510 / 505 in RTIL respectively. Figure 5.2 shows emission spectra of the employed dyes in RTIL. The dyes exhibited a little bit red shifted (5 nm), but similar excitation and emission wavelengths to EC (See Table 4.3).

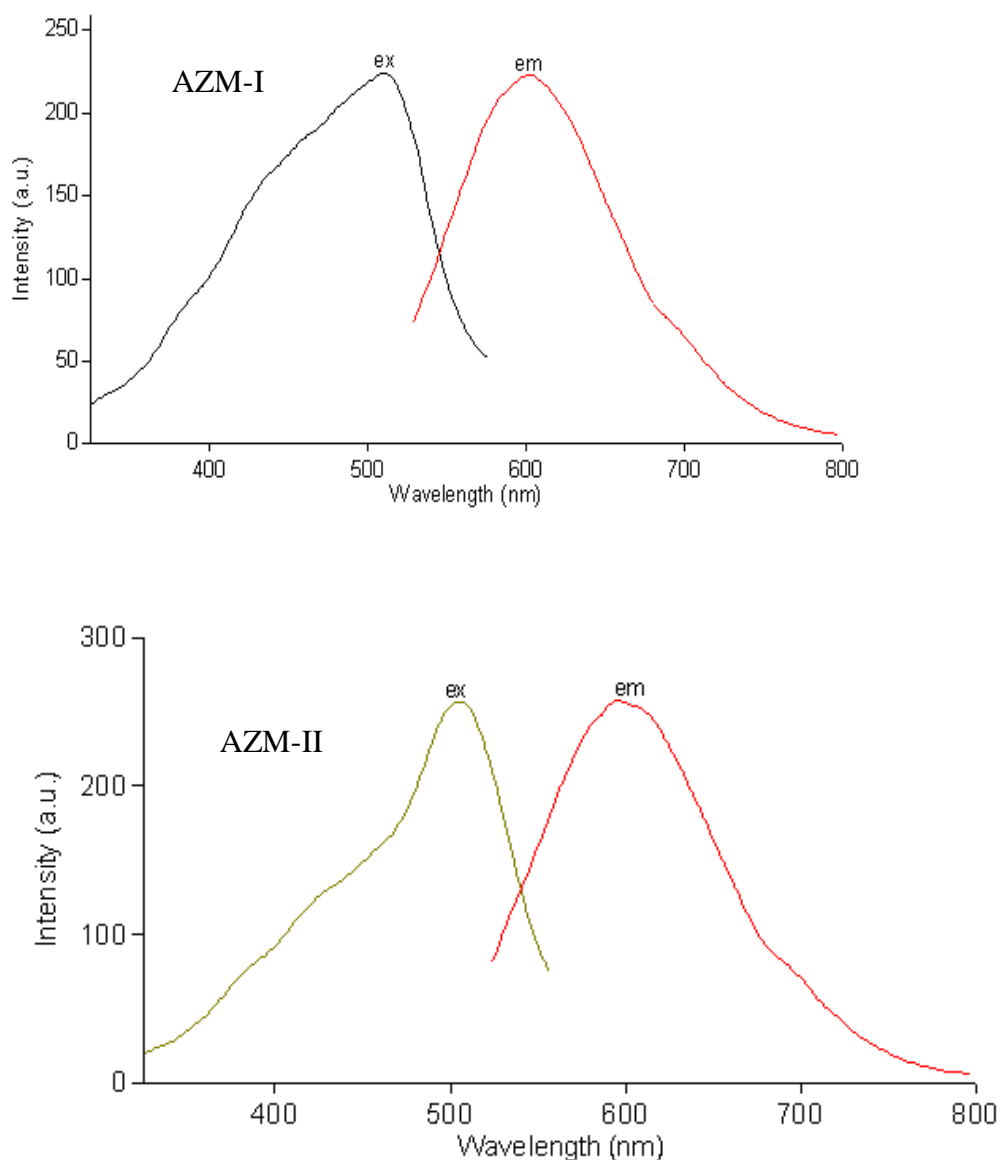


Figure 5.2 Excitation and corrected emission spectra of the **AZM-I** and **AZM-II** dyes

AZM-I: AZM-I I in RTIL.

AZM-II: AZM-II I in RTIL.

Figure 5.3 shows the emission spectra and related calibration curve of the AZM-I dye in RTIL after addition of HCO_3^- solutions in the concentration range of 2.0×10^{-6} to $10.4 \times 10^{-4} \text{ mol L}^{-1}$. From Figure 5.3 the linear calibration plot of $y = -0.1469x + 1.2872$ and regression coefficient of $R^2 = 0.9838$ can be seen. The slope of the plot is not satisfactory.

Figure 5.4 and 5.5 show spectral performances of CC-2 and CC-3 after exposure to HCO_3^- solutions in the concentration range of 2.0×10^{-6} to $74.0 \times 10^{-4} \text{ mol L}^{-1}$, respectively. Both the cocktails of CC-2 and CC-3 did not exhibit significant linear calibration plots for dissolved carbon dioxide sensing.

However, the additive containing AZM-II dye exhibited better response to dissolved CO_2 with respect to AZM-I yielding enhanced slope and R^2 values (See Figure 5.6).

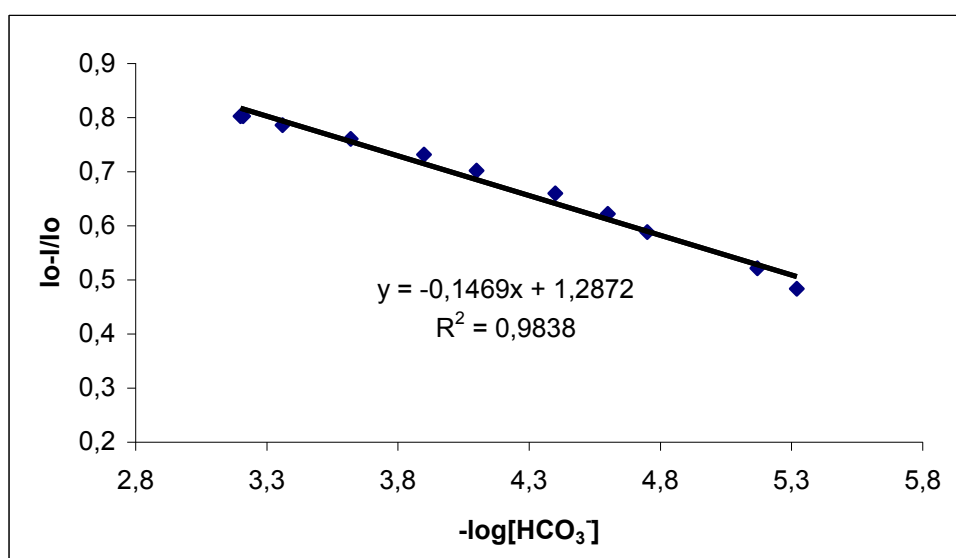
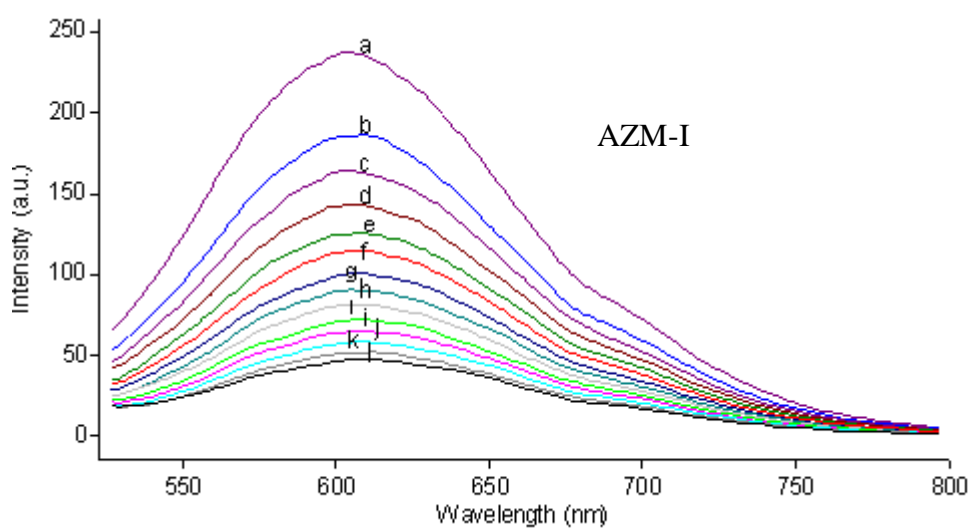


Figure 5.3 Emission spectra of immobilized AZM-I in RTIL after exposure to different HCO_3^- concentrations [CC-1].

- a) 0 M; b) 2.00×10^{-6} M; c) 3.20×10^{-6} M; d) 4.40×10^{-6} M; e) 5.60×10^{-6} M; f) 6.80×10^{-6} M;
 g) 1.88×10^{-5} M; h) 2.28×10^{-5} M; i) 3.48×10^{-5} M; j) 4.68×10^{-5} M; k) 1.20×10^{-4} M;
 l) 4.40×10^{-4} M; m) 6.40×10^{-4} M, 10.4×10^{-4} M

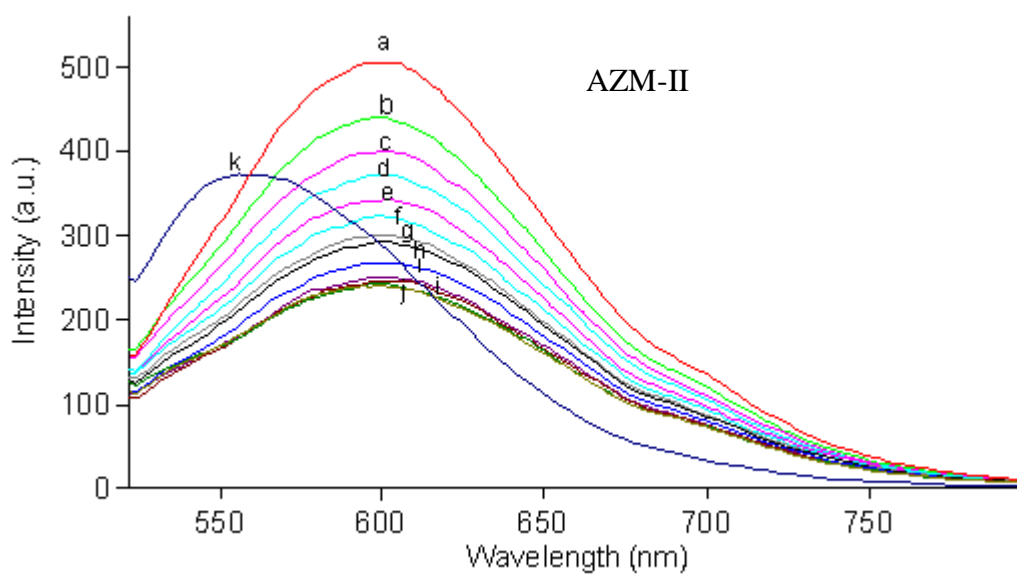


Figure 5.4 Emission spectra of immobilized AZM-II in RTIL after exposure to different HCO_3^- concentrations [CC-2].

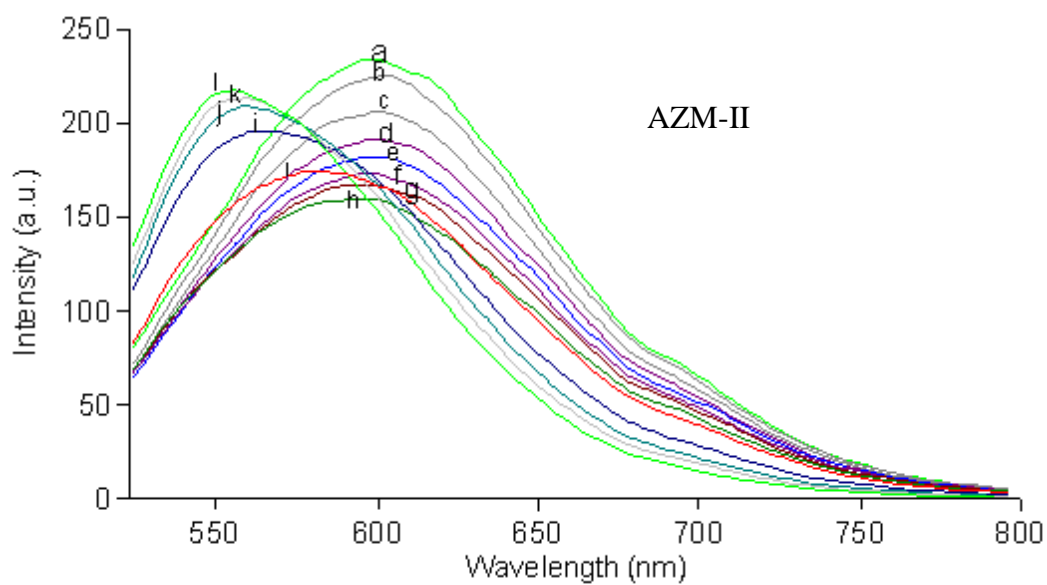


Figure 5.5 Emission spectra of immobilized AZM-II in RTIL after exposure to different HCO_3^- concentrations [CC-3].

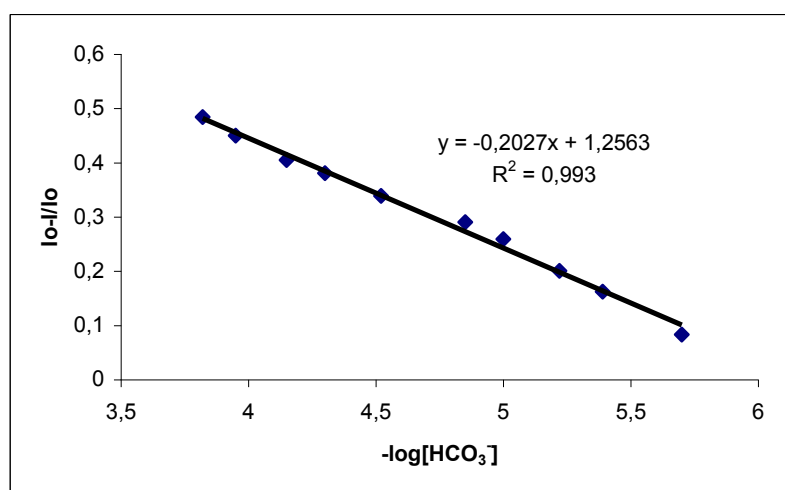
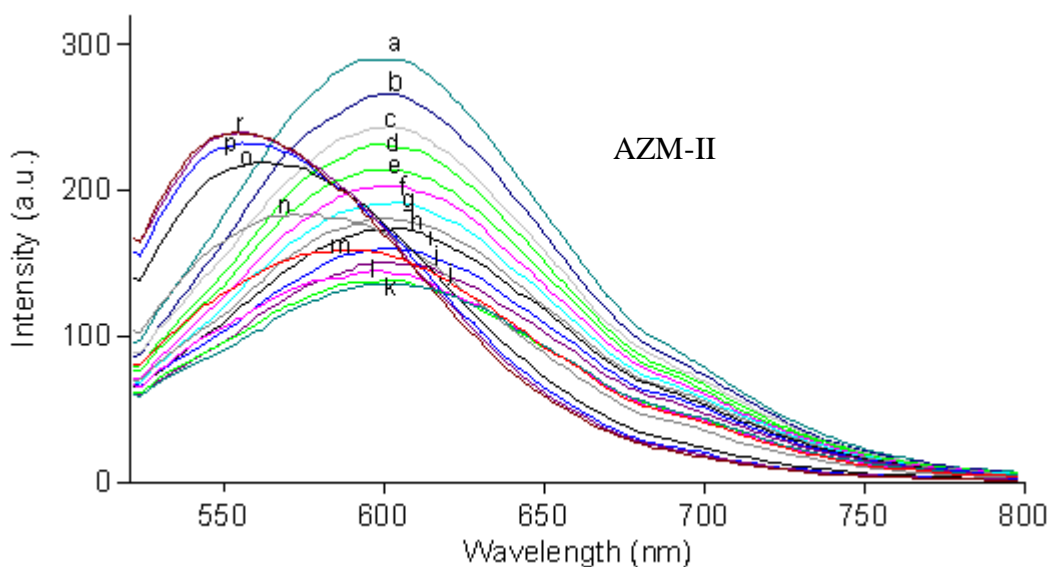


Figure 5.6 Emission spectra of immobilized AZM-II in RTIL after exposure to different HCO_3^- concentrations [CC-4].

a) 0 M; b) 2.00×10^{-6} M; c) 4.00×10^{-6} M; d) 6.00×10^{-6} M; e) 8.00×10^{-6} M;
 f) 1.00×10^{-5} M; g) 3.00×10^{-5} M; h) 5.00×10^{-5} M; i) 7.00×10^{-5} M;
 j) 1.10×10^{-4} M; j) 1.50×10^{-4} M; k) 7.40×10^{-4} M

Figure 5.7 and 5.8 show emission spectra of EC doped AZM dyes after exposure to different HCO_3^- concentrations. Both dyes exhibited well shaped and linear response for dissolved carbon dioxide in the concentration range of 1.33×10^{-6} to 2.26×10^{-4} and 1.73×10^{-5} to 1.08×10^{-3} for AZM-I and AZM-II, respectively.

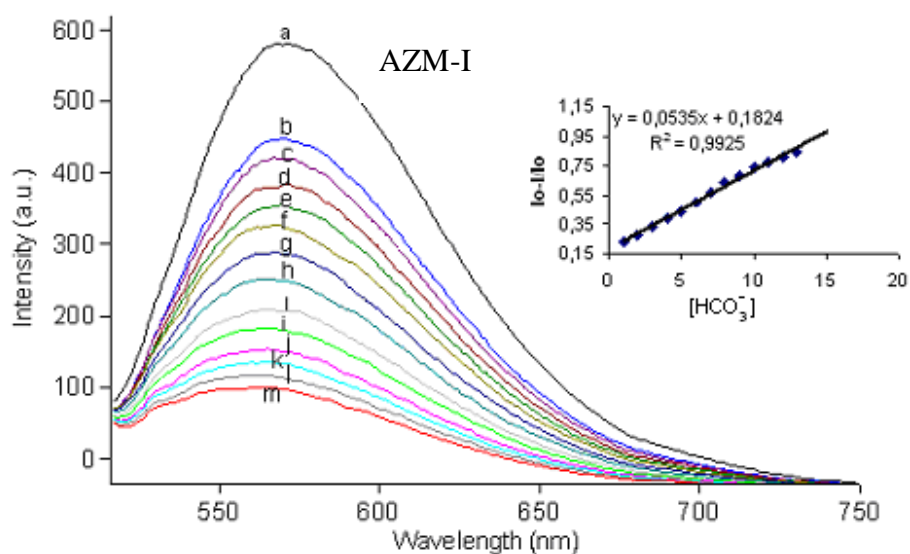


Figure 5.7 Emission spectra of immobilized AZM-I in EC matrix after exposure to different HCO_3^- concentrations.

a) 0 M; b) 1.33×10^{-6} M; c) 2.80×10^{-5} M; d) 9.33×10^{-5} M; e) 1.60×10^{-4} M; f) 2.26×10^{-4} M; g) 2.93×10^{-4} M; h) 3.60×10^{-4} M; i) 4.27×10^{-4} M; j) 4.93×10^{-4} M; k) 5.60×10^{-4} M; l) 6.27×10^{-4} M; m) 6.93×10^{-4} M.

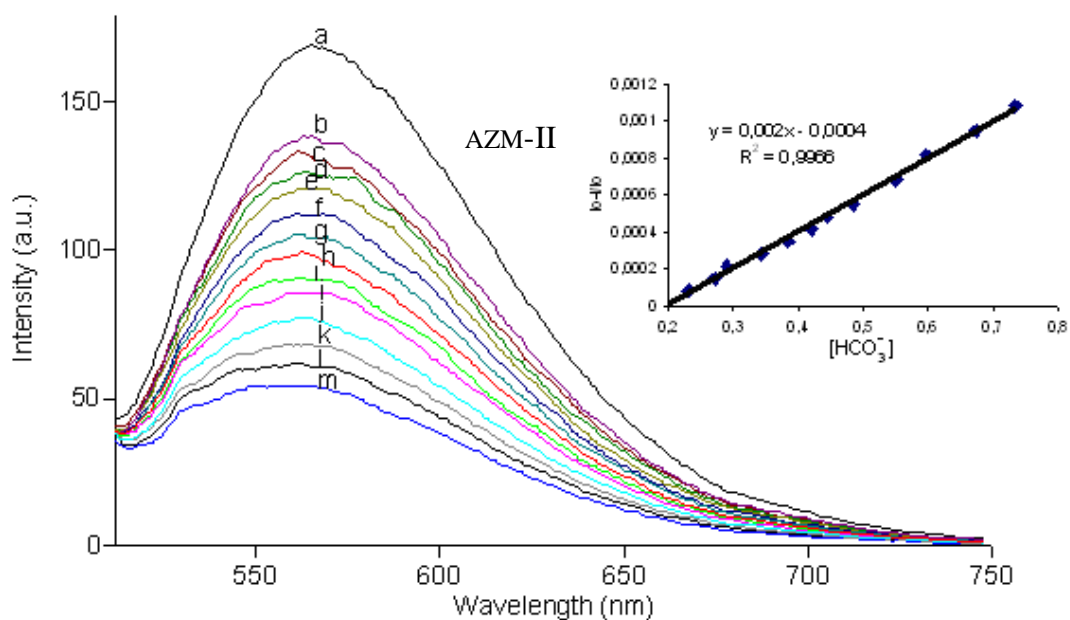


Figure 5.8 Emission spectra of immobilized AZM-II in EC matrix after exposure to different HCO_3^- concentrations.

a) 0 M; b) 1.73×10^{-5} M; c) 8.00×10^{-5} M; d) 1.47×10^{-4} M; e) 2.13×10^{-4} M; f) 2.80×10^{-4} M; g) 3.47×10^{-4} M; h) 4.13×10^{-4} M; i) 4.80×10^{-4} M; j) 5.47×10^{-4} M; k) 6.80×10^{-4} M; l) 8.13×10^{-4} M; m) 9.47×10^{-4} M.

5.5 Conclusion

The relative signal changes of emission spectra of the cocktails 1–4 were monitored after addition of certain concentrations of HCO_3^- solutions. The cocktail 1 (CC-1) and cocktail 4 (CC-4), which contained 1-ethyl-3-methylimidazolium tetrafluoroborate, exhibited the best response to different concentrations of HCO_3^- solutions in the direction of a decrease in signal intensity at 600 nm for AZM-I and AZM-II, respectively.

The linearized calibration curves of the sensor compositions for CC-1 and C-4 are shown in Figure 5.3 and Figure 5.6.

The dynamic working range is logarithmic and covers the concentration range of 5.60×10^{-6} to $10.40 \times 10^{-4} \text{ mol L}^{-1}$ and 2.00×10^{-6} to $7.40 \times 10^{-4} \text{ mol L}^{-1}$ [HCO_3^-] for AZM-I and AZM-II, respectively.

In most of the sensor designs, TBAOH and/or perfluoro compound (PFCs) was added into the sensing cocktail as a counter ion in order to increase the sensitivity and lifetime. However, we did not observe any significant enhancement in sensor response after addition of TBAOH into cocktail compositions for AZM-I. However, we observed an enhancement in sensor performance after addition of PFCs into cocktail composition CC-4 for AZM-II dye in terms of working range and linearity.

CHAPTER SIX

EMISSION BASED FIBER OPTIC CO₂ AND pH SENSING WITH LONG WAVELENGTH EXCITABLE SCHIFF BASES

6.1 Introduction

Most of the optical CO₂ sensor designs utilize indicator dyes with p*K*_a values between 7.4 and 10.0, which are doped into the polymer matrices. The number of the fluorescent pH indicators for carbon dioxide sensing is rather limited.

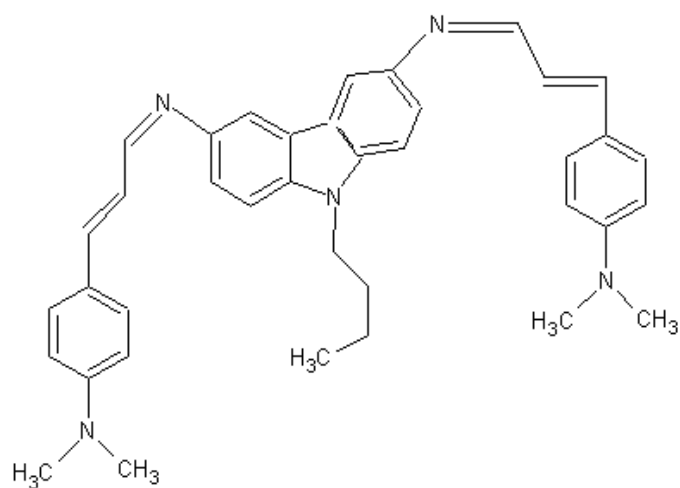
Most of the fluorescent pH probes work near neutral or acidic regions of the pH scale. In this work three different fluorescent schiff bases have been investigated for CO₂ and pH sensing in the pH range of 6.0-12.0 in plasticized PVC and EC with or without additives. Firstly absorption and emission based spectral data and acidity constant (p*K*_a) of the schiff bases were determined in conventional solvents and in PVC and EC. Then the gaseous and dissolved CO₂ sensitivity of the indicator dyes were investigated.

The newly synthesized fluorophores have been used for carbon dioxide sensing together with “carbon dioxide carrier” perfluorochemical (PFC) in ethyl cellulose matrix. It should be noted that the solubility of CO₂ in fluorocarbons is about 10–20 times as that observed in the parent hydrocarbons or in water, respectively, and once doped into the sensing film, considerably enhance the response of the sensing agent (Ertekin & Alp, 2005).

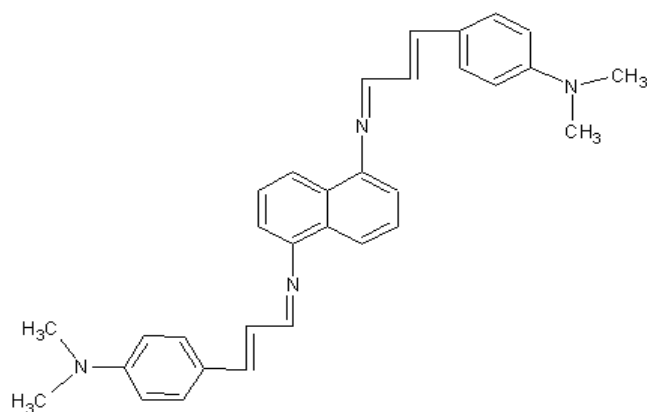
The long wavelength excitable immobilized schiff bases CY-1 ($\lambda_{\text{ex}} = 595 \text{ nm}$), CY-2 ($\lambda_{\text{ex}} = 585 \text{ nm}$) and CY-3 ($\lambda_{\text{ex}} = 655 \text{ nm}$) exhibited absorption and emission based optical response to proton in the pH range of 6.0-12.0. Responses of the CY-1, CY-2 and CY-3 were reversible within the dynamic working range. The response times were less than 1 min.

6.2 Synthesis of the Schiff Bases (CY-1, CY-2 and CY-3)

The Schiff bases CY-1, CY-2 and CY-3 were synthesized in our laboratories by Associated Prof. Dr. Yavuz Ergün. Schematic structures of the employed molecules are shown in Figure 6.1. Studies regarding IR and NMR related data of newly synthesized molecules are on going.



CY-1



CY-2

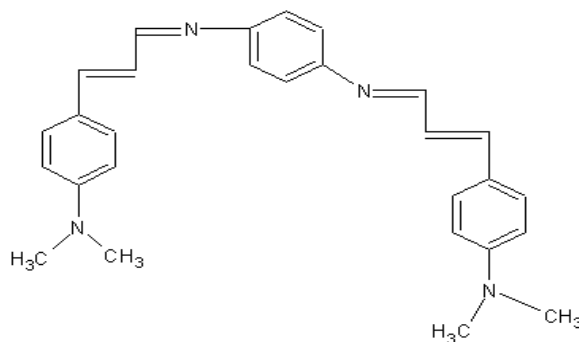
**CY-3**

Figure 6.1 Schematic structures of the employed molecules.

6.3 PVC Cocktail Preparation

The membranes were prepared to contain the proper amount of the dye (approximately 2 mg dye/kg polymer), 33% PVC and 66% plasticizer and equivalent amount of potassium tetrakis-(4-chlorophenil) borate (PTCPB). The mixture was dissolved in the solvent of tetrahydrofuran and mixed by several hours by the help of a magnetic stirrer.

6.4 Ethyl Cellulose Cocktail Preparation

The membranes were prepared to contain the dye, 33% ethyl cellulose and 66% plasticizer by weight. The mixture was dissolved in the solvent of tetrahydrofuran and mixed by several hours by the help of a magnetic stirrer. As mentioned earlier different cocktails (see table 6.1) were prepared namely M-1, M-2 and M-3 for gaseous CO₂ sensing purposes.

Table 6.1 Coctail compositions for CY-1, CY-2 and CY-3.

Compound	Coctail No	Additive
CY-1, CY-2, CY-3	M-1	---
CY-1, CY-2, CY-3	M-2	20 μ l 0.1 M TBAOH
CY-1, CY-2, CY-3	M-3	perfluoro
CY-1, CY-2, CY-3	M-4	20 μ l 0.1 M TBAOH+perfluoro

6.5 Results and Discussion

6.5.1 Spectral Characterization Studies in Solvents

For spectral characterization of the CY-1, CY-2 and CY-3 absorption excitation and corrected emission spectra were recorded in the solvents of DMF, EtOH, DCM, THF and toluene/ethanol (To: EtOH; 80:20) mixture. The UV-Vis spectroscopy related data (absorption maxima; λ_{Abs}), were shown in Table 6.2 and 6.3.

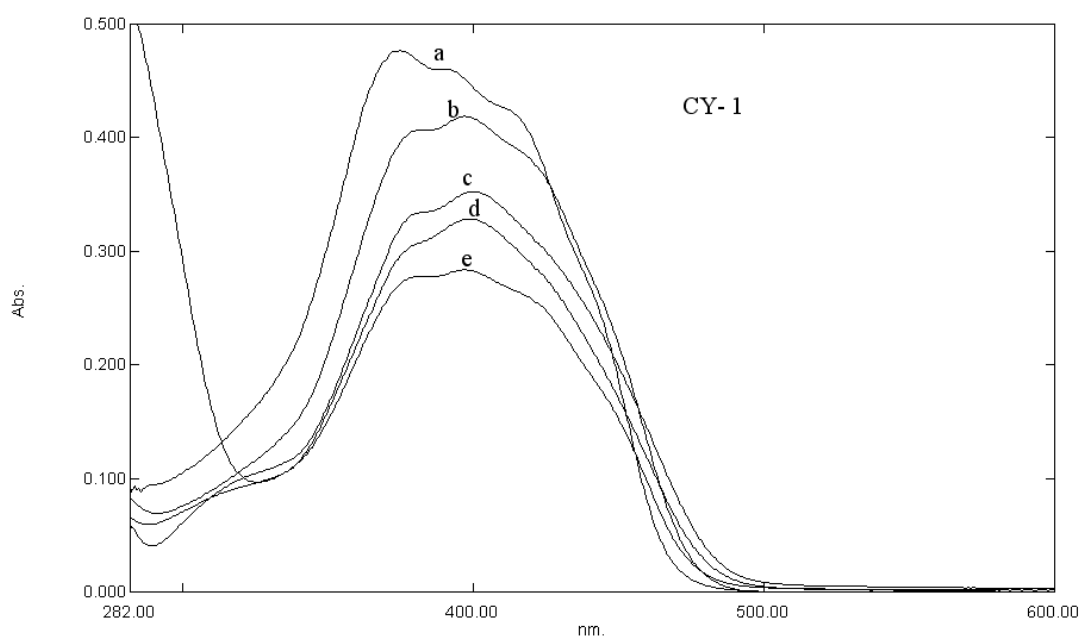


Figure 6.2.1 Absorption spectra of the CY-1 dye: a) THF b) DCM c) To:ETOH d) ETOH e) DMF

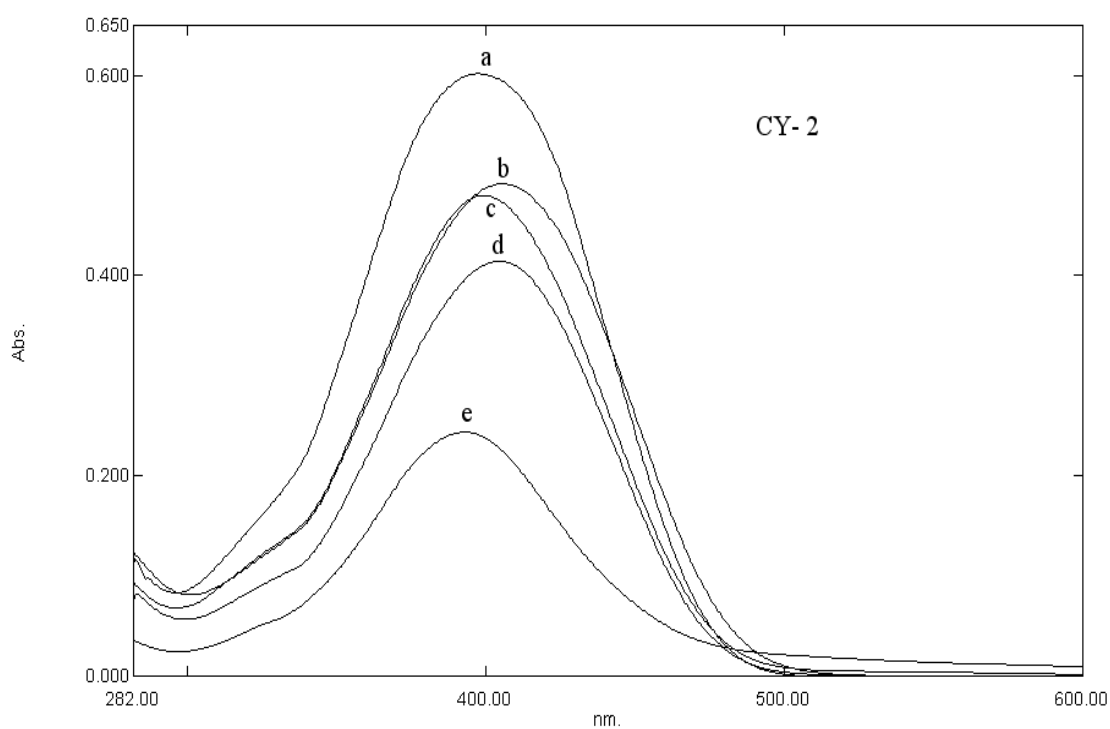


Figure 6.2.2 Absorption spectra of the CY-2 dye a) THF b) DMF c) DCM d) To:ETOH e) ETOH

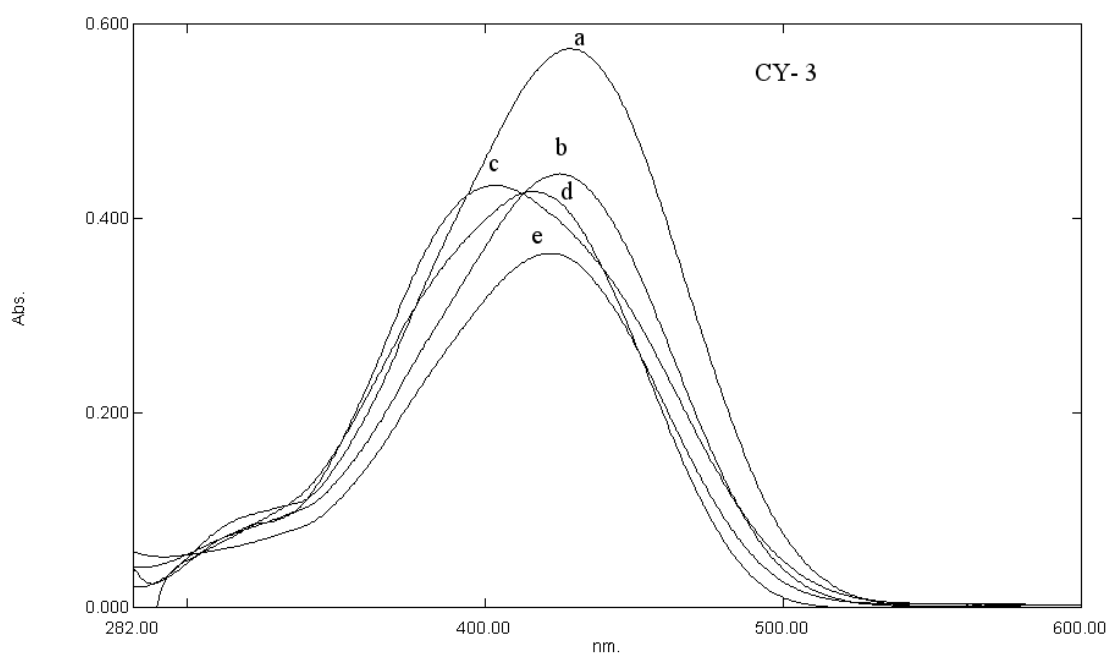


Figure 6.2.3 Absorption spectra of the CY-3 dye a) To:EtOH b) DMF c) EtOH d) THF e) DCM

Table 6.2 UV-Vis spectra related data of CY-1, CY-2 and CY-3 in the solvents of DMF, EtOH, DCM, THF and toluene/ ethanol mixture (80:20).

Compound	Matrix	λ_{abs}^1	λ_{abs}^2
CY-1	EtOH	252	400
CY-1	DCM	250	397
CY-1	THF	251	377
CY-1	To: EtOH	--	400
CY-1	DMF	--	398
CY-2	EtOH	--	394
CY-2	DCM	--	400
CY-2	THF	--	400
CY-2	To: EtOH	--	406
CY-2	DMF	--	407
CY-3	EtOH	--	404
CY-3	DCM	--	423
CY-3	THF	--	417
CY-3	To: EtOH	--	430
CY-3	DMF	--	425

6.5.2 Spectral Evaluation, Interpretation of Emission Spectra

For spectral characterization of CY-1, CY-2 and CY-3, excitation and corrected emission spectra were recorded. The emission spectra were corrected using commercially available silica ground of the instrument. Figure 6.3.1, 6.3.2, 6.3.3 and Table 6.3 reveal emission based spectral characteristics of Schiff bases in the employed solvents (EtOH, DCM, THF and To: EtOH) and in PVC.

Upon excitation the CY-1 displayed maximum emission wavelengths of 595, 390, 390, 390, 395 and 390 in the solvents of EtOH, DCM, THF, DMF and To: EtOH, respectively. When doped in plasticized PVC, the emission maximum of the dye was red shifted more than 46 nm and appeared at 641 nm (See Fig. 6.3 and 6.7).

Upon excitation the CY-2 displayed maximum emission wavelengths of 585, 390, 385, 380, 395 and 380 in the solvents of EtOH, DCM, THF, DMF and To: EtOH, respectively. When doped in plasticized PVC, the emission maximum of the dye was red shifted more than 31 nm and appeared at 616 nm (See Fig. 6.4 and 6.8).

Upon excitation the CY-3 displayed maximum emission wavelengths of 655, 390, 380, 380, 380 and 390 in the solvents of EtOH, DCM, THF, DMF and To: EtOH, respectively. When doped in plasticized PVC, the emission maximum of the dye was red shifted more than 35 nm and appeared at 690 nm (See Fig. 6.5 and 6.9).

Table 6.3. Spectral characterization of CY-1, CY-2 dyes. λ_{ex}^{em} : excitation wavelength for emission in nm; λ_{ex}^{ex} : excitation wavelength for excitation in nm; λ_{max}^{em} : maximum emission wavelength in nm; λ_{max}^{ex} : maximum excitation wavelength in nm; $\Delta\lambda_{ST}$: Stoke's shift.

Compound	Matrix	λ_{ex}^{em} (excitation wavelength for emission)	λ_{ex}^{ex} (emission wavelength for excitation)	λ_{max}^{em}	λ_{max}^{ex}	$\Delta\lambda_{ST}$ (Stoke's shift)
CY-1	EtOH	390	471	471	390	81
CY-1	DCM	390	460	460	390	70
CY-1	THF	390	437	437	390	47
CY-1	To: EtOH	395	469	469	395	74
CY-1	DMF	390	470	470	390	80
CY-1	PVC	595	641	641	595	46
CY-2	EtOH	390	469	469	390	79
CY-2	DCM	385	461	461	385	76
CY-2	THF	380	445	445	380	65
CY-2	To: EtOH	395	468	468	395	73
CY-2	DMF	380	472	472	380	92
CY-2	PVC	585	616	616	585	31
CY-3	EtOH	390	475	475	390	85
CY-3	DCM	380	460	460	380	80
CY-3	THF	380	440	440	380	60
CY-3	To: EtOH	390	474	474	390	84
CY-3	DMF	380	460	460	380	80
CY-3	PVC	655	690	690	655	35

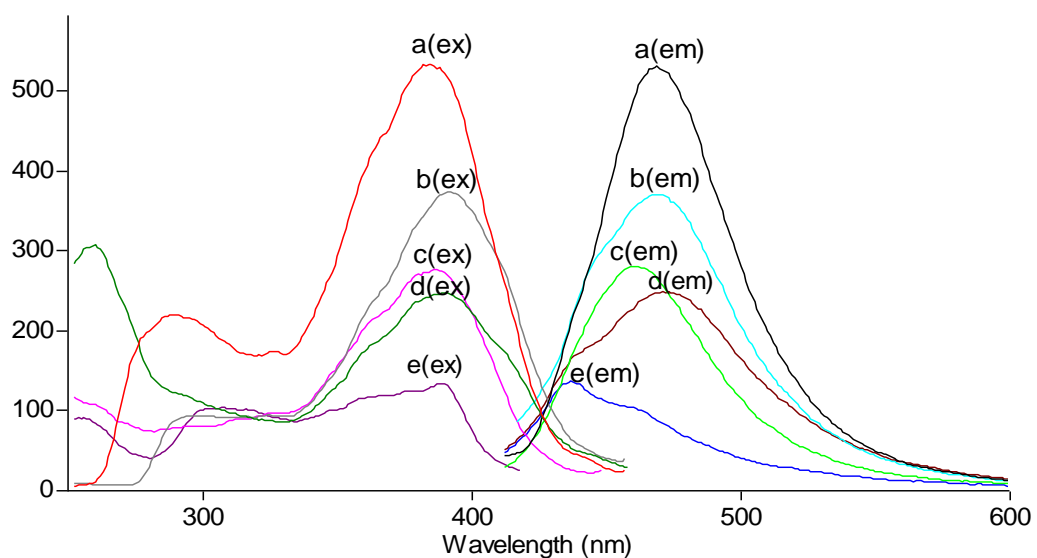


Figure 6.3.1 Excitation and corrected emission spectra of the CY-1 dye (10^{-6} M dye or 2.5 mmol dye/kg polymer).

CY-1: a) DMF b) To:ETOH c) DCM d) ETOH e) THF

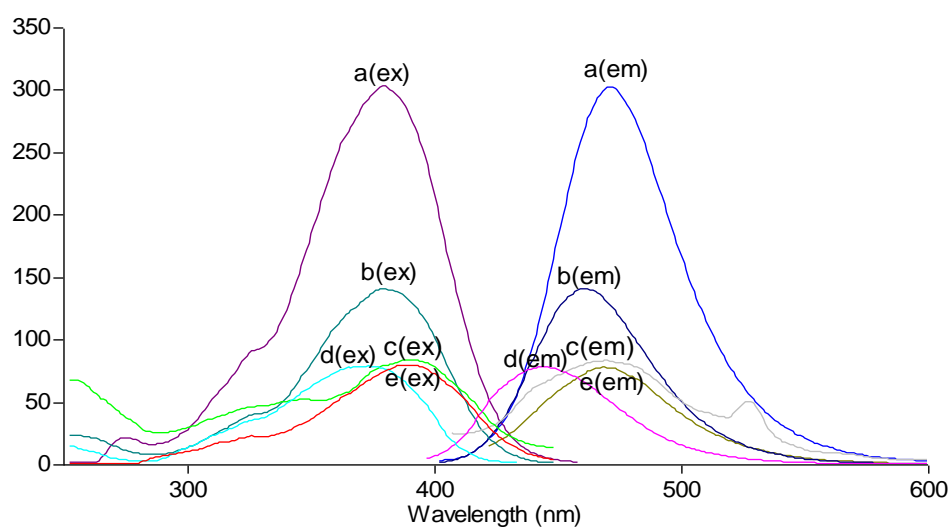


Figure 6.3.2 Excitation and corrected emission spectra of the CY-2 dye (10^{-6} M dye or 2.5 mmol dye/kg polymer).

CY-2: a) DMF b) DCM c) ETOH d) THF e) To:ETOH

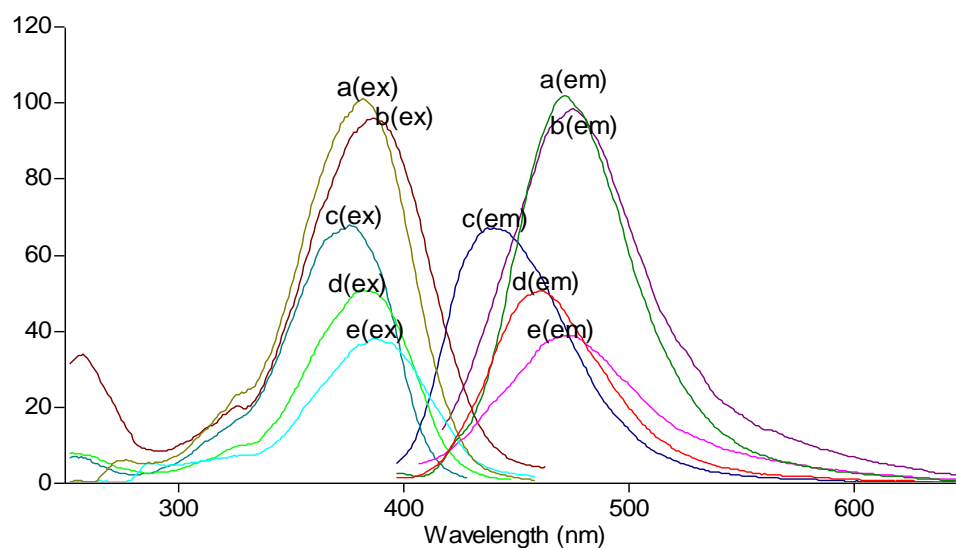


Figure 6.3.3 Excitation and corrected emission spectra of the CY-3 dye (10^{-6} M dye or 2.5 mmol dye/kg polymer).

CY-3: a) DMF b) ETOH c) THF d) DCM e) To:ETOH

6.5.3 pK_a Calculations of CY-1, CY-2 and CY-3 in PVC Matrix

The immobilized Schiff bases reversibly responded to H^+ ions in PVC. The relative signal change of absorption spectra of the CY-1, CY-2 and CY-3 was monitored after addition of certain concentrations of buffered acid solutions at different pH ranges. The immobilized CY-1, CY-2 and CY-3 exhibited the best response to different concentrations of acid solutions between pH=6.0-12.00 in the direction of a decrease in signal intensity at 535 nm, 590 nm and 644 nm, respectively in absorption spectrum. Due to the presence of the isobestic point at 485, 490 and 496 nm, respectively, the CY-1, CY-2 and CY-3 dyes allow absorption-based ratiometric measurements in plasticized polymer PVC matrix. Upon exposure to the solutions between pH 6.0–12.0, the CY-1, CY-2 and CY-3 dyes exhibited a 95% relative signal change in direction of decrease in absorbance intensity. (See Figure 6.4, 6.5 and 6.6).

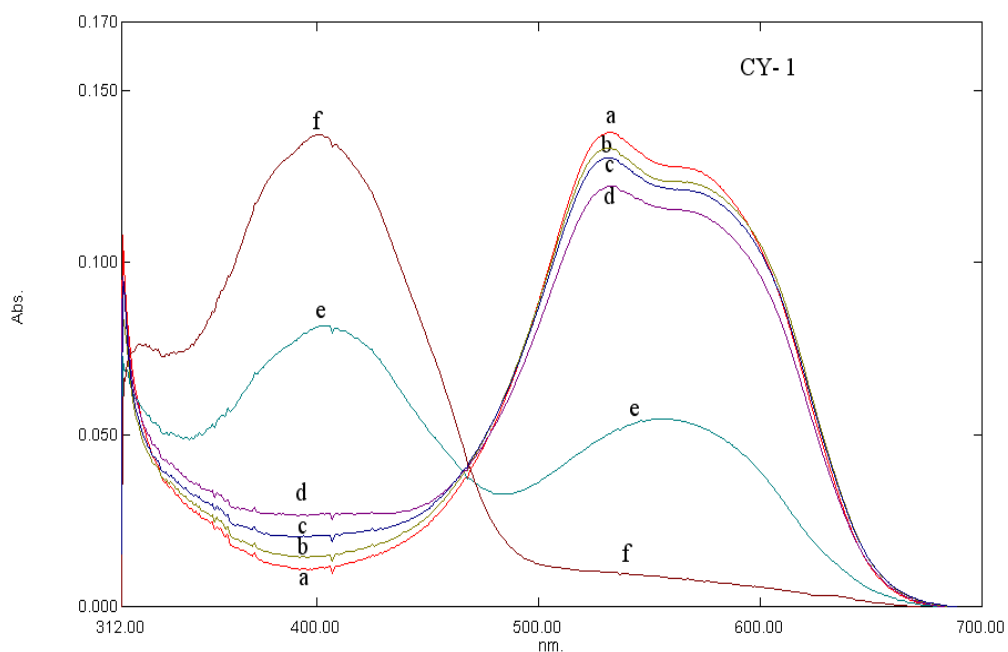


Figure 6.4 Absorption spectra of CY-1 in PVC after addition of acid solutions in the pH range of 7.00-12.00

pH: a) 7.00 b) 8.00 c) 9.00 d) 10.00 e) 11.00 f) 12.00

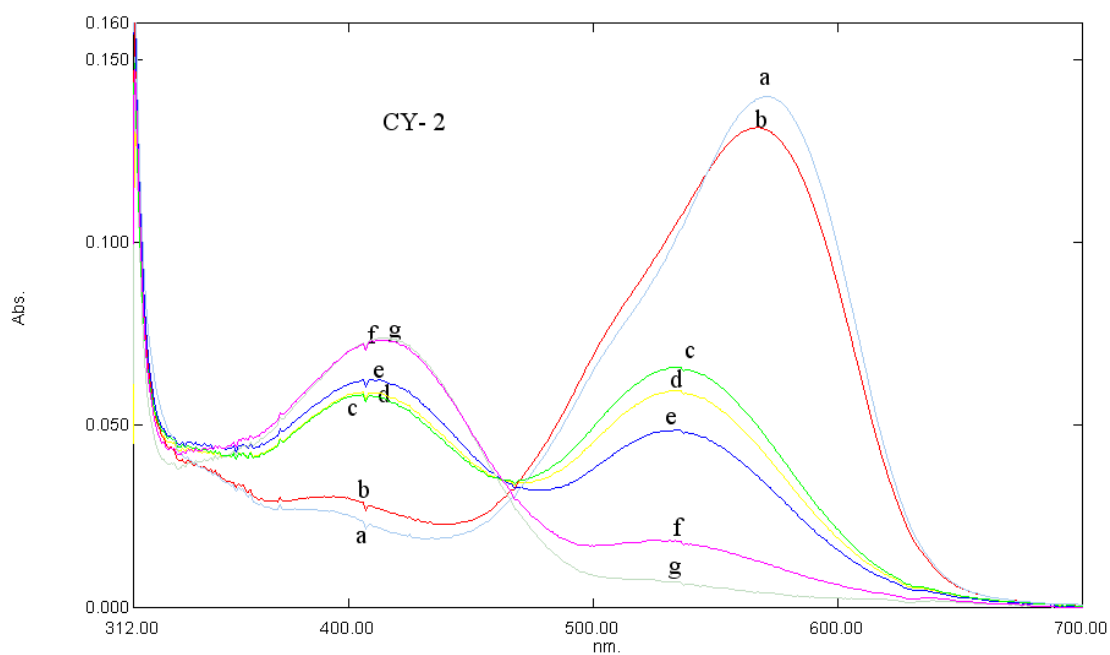


Figure 6.5 Absorption spectra of CY-2 in PVC after addition of acid solutions in the pH range of 6.00-12.00

pH: a) 6.00 b) 7.00 c) 8.00 d) 9.00 e) 10.00 f) 11.00 g) 12.00

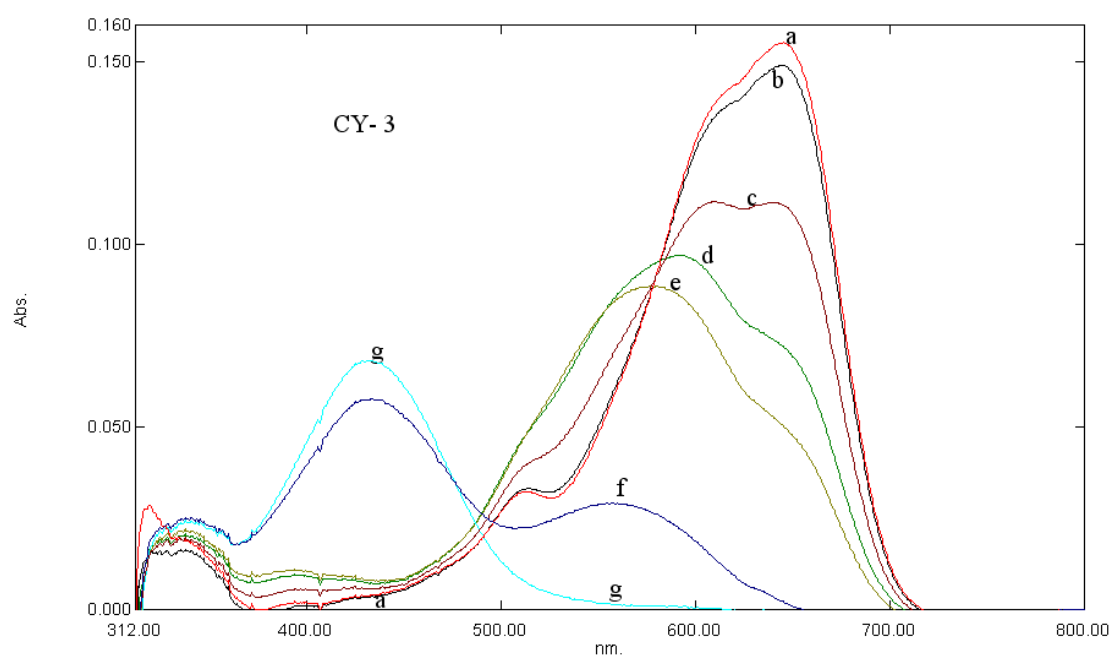


Figure 6.6 Absorption spectra of CY-3 in PVC after addition of acid solutions in the pH range of 6.00-12.00

pH: a) 6.00 b) 7.00 c) 8.00 d) 9.00 e) 10.00 f) 11.00 g) 12.00

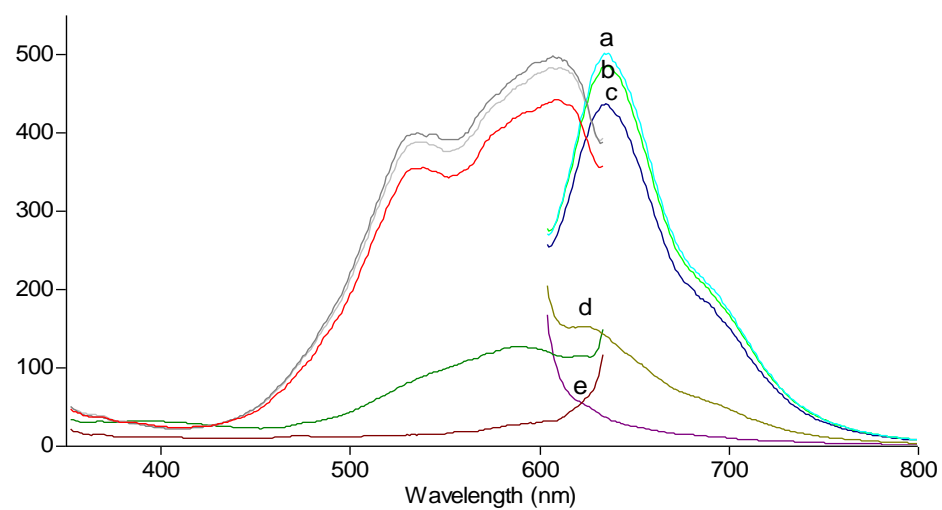


Figure 6.7 pH induced emission based spectral response of the PVC doped CY-1 in the pH range of 6.00-12.00.

pH: a) 7.00, 8.00 b) 9.00 c) 10.00 d) 11.00 e) 12.00

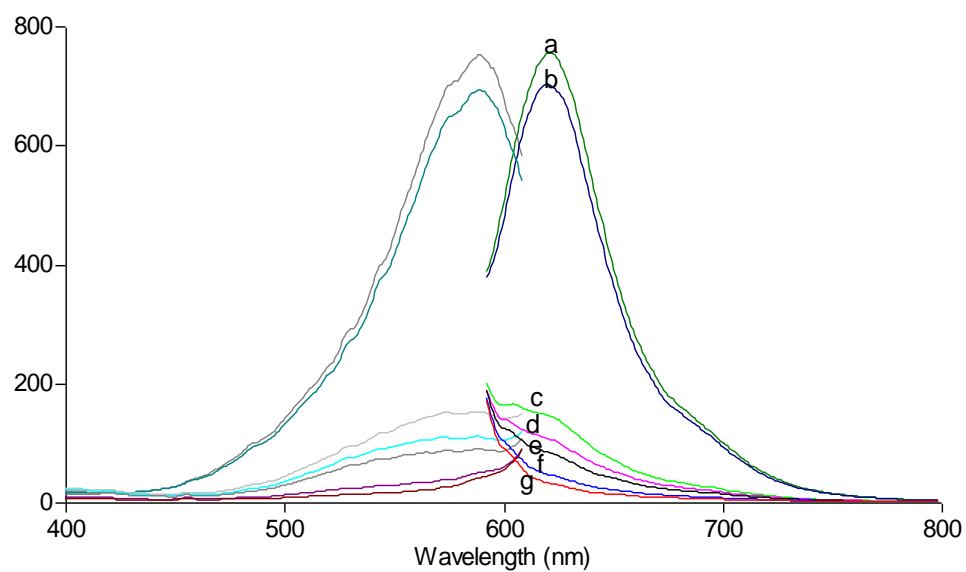


Figure 6.8 pH induced emission based spectral response of the PVC doped CY-2 in the pH range of 6.00-12.00. pH: a) 6.00 b) 7.00 c) 8.00 d) 9.00 e) 10.00 f) 11.00 g) 12.00

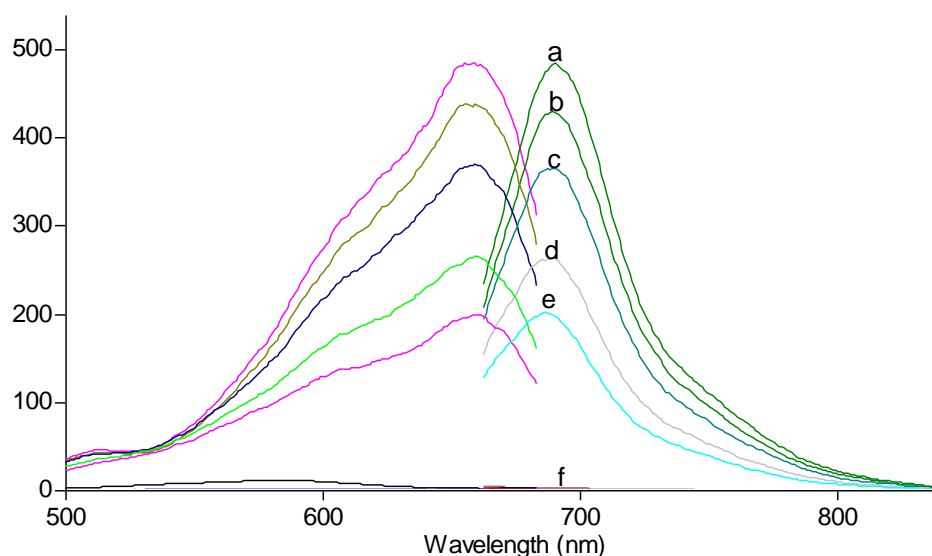


Figure 6.9 pH induced emission based spectral response of the PVC doped CY-3 in the pH range of 6.00-12.00. pH: a) 6.00 b) 7.00 c) 8.00 d) 9.00 e) 10.00 f) 11.00; 12.00

For all dyes, pK_a values were calculated via equation

$$pK_a = pH + \log \left[\frac{(I_x - I_b)}{(I_a - I_x)} \right] \quad (1)$$

where I_a and I_b are the signal intensities of the dyes in their acid and conjugate base form respectively (Mills & Chang, 1992). The pK_a values were found to be 10.5, 7.4 and 8.8 for CY-1, CY-2 and CY-3, respectively.

6.5.4 Gas Phase Sensing Studies for EC Doped CY-1, CY-2 and CY-3

Gaseous CO_2 and N_2 were mixed in the concentration range 0–100% in a gas diluter (Sonimix 7000A gas blending system). The output flow rate of the gas mixture was maintained at 250 mL min^{-1} . Gas mixtures were introduced into the sensor agent-containing cuvette via a diffuser needle under ambient conditions either directly or after humidification of the gas by bubbling through water at $35 \text{ }^\circ\text{C}$.

In order to investigate the effect of the additives; PFC and TBAOH, the absorption and emission based characteristics of cocktails; M-1, M-2 and M-3 were recorded.

Figure 6.10 shows absorption based gathered spectra of the employed cocktail CY-1 with/without additives (See also Table 6.1).

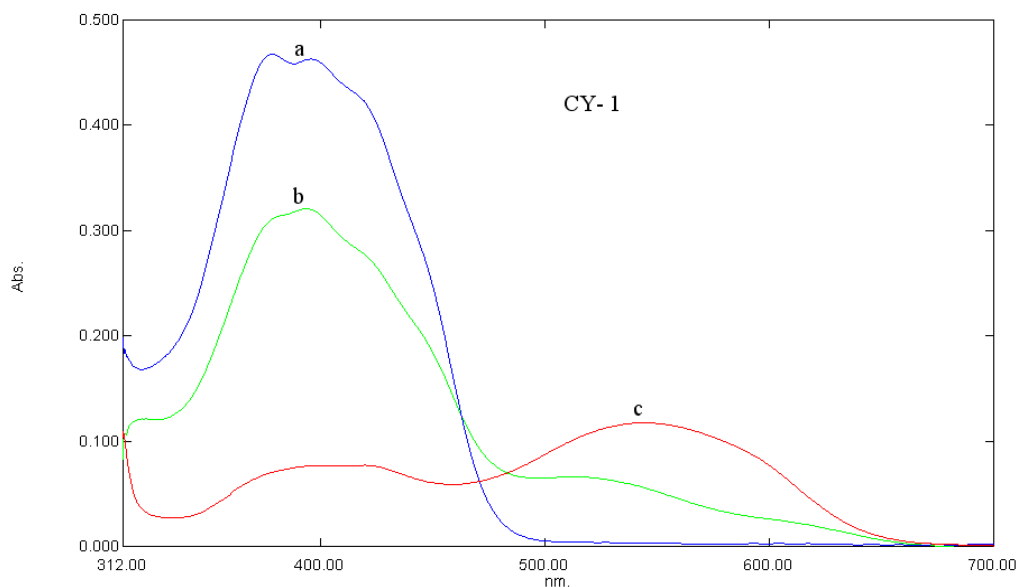


Figure 6.10 Absorption spectra of different cocktail membranes of CY-1 (EC).
a) 20 μ l TBAOH M-2, b) 20 μ l TBAOH +perfluoro M-3, c) CY-1 (EC) M-1

Figure 6.11 shows response of CY-1 to different concentrations of CO₂. Addition of additives of TBAOH and PFC caused a distinct decrease in emission peaks at 641 nm.

As mentioned earlier TBAOH is usually added as a lipophilic counter ion to stabilize the sensor dye in the matrix. The presence of TBAOH tunes the sensitivity of the sensor and enhances the stability since it also acts as a sink for acidic species. However, the dye was not functional in TBAOH containing cocktail (See Fig. 6.12-a). Exposure to gaseous CO₂ in the concentration range of 20-100% resulted with insignificant response. Similar results were observed for PFC containing matrix material (See Fig. 6.13). The observed quenching in the emission spectra of the pH sensitive dye; CY-1 in additive containing matrices can be attributed to the interaction of the dye with strongly basic quaternary ammonium hydroxide and slightly acidic PFC.

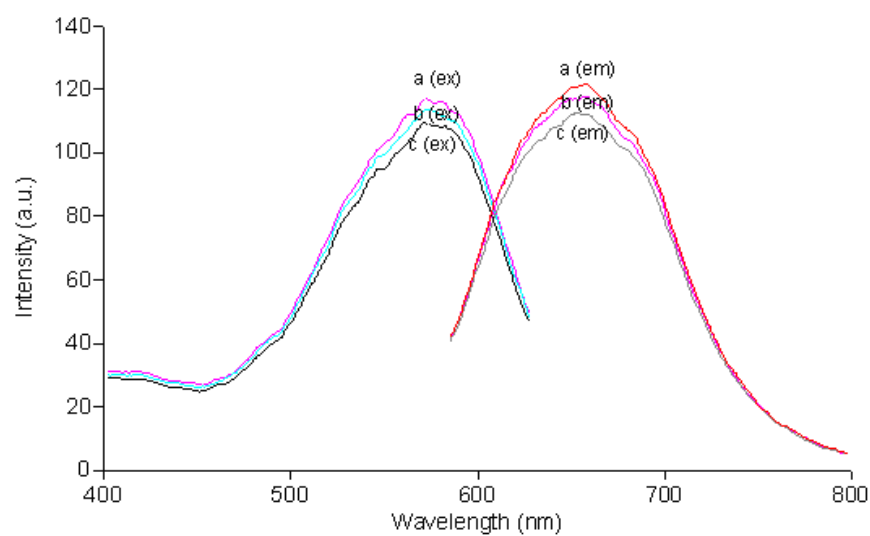


Figure 6.11 Emission and excitation spectra of M-1 coctail membrane of CY-1 (EC).

a) CY-1 (EC) M-1 b) 20% CO₂ c) 100% CO₂

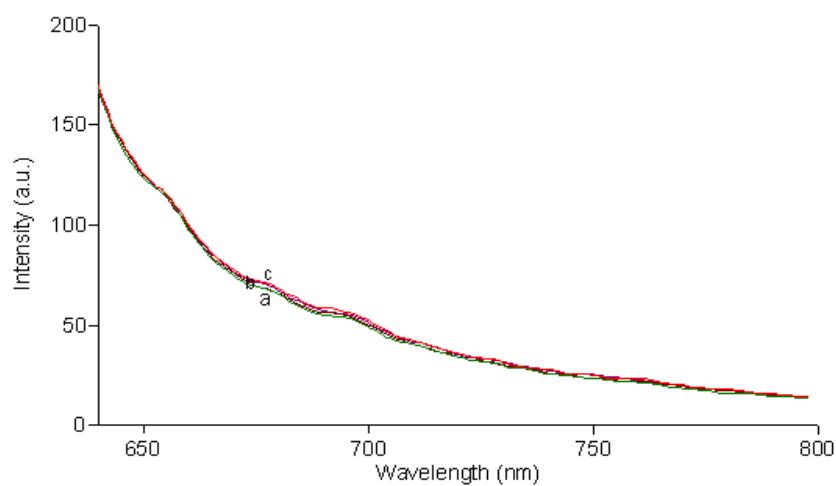


Figure 6.12 Emission spectra of M-2 (CY-1+TBAOH) coctail membrane of CY-1 (EC).

a) CY-1 (EC) M-2 b) 20% CO₂ c) 100% CO₂

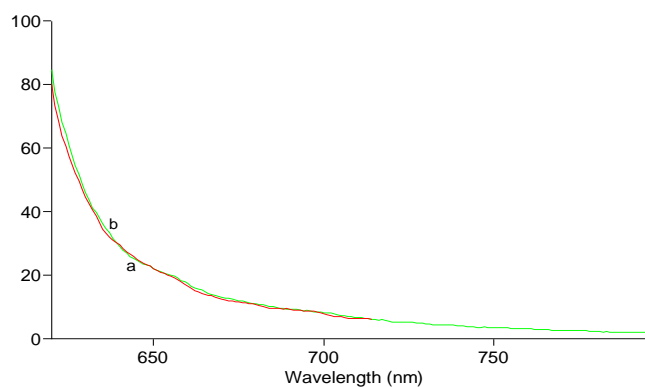


Figure 6.13 Emission spectra of M-3 (CY-1+perfluoro) cocktail membrane of CY-1 (EC).

a) CY-1 (EC) M-3 b) 20% CO₂

Spectral responses of CY-2 and CY-3 dyes were also examined in similar matrix materials. Fig. 6-14 – 6.19 show spectral response of CY-2 and CY-3 in additive containing matrix materials. Since the structures of the employed dyes have been similar, they exhibited similar reaction in presence of the additives of TBAOH and PFC.

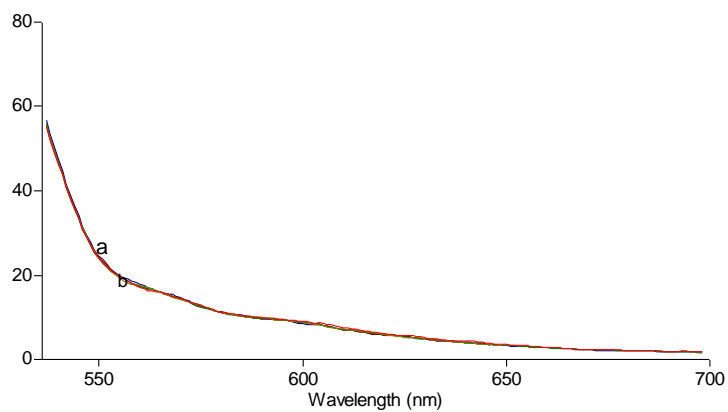


Figure 6.14 Emission spectra of M-1 (CY-2 (EC)) cocktail membrane of CY-2.

a) 0% CO₂ b) 100% CO₂

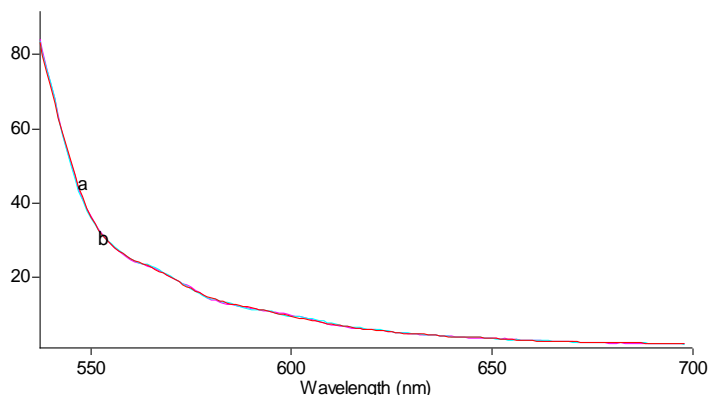


Figure 6.15 Emission spectra of M-2 (CY-2 (EC) +TBAOH) cocktail membrane of CY-2.

a) 0% CO₂ b) 100% CO₂

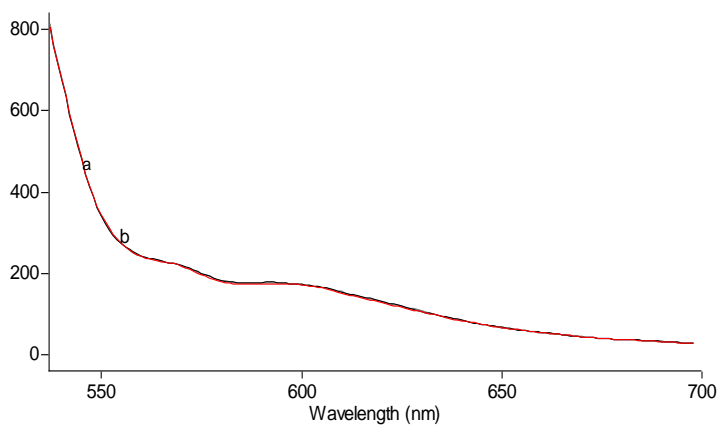


Figure 6.16 Emission spectra of M-3 (CY-2 (EC) +perfluoro) cocktail membrane of CY-2.

a) 0% CO₂ b) 100% CO₂

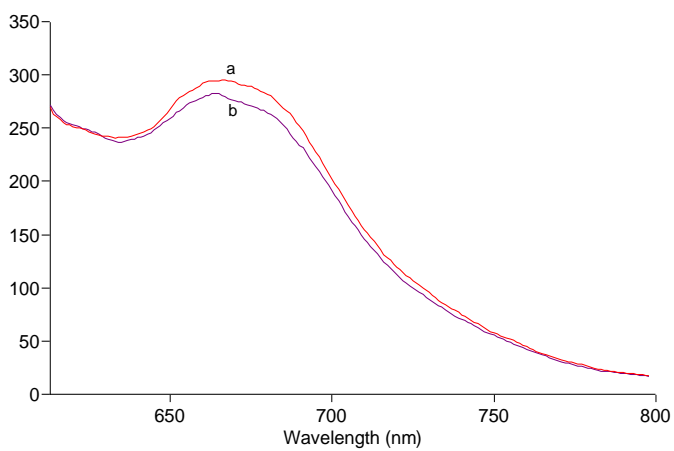


Figure 6.17 Emission spectra of M-1 (CY-3 (EC)) cocktail membrane of CY-3.

a) 0% CO₂ b) 100% CO₂

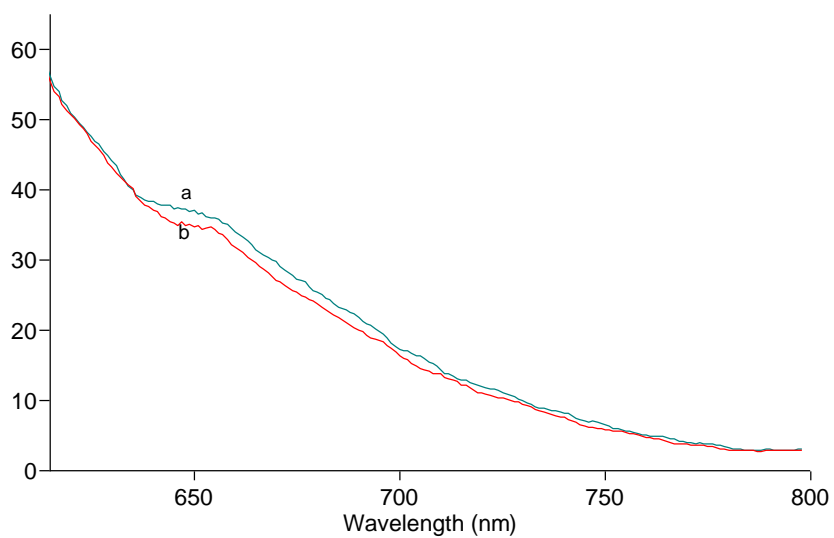


Figure 6.18 Emission spectra of M-3 (CY-3 (EC) +perfluoro) cocktail membrane of CY-3.

a) 0% CO₂ b) 100% CO₂

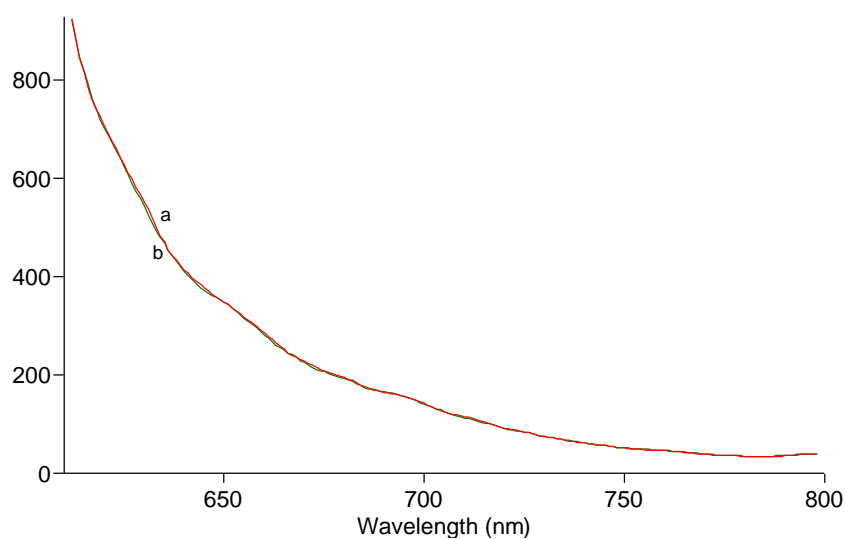


Figure 6.19 Emission spectra of M-4 (CY-3 (EC) +perfluoro+TBAOH) cocktail membrane of CY-3
a) 0% CO₂ b) 100% CO₂

The CY-1, CY-2 and CY-3 doped sensor compositions did not exhibit significant spectral response for gas-phase carbon dioxide.

6.5.5 Dissolved CO₂ Sensing Studies with CY-1, CY-2 and CY-3 in EC

Sensor performances of all of the employed cocktail compositions were also tested for dissolved CO₂. Standard solutions were prepared freshly from 1 mol L⁻¹ NaHCO₃ stock solution prior to the measurements. CO₂-free standard solutions were prepared with doubly distilled water after boiling and bubbling with nitrogen; they were stored in closed containers. Microlitre volumes of (10 μL) of standard solutions of NaHCO₃ were added to the sensing agent-containing cuvette, mixed and the changes in fluorescence intensity caused by addition of different concentrations of dissolved CO₂ were measured. All the experiments were performed at room temperature (25 °C). 10 microlitres of standard HCO₃⁻ solutions were added by using a micro syringe onto the sensing agent, so dilution was avoided. Figure 6.20 shows absorption and emission based response of additive-free cocktail; CY-1 for dissolved CO₂ in the concentration range of 2.67x10⁻⁶ – 5.94x10⁻³ M.

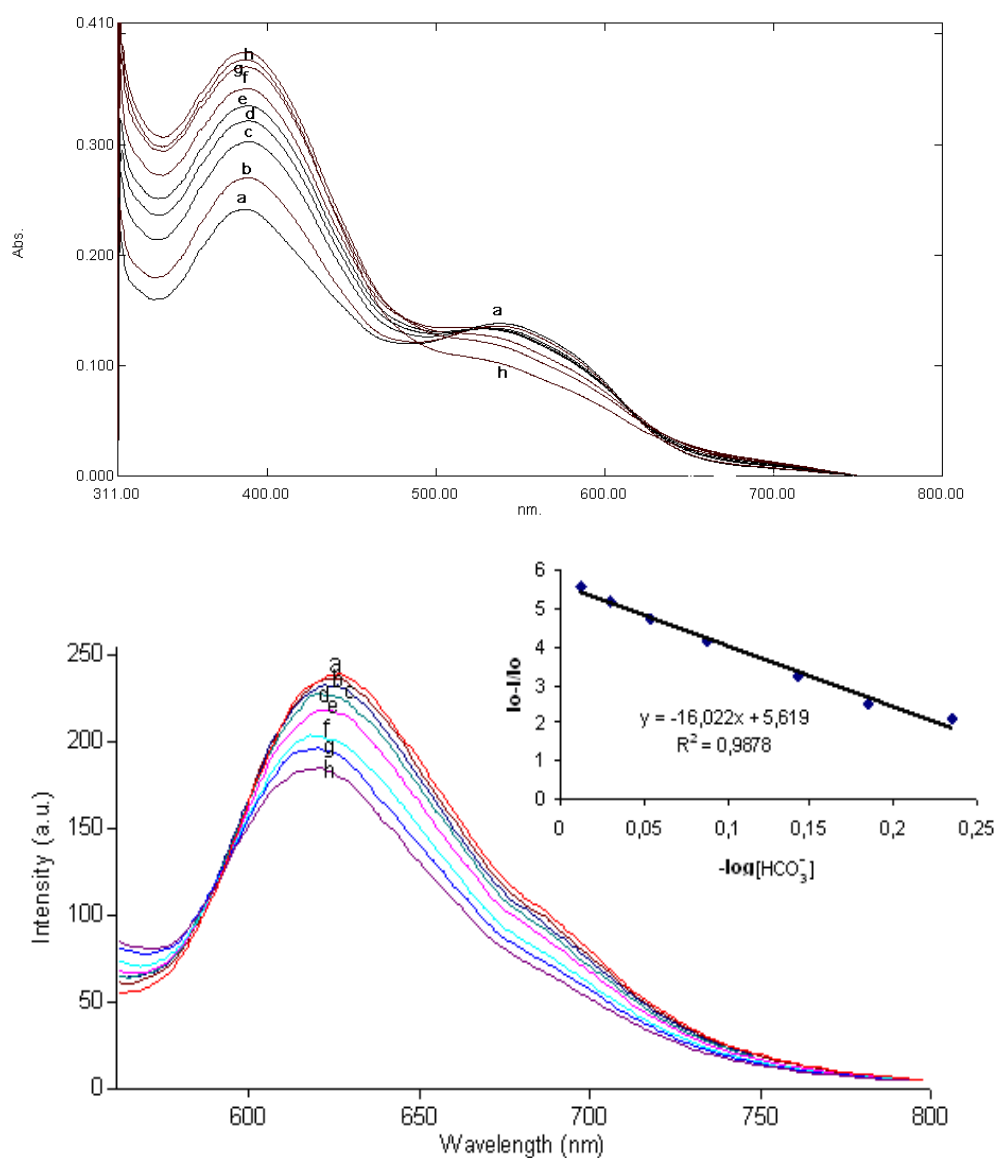


Figure 6.20 Absorption/Emission spectra of immobilized CY-1 (coctail M-1) in EC matrix after exposure to different HCO_3^- concentrations.

a) 0 M b) 2.67×10^{-6} M c) 6.67×10^{-6} M d) 2.00×10^{-5} M e) 7.33×10^{-5} M f) 6.07×10^{-4} M
g) 3.27×10^{-3} M h) 5.94×10^{-3} M

The dynamic range for the detection of H_2CO_3 ($\text{CO}_2 + \text{H}_2\text{O}$) was between 2.67×10^{-6} – 5.94×10^{-3} M. The corresponding calibration graph exhibited good linearity. It should be noted that the X-axis (concentration) of the calibration graph is logarithmic ($y = -16.022x + 5.619$ and $R^2 = 0.9878$) and covers a large scale. However, in solution phase studies attained relative signal change was not high. For

absorption and emission based measurements relative signal changes of 50% and 33% were recorded respectively.

Figure 6.21, 6.22 and 6.23 show the spectral response of CY-1 dye in additive containing cocktails; M-2, M-3 and M-4.

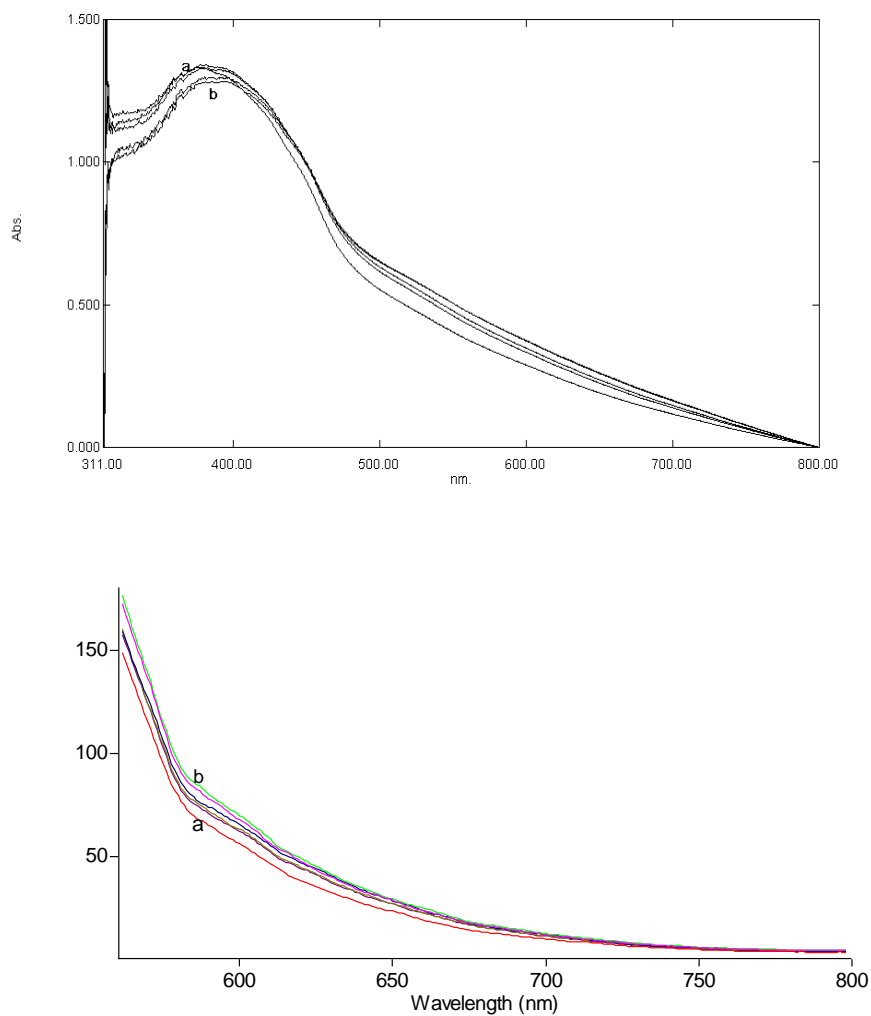


Figure 6.21 Emission/absorption spectra of immobilized CY-1 (cocktail M-2) in EC matrix after exposure to different HCO₃⁻ concentrations.

a) 0 M b) 5.33×10^{-3} M

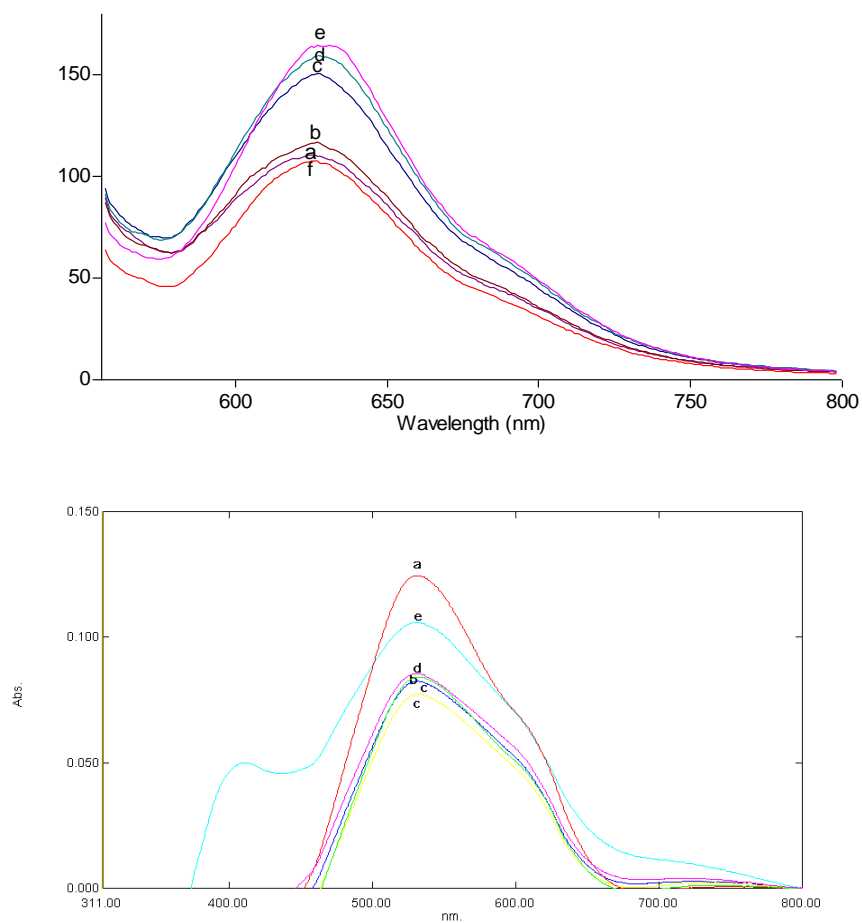


Figure 6.22 Emission/absorption spectra of immobilized CY-1 (coctail M-3) in EC matrix after exposure to different HCO_3^- concentrations.

a) 0 M b) 2.67×10^{-6} M c) 8.00×10^{-6} M d) 1.33×10^{-4} M e) 5.87×10^{-4} M
f) 5.92×10^{-3} M

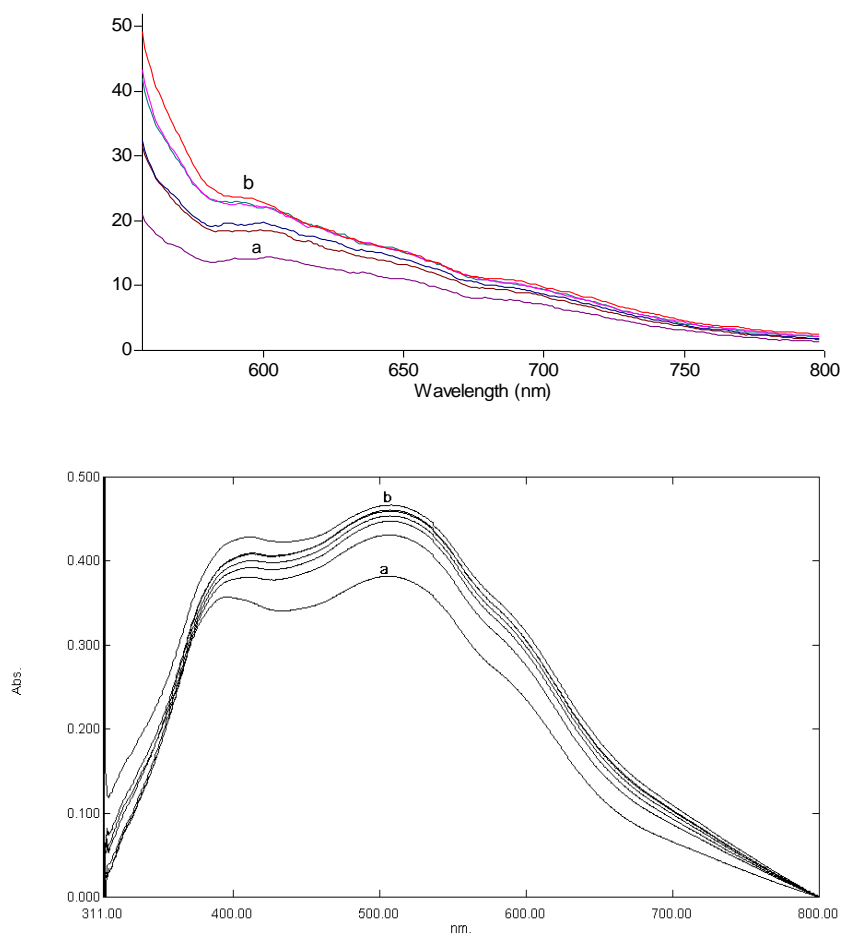


Figure 6.23 Emission/absorption spectra of immobilized CY-1 (cocktail M-4) in EC matrix after exposure to different HCO_3^- concentrations.

a) 0 M b) 5.33×10^{-3} M

The attempts for dissolved CO_2 sensing in additive containing matrix materials resulted with low relative signal changes with respect to additive-free composition. This can be attributed to the quenching effect of the additives on sensing performance of fluorescent dye; CY-1.

The CY-2 dye exhibited excellent performance in additive-free cocktail M-1 and additive containing M-3. Figure 6.24 and 6.25 show the spectral response of CY-2 in above mentioned matrices.

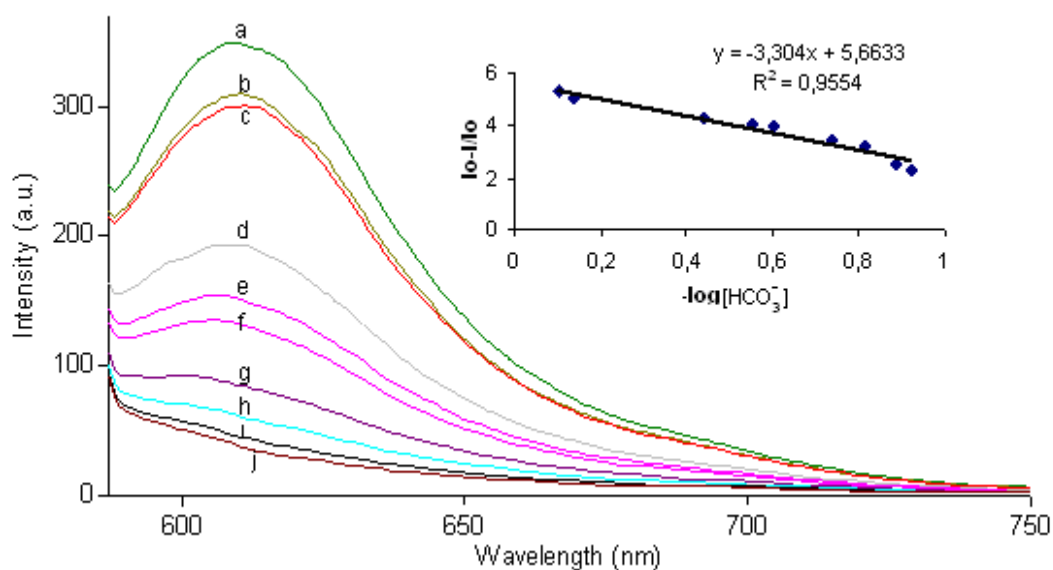


Figure 6.24 Emission/absorption spectra of immobilized CY-2 (cocktail M-1) in EC matrix after exposure to different HCO_3^- concentrations.

a) 0 M b) 5.33×10^{-6} M c) 10.67×10^{-6} M d) 6.40×10^{-5} M e) 9.07×10^{-5} M f) 11.73×10^{-5} M
g) 4.80×10^{-4} M h) 6.51×10^{-5} M i) 3.32×10^{-3} M j) 5.98×10^{-3} M

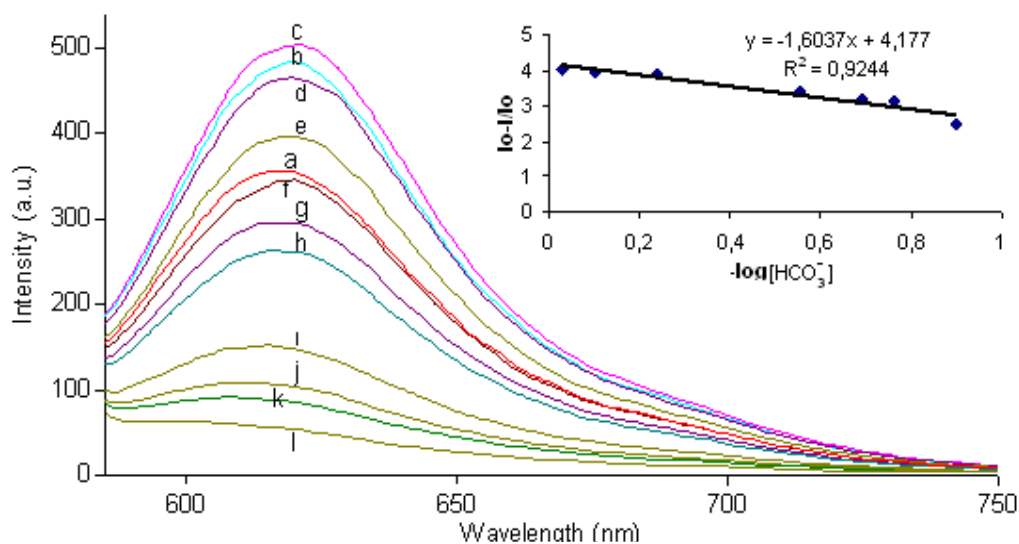


Figure 6.25 Emission/absorption spectra of immobilized CY-2 (cocktail M-3) in EC matrix after exposure to different HCO_3^- concentrations.

a) 0 M b) 5.33×10^{-6} M c) 8.00×10^{-6} M d) 3.47×10^{-5} M e) 6.13×10^{-5} M f) 8.80×10^{-5} M
g) 11.47×10^{-5} M h) 14.13×10^{-5} M i) 4.80×10^{-4} M j) 6.75×10^{-4} M k) 9.41×10^{-4} M
l) 3.61×10^{-3} M

After addition of HCO_3^- solutions in the concentration range of 5.33×10^{-6} - $5.98 \times 10^{-3} \text{ mol L}^{-1}$; approximately 90% of relative signal change was attained.

The X-axis (concentration) of the calibration graph is logarithmic again ($y = -3.304x + 5.6633$ and $R^2 = 0.9554$) and covers a large scale for M-1. Similarly in C-3, response for bicarbonate was linear and was very satisfactory in terms of relative signal change (See Fig. 6.25). The CY-2 dye exhibited excellent performance in PFC containing matrix material for dissolved CO_2 . This can be attributed to the well known wet carbon dioxide carrier characteristic of the PFC; in which all hydrogen atoms have replaced with fluorine atoms, and therefore they can dissolve large volumes of oxygen and carbon dioxide (Ertekin K & Alp S, 2005).

Response of CY-2 in TBAOH containing cocktail; M-2 was not satisfactory (See Fig. 6. 26). The CY-3 dye exhibited significant spectral response in M-1 for dCO_2 in the concentration range of 8.0×10^{-6} - $3.48 \times 10^{-3} \text{ M}$ (See Fig. 6.27). Figure 6.28 shows emission spectral response of CY-3 dye in M-3. The response was noticeable but was not very satisfactory in terms of relative signal change.

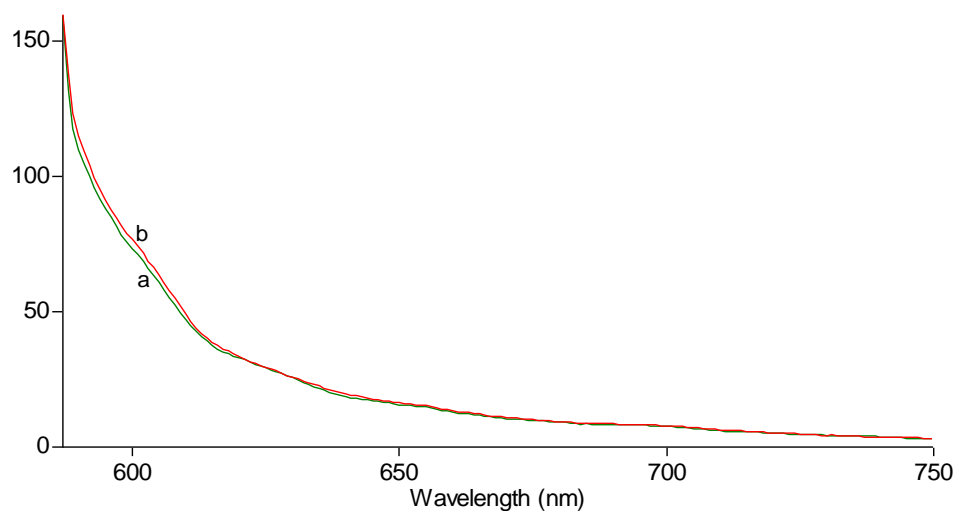


Figure 6.26 Emission/absorption spectra of immobilized CY-2 (coctail M-2) in EC matrix after exposure to different HCO_3^- concentrations.

a) 0 M b) 8.67×10^{-3} M

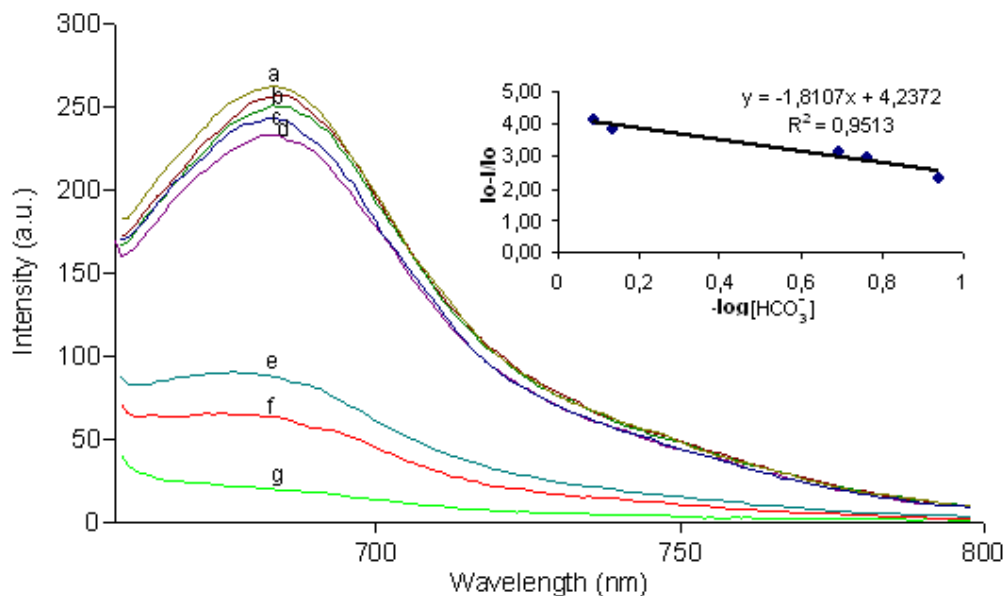


Figure 6.27 Emission/absorption spectra of immobilized CY-3 (coctail M-1) in EC matrix after exposure to different HCO_3^- concentrations.

a) 0 M b) 8.00×10^{-6} M c) 3.33×10^{-6} M d) 6.67×10^{-5} M e) 6.80×10^{-4} M

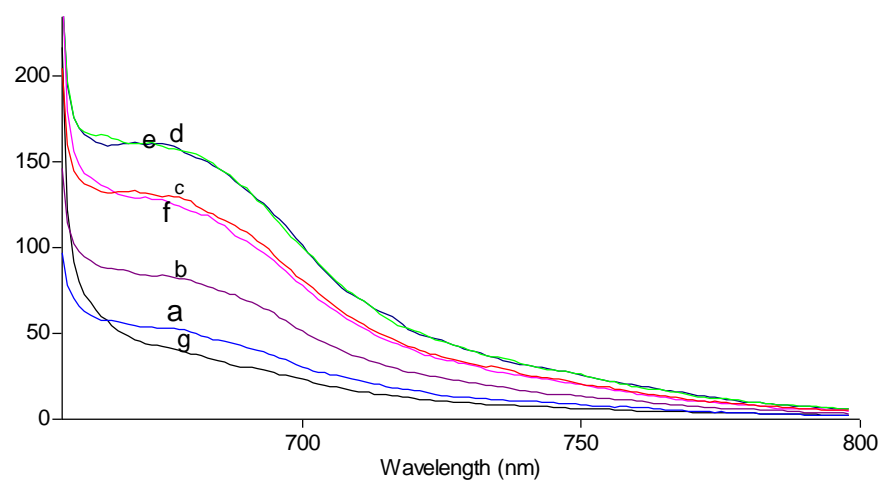


Figure 6.28 Emission/absorption spectra of immobilized CY-3 (coctail M-3) in EC matrix after exposure to different HCO_3^- concentrations.

a) 0 M g) 5.33×10^{-3} M

CHAPTER SEVEN

CO₂ SENSING STUDIES WITH ELECTROSPUN PMMA FIBERS

7.1 Introduction

In the last years the interest for the production of polymer fibers ranging from 100 nm to 1 mm has grown. These materials have many applications in industrial field for their characteristic, like stability, and the easy and reproducible mechanism for the fiber growth. Electrospinning is a novel and efficient fabrication process that can be utilized to form polymer nanofibers (Reneker, Yarin, Fong & Koombhongses, 2000, Yarin, Koombhongses & Reneker, 2001, Theron, Zussman & Yarin, 2001; Bognitzki and et al, 2001).

The electrospinning process is a way to produce nano size polymer fibers. In this process a high electric field is applied to viscous polymer solution, held in capillary tube, inducing a charge density on the liquid surface. Mutual charge repulsion causes a force directly opposite to the surface tension. When the electric field is sufficiently high, the surface of the solution in proximity of the tip of the capillary tube elongates and forms a cone, named Taylor cone. A critical value of the electric field exists, for which the repulsive electrical force overcomes the surface tension. As the critical value is reached a charge jet of the solution is ejected from the tip of the Taylor cone. As the jet accelerates and thins in the electric field, radial charge repulsion results in splitting of the primary jet into multiple filaments, in a process known as “splaying.” (Doshi & Reneker, 1995).

In this view the final fiber size is determined primarily by the number of subsidiary jets formed. When the filaments dry and solidify, electrically charged fibers remain. These charged fibers can be directed or accelerated by electrical forces and then collected in sheets or other useful geometrical forms.

Following parameters effect size and morphology of the obtained fiber.

1. Molecular Weight, Molecular-Weight Distribution and Architecture (branched, linear etc.) of the polymer
2. Solution properties (viscosity, conductivity & and surface tension)
3. Electric potential, Flow rate & Concentration
4. Distance between the capillary and collection screen
5. Ambient parameters (temperature, humidity and air velocity in the chamber)
6. Motion of target screen (collector).

In this work we report preparation and characterization of dye-doped PMMA (poly-methyl-methacrylate) micro fibers obtained by electrospinning.

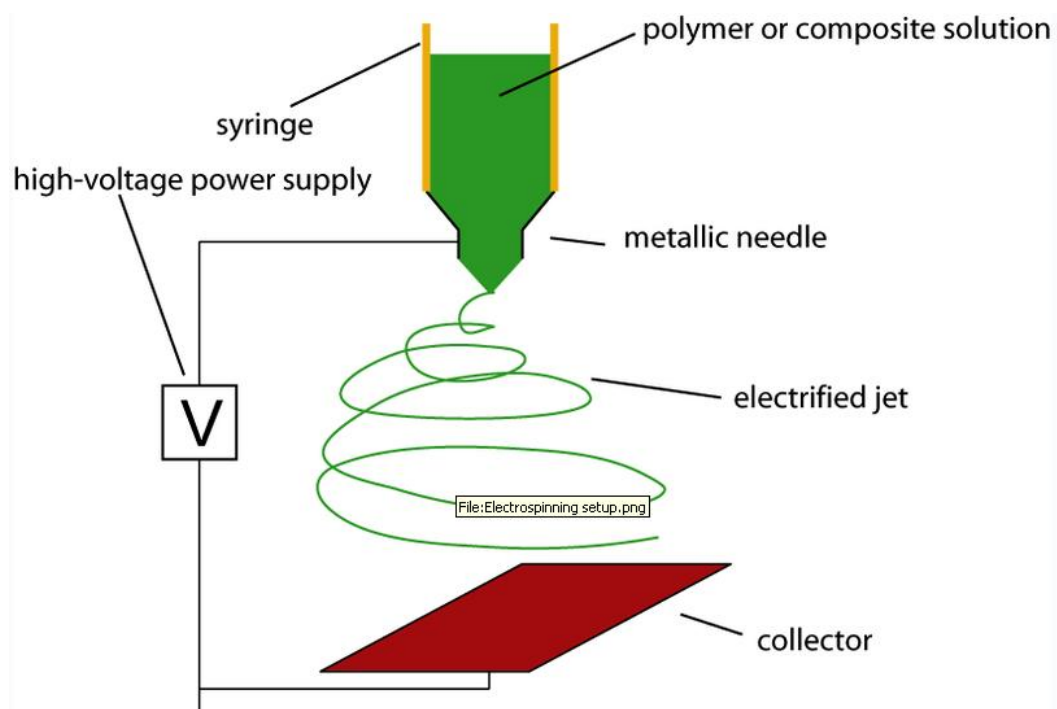


Figure 7.1 Electrospinning instrument. Schematic of an electrospinning setup (retrieved from http://en.wikipedia.org/wiki/File:Electrospinning_setup.png.)

7.2 Materials and Equipment

PMMA based nano fibers were prepared in three different composition.

First one (C-1) contains 240 mg of PMMA, 72 mg of ionic liquid (**RTIL**; 1-ethyl-3-methylimidazolium tetrafluoroborate), 168 mg of plasticizer (DOP), 1.0 mg of AZM-I or AZM-II (2.5 mmol dye/kg polymer), stoichiometric amount of potassium tetrakis (4- chlorophenyl) borate and 1.5mL of THF.

Second one (C-2) contains 240 mg of PMMA, 96 mg of ionic liquid (**RTIL**; 1-ethyl-3-methylimidazolium tetrafluoroborate), 144 mg of plasticizer (DOP), 1.0 mg of AZM-I or AZM-II (2.5 mmol dye/kg polymer), stoichiometric amount of potassium tetrakis (4- chlorophenyl) borate and 1.5mL of THF.

Third one (C-3) contains 240 mg of PMMA, 120 mg of ionic liquid (**RTIL**; 1-ethyl-3-methylimidazolium tetrafluoroborate), 120 mg of plasticizer (DOP), 1.0 mg of AZM-I or AZM-II (2.5 mmol dye/kg polymer), stoichiometric amount of potassium tetrakis (4- chlorophenyl) borate and 1.5mL of THF.

Chemical structures of the AZM dyes were shown in chapter four. Figure 7.2 shows SEM photo of the electrospun PMMA fibers.

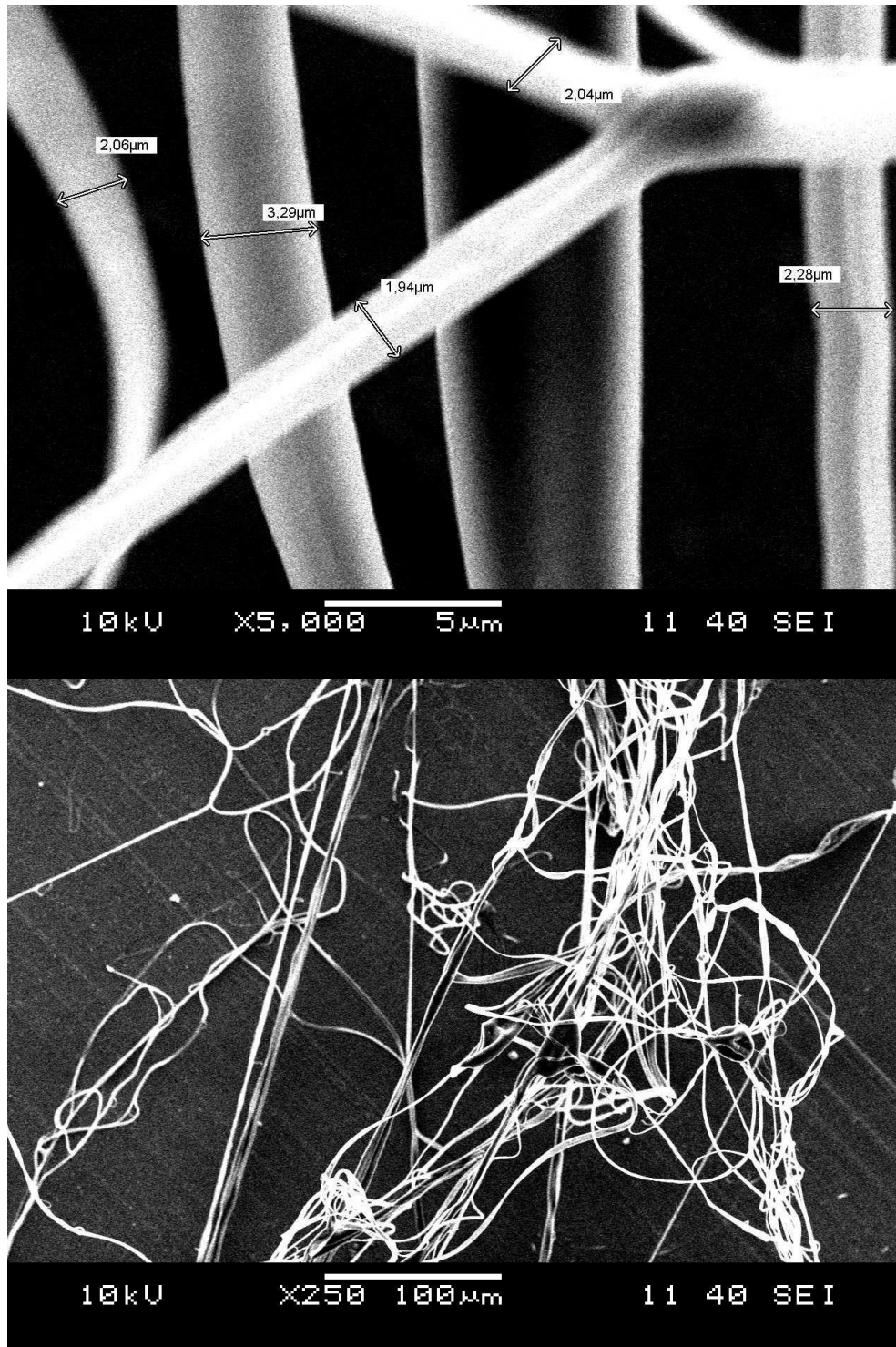


Figure 7.2 SEM photo of the electrospun PMMA fibers (fiber diameter 2 μm.) Morphology of electrospun PMMA fibers with an average diameter of 2 μm.

7.3 Gases and Dissolved CO₂ Sensing Studies in PMMA

Gaseous CO₂ and N₂ were mixed in the concentration range 0–100% in a gas diluter (Sonimix 7000A gas blending system). The output flow rate of the gas mixture was maintained at 250 mL min⁻¹. Gas mixtures were introduced into the sensor agent-containing cuvette via a diffuser needle under ambient conditions either directly or after humidification of the gas by bubbling through water at 35 °C.

7.4 Results and Discussion

In this work a series of CO₂ sensitive nanofibers with various compositions of poly-methyl-methacrylate (PMMA)/plasticizer and ionic liquid were produced by electrospinning.

Quenching-based optical chemical sensors were then fabricated by the electrospinning technique. The fluorescent AZM-I dye has been used as CO₂ sensing agent together with ionic liquid; 1-ethyl-3-methylimidazolium tetrafluoroborate in PMMA. The characterization, electrospinning fabrication, and sensing capability of these fibers were also discussed.

Figure 7.3-7.5 show emission spectra of AZM-I dye in C-1, C-2 and C-3 (PMMA) after exposure to gaseous CO₂. We could not observe a significant response for gas phase measurements. However, the PMMA doped fibers yielded an emission based spectral response for wet CO₂. Figure 7.6, 7.7 and 7.8 show fluorescence quenching based response of AZM-I dye after exposure to dissolved CO₂. In all cases the electrospun fibers exhibited significant response for dCO₂ in the concentration range of 2×10^{-4} - 9.6×10^{-3} , 8×10^{-4} - 10^{-2} and 10^{-5} - 10^{-2} for C-1, C-2 and C-3 respectively. The observed relative signal change was about 70% in all compositions.

The interference effects of other anions in fluorescence intensities in the presence of NO₃⁻, ClO₄⁻, AcO⁻, C₂O₄²⁻ and SO₄²⁻ were tested with 10⁻³ M solutions of the

anions in separate solutions for AZM-I dye. Results of this study were given at the end of the chapter four.

The expected results for PMMA fiber sensors are an order of magnitude higher sensitivity to the dissolved CO₂ than sensor slides formed from continuous thin films. This is believed to be due to the higher surface area to volume ratio of the electrospun nanofibrous materials. However, our preliminary results were not in accordance with expectations. The sensitivity can be tuned with the fiber size, experimental measurement set up, flow rate and length of tubings. Additionally, the type of polymer is also effective in terms of diffusion.

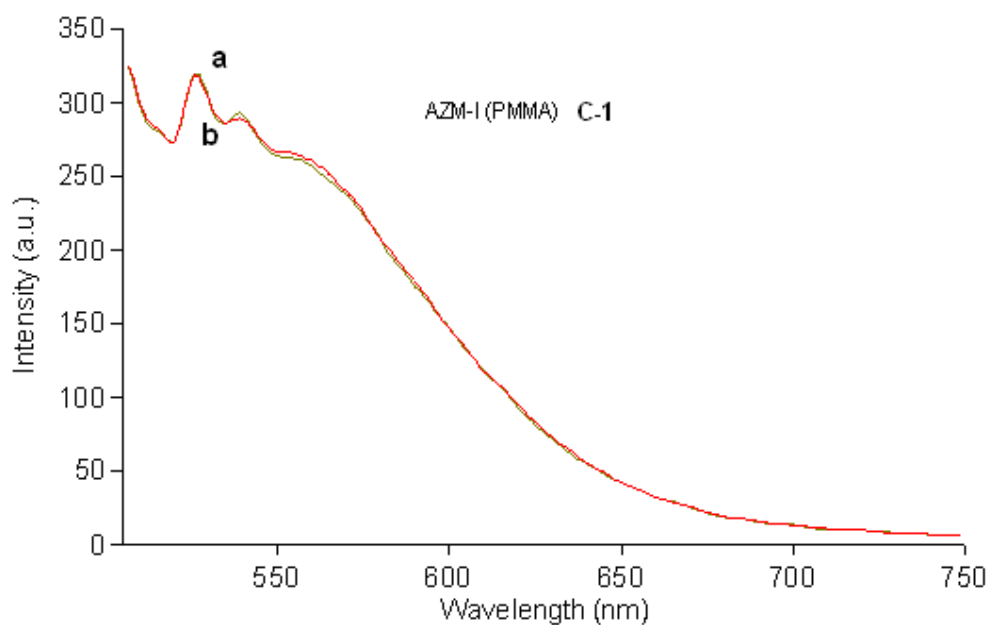


Figure 7.3 Emission spectra of AZM-I, C-1 (PMMA).

a) 0% CO₂ b) 100% CO₂

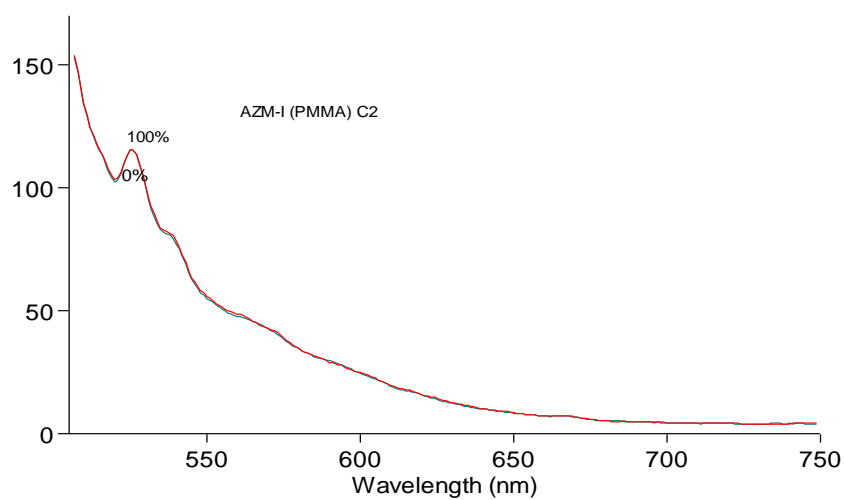


Figure 7.4 Emission spectra of AZM-I, C-2 (PMMA).

a) 0% CO₂ b) 100% CO₂

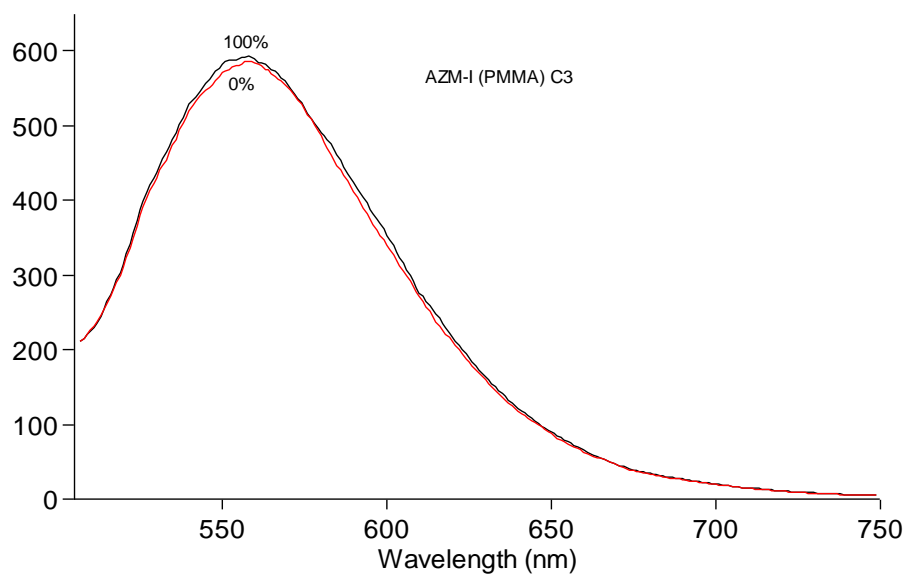


Figure 7.5 Emission spectra of AZM-I, C-3 (PMMA).

a) 0% CO₂ b) 100% CO₂

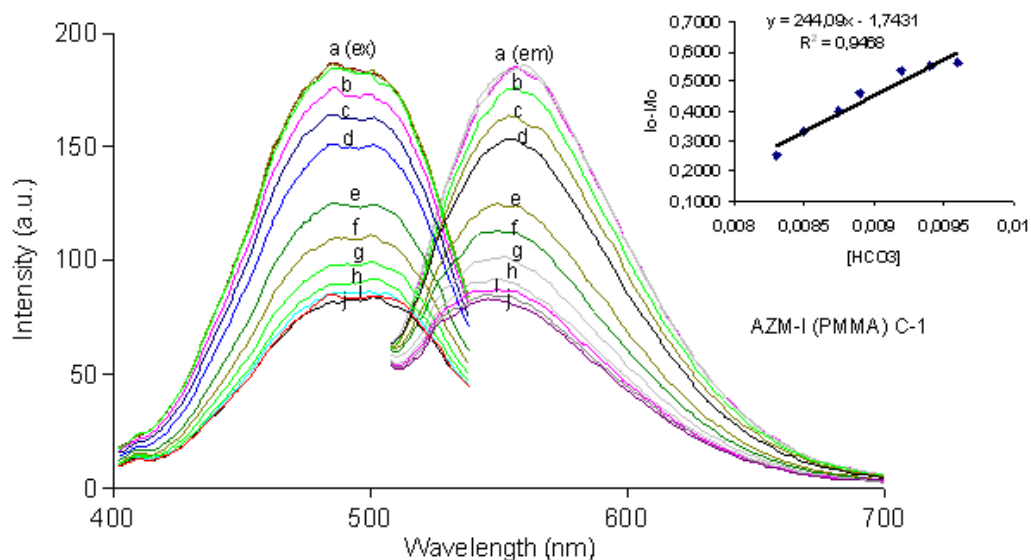


Figure 7.6 Emission spectra of immobilized AZM-I in PMMA (C-1) nano fibers after exposure to different HCO_3^- concentrations.

a) 0 M; 2.00×10^{-4} M; 6.00×10^{-4} M; b) 2.60×10^{-3} M; c) 4.60×10^{-3} M; d) 8.30×10^{-3} M; e) 8.50×10^{-3} M; f) 8.75×10^{-3} M; g) 8.80×10^{-3} M; h) 8.90×10^{-3} M; i) 9.40×10^{-3} M; j) 9.60×10^{-3} M.

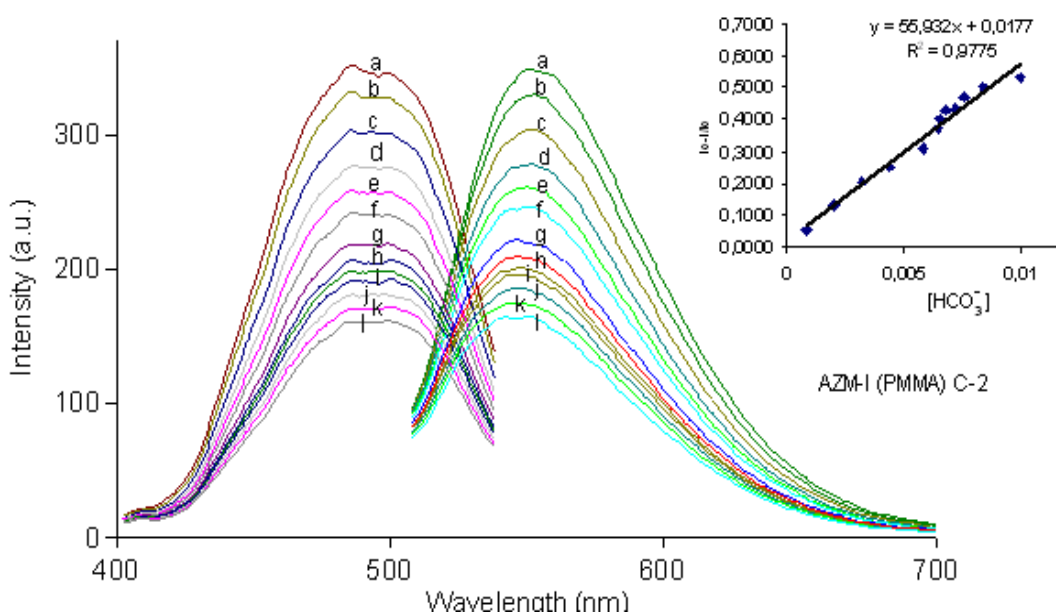


Figure 7.7 Emission spectra of immobilized AZM-I in PMMA (C-2) nano fibers after exposure to different HCO_3^- concentrations.

a) 0 M; b) 8.00×10^{-4} M; c) 2.00×10^{-3} M; d) 3.20×10^{-3} M; e) 4.40×10^{-3} M; f) 5.80×10^{-3} M; g) 6.45×10^{-3} M; h) 6.50×10^{-3} M; i) 6.80×10^{-3} M; j) 7.20×10^{-3} M; k) 8.40×10^{-3} M; l) 1.00×10^{-2} M

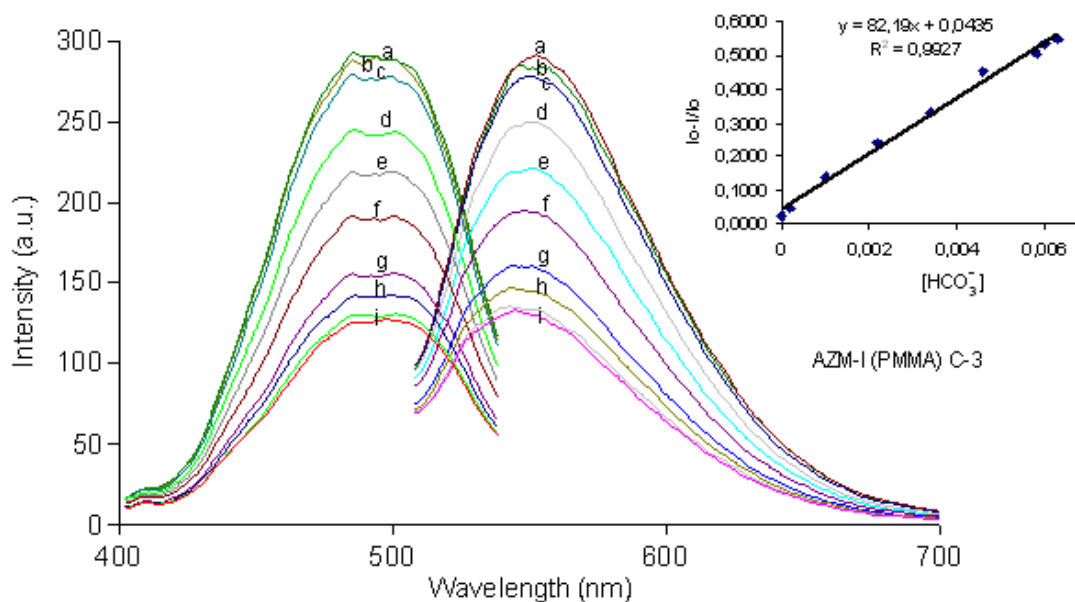


Figure 7.8 Emission spectra of immobilized AZM-I in PMMA (C-3) nano fibers after exposure to different HCO_3^- concentrations.

a) 0 M; b) 1.60×10^{-5} M; c) 2.00×10^{-4} M; d) 1.00×10^{-3} M; e) 2.20×10^{-3} M; f) 3.40×10^{-3} M; g) 4.60×10^{-3} M; h) 5.80×10^{-3} M; i) 6.00×10^{-3} M; 6.30×10^{-3} M.

The relative signal changes of emission spectra of the cocktails 1–3 were monitored after addition of certain concentrations of HCO_3^- solutions. The linearized calibration curve of the sensor compositions C-1, C-2 and C-3 are shown in Figure 7.4, Figure 7.5 and Figure 7.6. The dynamic working range is logarithmic and covers the concentration range of 8.30×10^{-3} to 9.60×10^{-3} mol L⁻¹ for C-1; 8.00×10^{-4} to 1.00×10^{-2} mol L⁻¹ for C-2 and 1.60×10^{-5} to 6.30×10^{-3} mol L⁻¹ for C-3.

7.5 Conclusion

CO_2 sensitive nanofibers with various compositions of poly-methyl-methacrylate (PMMA)/plasticizer and ionic liquid were produced by electrospinning with different cocktail compositions.

Figure 7.3-7.5 show emission spectra of AZM-I dye in C-1, C-2 and C-3 (PMMA) after exposure to gaseous CO_2 . We could not observe a significant response for

gaseous CO₂. But, in all cases the electrospun fibers exhibited significant response for dCO₂ in the concentration range of 2.00×10^{-4} - 9.60×10^{-3} , 8.00×10^{-4} - 10^{-2} and 10^{-5} - 10^{-2} for C-1, C-2 and C-3 respectively for wet CO₂.

CHAPTER EIGHT

CONCLUSION

There are only a limited number of fluorescent “proton driven” molecular switches available covering the neutral-alkaline pH region. In this thesis the AZM derivatives; with fast switching speeds; contain available active centers for proton attacks and are appropriate for use as fluorescent pH probes between pH 6.0–11.0. The pK_a values and large dynamic working range make the EC-doped AZM molecules promising indicators for dissolved CO_2 sensing in environmental and physiological samples. Also the compatibility of the employed molecules with the solid-state optical components (in particular LED’s emitting in the wavelength range of 500–510 nm) and fiber optics can be useful in construction of inexpensive and miniaturized field available instrumentation.

In most of the sensor designs, TBAOH and/or perfluoro compound (PFCs) was added into the sensing cocktail as a counter ion in order to increase the sensitivity and lifetime. However, we did not observe any significant enhancement in sensor response after addition of TBAOH into cocktail compositions for AZM-I. But we observed an enhancement in sensor performance after addition of PFCs into cocktail composition for AZM-II dye in terms of working range and linearity.

CO_2 sensitive nanofibers with various compositions of poly-methyl-methacrylate (PMMA)/plasticizer and ionic liquid were produced by electrospinning with different cocktail compositions. We could not observe a significant response for gaseous CO_2 . But, in all cases the electrospun fibers exhibited significant response for dCO_2 .

REFERENCES

- Ambroziak, K., Szypa, M. A. (2007). Synthesis of unsymmetrical chiral salen ligands derived from 2-hydroxynaphthaldehyde and substituted salicylaldehydes. *Tetrahedron Lett*, 48, 3331-3335.
- Amao, Y. and Nakamura, N. (2004). Optical CO₂ sensor with the combination of colorimetric change of á-naphtholphthalein and internal reference fluorescent porphyrin dye. *Sensors and Actuators B*, 100 (3), 347-351.
- Baker, S. N., Baker, G. A., & Bright, F. V. (2002). Temperature-dependent microscopic solvent properties of dry and wet 1-butyl-3-methylimidazolium hexafluorophosphate: correlation with ET (30) and Kamlet-Taft polarity scales. *Green Chem.* 4, 165–169.
- Baldini, F., Falai, A., De Gaudio, A. R., Landi, D., Lueger, A.; Mencaglia, A. (2003). Continuous Monitoring of Gastric Carbon Dioxide with Optical Fibres. *Sensors and Actuators B*, B90 (1-3), 132-138.
- Baldini F., Chester A.N., Homola J. & Martellucci S. (2004). *Springer*, Proceedings of the NATO Advanced Study Institute on Optical Chemical Sensors.
- Baldini F. et al. (eds.) (2006). Optical Chemical Sensors, 99–116, *Springer*. Printed in the Netherlands.
- Baldini F. et al. (eds.) (2006). Optical Chemical Sensors, 297–321, *Springer*. Printed in the Netherlands.
- Becuwe, M., Cazier, F., Bria, M., Woisel, P., Delattrea, F. (2007). Tuneable fluorescent marker appended to b-cyclodextrin: a pH-driven molecular switch. *Tetrahedron Lett.*, 48, 6186-6188.

- Bognitzki M., Czado W., Frese T., Schaper A., Hellwig M., Steinhart M., Greiner A., Wendorff J.H. (2001). *Adv. Mater.* 13 70.
- Brown, G. J., Silva, A. P., James, M. R., McKinney, B. O. F., Pears, D. A., Weir, S. M. (2008). a Solid-bound, proton-driven, fluorescent 'off-on-off' switches based on PET (photoinduced electron transfer). *Tetrahedron*, 64, 8301-8306.
- Burke C. S., Markey A., Nooney R. I., Byrne P., McDonagh C. (2006). *Sensors and Actuators B*, 119 288–294, Development of an optical sensor probe for the detection of dissolved carbon dioxide.
- Bültzingslöwen, C., McEvoy, A. K., McDonagh, C., MacCraith, B. D., Klimant, I., Krause, C. & Wolfbeis, O. S. (2002). Sol-Gel Based Optical Carbon Dioxide Sensor Employing Dual Luminophore Referencing for Application in Food Packaging Technology. *Analyst*, 127 (11), 1478-1483.
- Bultzingslowen C. von, McEvoy A.K., McDonagh C., MacCraith B.D. (2003). Lifetime-based optical sensor for high-level pCO₂ detection employing fluorescence resonance energy transfer, *Anal. Chim. Acta*, 480 (2) 275–283.
- Cheng, F., Tang, N. (2008). pH-induced molecular switch of a novel trinuclear Ru(II) polypyridyl complex., *Inorg. Chem. Commun.*, 11, 506-508.
- Dasgupta K.P., Zhang G., Poruthoor S.K., Caldwell S., Shen D., Liu S.Y. (1998). *Anal. Chem.*, 70 4661–4669.
- DeGrandpre M.D., Hammar T.R., Smith S.P., Sayles F.L. (1995). *Limnol. Oceanogr.* 40 969–975.
- Diaz-Garcia M.E., Badia R. (2004). Molecularly imprinted polymers for optical sensing devices" in *Optical Sensors: Industrial, Environmental and Diagnostic Applications*, R.Narayanaswamy, O. S. Wolfbeis, (Eds.), *Springer*.

- Dhami, S., Mello A. J., Rumbles, G., Bishop, S. M., Phillips, D. & Beeby, A. (1995). Phthalocyanine fluorescence at high concentration: dimers or reabsorption effect? *Photochem. Photobiol.*, 61, 341.
- Dinten O. (1988). Experimental and theoretical contributions in order to improve ion-selective electrodes based on PVC liquid membranes in terms of membrane technology, ETH Ph.D. thesis No. 8591.
- Doshi J., Reneker D.H. (1995). A model of steady state jet in the electrospinning process, *Mechanics Research Communications*, 35 151.
- Ertekin, K., Klimant, I., Neurauder, G. & Wolfbeis, O. S. (2003). Characterization of a Reservoir-Type Capillary Optical Microsensor for pCO₂ Measurements. *Talanta*, 59 (2), 261-267.
- Ertekin K., Alp S., Karapire C., Yenigül B, Henden E., Icli S. (2000) *J. Photochem. Photobiol., A*, 137, 155–161.
- Ertekin K., Alp. (2006) *Sensors and Actuators*, 115 672–677 Enhanced emission based optical carbon dioxide sensing in presence of perfluorochemicals (PFCs)
- Fu, L., Cao, L., Liu, Y. (2004). Molecular and nanoscale materials and devices in electronics. *Adv. Colloid Interface Sci.*, 111, 133-157.
- Ge X.D., Kostov Y., Rao G. (2003). High-stability non-invasive autoclavable naked optical CO₂ sensor, *Biosens. Bioelectron.* 18 (7) 857–865.
- Giordani, S., Mabel, A., Cejas, A. M., Raymo, F. M. (2004). Photoinduced proton exchange between molecular switches. *Tetrahedron*, 60, 10971-10981.

Goyet C., Walt D.R., Brewer P.G. (1992). *Deep-Sea Res.* 39 1015–1026.

Göpel W., Hesse J., Zemel J.N. (Eds.) (1991). *Sensors: A Comprehensive Survey*, Vol. 1: Fundamentals and General Aspects, VCH, Weinheim, Germany.

Göpel W., Hesse J., Zemel J.N. (eds.) (1991-1993). *Sensors - A Comprehensive Survey*, VCH, Weinheim.

Grigoras, M., Antonoaia, N. C. (2005). Synthesis and characterization of some carbazole-based imine polymers. *Eur. Polym. J.*, 41, 1079-1089.

Haupt K. (2001). Molecularly imprinted polymers in analytical chemistry, *Analyst*, 126:747-756.

Huber C., Krause C., Werner T., Wolfbeis O.S. (2003). Serum chloride optical sensors based on dynamic quenching of the fluorescence of photo-immobilized lucigenin, *Microchimica Acta*, 142: 245-253.

Ines Oehme (1995). Doctoral Thesis, Chemical Optical Sensors for Determination of Heavy Metals. Innovations section of Environmental Health Perspectives, Volume 104, Number 5.

IUPAC (1991). *Pure & Appl. Chem.* 63, 1247.

Janata J. (1990). *Anal. Chem.*, 62 33R

Janata J. (1989). *Principles of Chemical Sensors*, Plenum Press, New York.

Klimant I., Wolfbeis O.S. (1995). Oxygen-sensitive materials based on silicone-soluble ruthenium complexes, *Anal. Chem.*; 67: 3160-3166.

- Koelling M., Hecht H. & Holst G.A. (2002). Simple plastic fiber based optode array for the in-situ measurement of ground air oxygen concentrations.- in: Advanced Environmental Sensing Technology II.- Tuan Vo-Dinh, Stephanus Böttgenbach (Eds.), *Proceedings of SPIE*, 4576, 75-86.
- Lakowicz, J. R. (1993). Principles of Fluorescence Spectroscopy. Plenum Press: New York and London.
- Lakowicz J.R. (1999). Principles of Fluorescence Spectroscopy, 2nd ed., Kluwer Academic/Plenum Publishers, New York.
- Lerchi, M., Bakker, E., Rusterholz, B. & Simon, W. (1992). Lead-selective bulk optodes based on neutral ionophores with subnanomolar detection limits. *Anal. Chem.*, 64 (14), 1534-1540.
- Lobnik A., Wolfbeis O.S. (1998). Sol-gel based sensor for dissolved ammonia, *Sensors and Actuators B*; 51: 203.
- MacCraith B.D., O'Keeffe G., McEvoy A.K., McDonagh C.M., McGilp J.F., O'Kelly B., O'Mahony J.D., Cavanagh M. (1994). LED-based oxygen sensing using evanescent wave excitation of a dye-doped sol-gel coating, *Journal of Optical Engineering*; 33: 3861-3866.
- Mayr, T. (1999). Neutral carrier based fluorosensor for silver (I) ions. Diploma Thesis, Graz.
- Mélares, C., Gandini, A. (1996). Polymeric schiff bases bearing furan moieties 2. Polyazines and polyazomethines. *Polym. Int.*, 40, 33-39.
- Mertz E., Zimmerman S.C. (2003). Cross-linked dendrimer hosts containing reporter groups for amine guests, *J. Amer. Chem. Soc.*; 125: 3424-3425.

Mills A., Chang Q., McMurray N. (1992). *Anal. Chem.* 64 1383.

Mills A., Chang Q. (1993). *Analyst* 118 839–843.

Mills A., Chang Q. (1993). Fluorescence plastic thin-film sensor for carbondioxide, *Analyst* 118 (7) 839–843.

Mills A., Chang Q. (1994). Colorimetric polymer film sensors for dissolved carbon-dioxide, *Sens. Actuator B: Chem.* 21 (2) 83–89.

Mills A., Lepre A., Wild L. (1997). Breath-by-breath measurement of carbon dioxide using a plastic film optical sensor, *Sens. Actuator B: Chem.* 39 (1–3) 419–425.

Mills, A., Chang, Q., McMurray, N. (1992). Equilibrium studies on colorimetric plastic film sensors for carbon dioxide. *Anal. Chem.*, 64, 1383-1389.

Miyatake K. (1988). *Sensor Gijutsu*, 8, 65

Mohr G.J. et al. (1997). Novel optical sensor materials based on solubilization of polar dyes in apolar polymers, *Advanced Materials*; 14: 1108.

Mohr G.J. and Wolfbeis O.S. (1994). Optical sensors for a wide pH range based on azo dyes immobilized on a novel support, *Analytica Chimica Acta*; 292: 41-48.

Mohr G.J. (2004). Chromo- and fluororeactands: Indicators for detection of neutral analytes using reversible covalent bond chemistry, *Chemistry, A European Journal*; 10:1083-1090.

Müller, B. & Hauser, P.C. (1996). Fluorescence optical sensor for low concentrations of dissolved carbon dioxide. *Analyst*, 121, 339-343.

Muller B., Hauser P.C. (1996). Fluorescence optical sensor for low concentrations of dissolved carbon dioxide, *Analyst*, 121 (3) 339–343.

Munkholm C., Walt D.R., Milanovich F.P. (1988). *Talanta* 35 109–112.

Munkholm C., Walt D.R., Milanovich F.P., Klainer S.M. (1986). Polymer modification of fiber optic chemical sensors as a method of enhancing fluorescence signal for pH measurement, *Analytical Chemistry*; 58: 1427-1430.

Narayanaswamy R., Wolfbeis O.S. (Eds.) (2004). Optical Sensors: Industrial, Environmental and Diagnostic Applications, Springer Series on Chemical Sensors and Biosensors Vol.1, *Springer*, Berlin-Heidelberg, Germany.

Neurauter, G., Klimant I. & Wolfbeis, O. S. (1999). Microsecond Lifetime-Based Optical Carbon Dioxide Sensor Using Luminescence Resonance Energy Transfer. *Anal. Chim. Acta*, 382, 67-75.

Nivens D.A., Schiza M.V., Angel S.M. (2002). Multilayer sol–gel membranes for optical sensing applications: single layer pH and dual layer CO₂ and NH₃ sensors, *Talanta* 58 (3) 543–550.

Oehme I. et al. (1994). LED-compatible copper (II)-selective optode membrane based on lipophilized Zincon, *Fresenius Journal of Analytical Chemistry*; 350: 563.

Paley M.S. et al. (1990). Solvatochromism. A new method for polymer characterization, *Macromolecules*; 23: 4557.

Parker, C. A. (1968). Photoluminescence of Solutions. *Elsevier*: Amsterdam.

Polymer handbook / ed.: J. Brandrup, E. H. Immergut and E. A. Grulke; Wiley cop. 1999.

Reichardt, C. (1988). Solvents and Solvent Effects in Organic Chemistry. (6th ed.) VCH: Weinheim.

- Reneker D.H., Yarin A.L., Fong H., Koombhongses S. (2000). *J. Appl. Phys.* 87 4531.
- Robert-Baldo G.L., Morris M.J., Byrne R.H. (1985). *Anal. Chem.* 57 2564–2567.
- Röhr, H., Trieflinger, C., Rurack, K., Daub, J. (2006). Proton- and Redox-Controlled Switching of Photo- and Electrochemiluminescence in Thiophenyl-Substituted Boron–Dipyrromethene Dyes. *Chem. Eur. J.*, 12, 689-700.
- Schaden S., Haberkorn M., Frank J., Baena J.R., Lendl B. (2004). Direct determination of carbon dioxide in aqueous solution using mid-infrared quantum cascade lasers, *Appl. Spectrosc.* 58 (6) 667–670.
- Schmidt, W. (1994). *Optische Spektroskopie*. VCH: Weinheim.
- Seiler K., Wang K., Bakker E., Morf W.E., Rusterholz B., Spichiger U.E., Simon W. (1991). Characterization of sodium-selective optode membranes based on neutral ionophores and assay of sodium in plasma, *Clinical Chemistry*; 37: 1350-1355.
- Seiler, K. & Simon, W. (1992). Theoretical aspects of bulk optode membranes. *Anal. Chim. Acta*, 266, 73-87.
- Seitz W.R. (1991). Optical ion sensing, in: *Fiber optic chemical sensors and biosensors II* (Wolfbeis O.S., ed.), CRC Press, Boca Raton, Florida.
- Shi, D., Yaowu, S. Y., Wang, F., Tian, Q. (2008) Macromolecules, Tuneable fluorescent marker appended to β -cyclodextrin: a pH-driven molecular switch. *Tetrahedron Letters*. 417 478-7484.
- Shiraishi, Y., Tokitoh, Y., Nishimura, G., Hirai, T. (2007). Solvent-Driven Multiply Configurable On/Off Fluorescent Indicator of the pH Diethylenetriamine Bearing Two End Pyrene Fragments. *J. Phys. Chem. B*, 111, 5090-5100.

- Shiraishi, Y., Miyamoto, M., Hirai, T. (2007). Temperature-driven on/off fluorescent indicator of pH window: an anthracene-conjugated thermo responsive polymer. *Tetrahedron Lett*, 48, 6660–6664.
- Shortreed M., Kopelman R., Kuhn M., Hoyland B. (1996). Fluorescent fiber-optic calcium sensor for physiological measurements, *Analytical Chemistry*; 68: 1414.
- Skoog D.A., West D.M., Holler F.J. (1994). *Analytical Chemistry*, Saunders College Publishing.
- Silva, S. A., Loo, K. C., Amorelli, B., Pathirana, S. P., Nyakirangani, M., Dharmasena, M., Demarais, S., Dorcley, B., Pullay, P., Salih, Y. A. (2005). A fluorescent “off-on-off” proton switch derived from natural products and further studies of first-generation fluorescent photoinduced electron transfer (PET) systems. *J. Mater. Chem.*, 15, 2791-2795.
- Stumm W., Morgan J.J. (1981). *Aquatic Chemistry*, 2nd ed., Wiley, New York.
- Tabacco M.B., Uttamlal M., McAllister M., Walt D.R. (1999). *Anal. Chem.* 71 154–161.
- Theron A., Zussman E., Yarin A.L. (2001). *Nanotechnology* 12 384.
- Uttamlal M., Walt D.R. (1995). *Biotechnology* 13 597–601.
- Yarin A.L., Koombhongses S., Reneker D.H. (2001). *J. Appl. Phys.* 89 3018.
- Wolfbeis, O.S. (1991). *Fiber Optic Chemical Sensors and Biosensors*, CRC, Boca Raton, Florida.
- Walt D.R., Gabor G. (1993). *Anal. Chim. Acta* 274 47–52.

- Wang Z., Wang Y., Cai W.-J. Liu S.-Y. (2002). *Talanta* 57 69–80, A long pathlength spectrophotometric $p\text{CO}_2$ sensor using a gas-permeable liquid-core waveguide.
- Weigl B.H., Wolfbeis O.S. (1995). New hydrophobic materials for optical carbon dioxide sensors based on ion-pairing, *Anal. Chim. Acta* 302 (2–3) 249–254.
- Williams, A. T. R., Winfield, S. A., Miller, J. N. (1983). Relative fluorescence quantum yields using a computer-controlled luminescence spectrometer. *Analyst*, 108, 1067-1071.
- Wolfbeis O.S. (ed.) (1991). *Fiber Optic Chemical Sensors and Biosensors*, Vols. I and II, CRC Press, Boca Raton.
- Wolfbeis O.S., Weis L.J., Leiner M.J.P., Ziegler W.E. (1988). *Anal. Chem.* 60 2028–2030.
- Wolfbeis O.S. (1995). Fluorescence-based ion sensing using potential-sensitive dyes, *Sensors & Actuators B*; 29: 140.
- Wong J., Angell C.A. (1977). *Glass Structure by Spectroscopy*, Marcel Dekker, New York.
- Xiao, Y., Fu, M., Qian, X., Cui, J. (2005). A proton sponge-based fluorescent switch. *Tetrahedron Lett.*, 46, 6289-6292.
- Zhang Z., Seitz W.R., 1984, *Anal. Chim. Acta* 160 305–309.